



Michael Rumetshofer, BSc

First-principles molecular transport calculations

MASTER'S THESIS

to achieve the university degree of

Diplom-Ingenieur

Master's degree programme: Technical Physics

submitted to

Graz University of Technology

Supervisor

Univ.-Prof. Dipl.-Phys. Dr.rer.nat. Wolfgang von der Linden

Co-Supervisor

Ass.Prof. Dr. Lilia Boeri

Institute of Theoretical and Computational Physics

Graz, April 2016

Abstract

Molecular charge transport is one of the most fascinating topics in solid-state physics. On one hand there is attempt for developing molecular devices which reproduce the properties of microelectronic components on the other hand it is an interesting topic because of the comparison between measurements and first-principles calculations. The aim of this work is a first-principles calculation of the charge transport through a benzene-1,4-dithiol (BDT) molecule contacted by two gold chains. The BDT transport system is a benchmark system in both, experiment and theory. There are significant differences between the measurements and the theoretical predictions to be worth the effort of further investigations. The aim of this thesis is to investigate the effect of strong correlations between the electrons in the BDT molecule on the transport properties.

In order to compute the transport properties the electronic band structure of the system is calculated using the plane-wave pseudopotential code *Quantum Espresso*. The Kohn-Sham eigenvalues and eigenfunctions are then transformed to a real-space basis of Maximally Localized Wannier Functions (MLWF) using the code *Wannier90*. This allows extracting a tight-binding Hamiltonian to describe the transport system. Strong electron correlations are then included using an extended Hubbard model. The many-body physics within Non-equilibrium Green functions (NEG) enable doing the transport calculation through a strongly correlated molecule connected by two leads.

First the transport over a single gold chain is studied. A tool for calculating the current through a lead-center-lead system is implemented. By comparing the electronic band structure of the gold chain with their transmission function, it is possible to check the algorithm. Then the transport properties of the gold-BDT-gold system are calculated. It turns out that in the case of single gold chains as leads, the transport properties are determined only by the orbitals coupling to the gold s -orbitals. Therefore transport through the benzene p_z -orbitals is suppressed. Strong correlations between the electrons in the central region are treated by use of many-body physics. The correlations lower the current flowing through the transport system.

Kurzfassung

Der Ladungstransport in Molekülen ist eines der faszinierendsten Gebiete der Festkörperphysik. Einerseits gibt es Bestrebungen molekulare Bauelemente zu entwickeln, die mikroelektronische Komponenten nachbilden, andererseits ist der Vergleich zwischen experimentellen Messungen und *Ab-initio*-Rechnungen ein interessantes Thema. Ziel dieser Arbeit ist die *Ab-initio*-Berechnung des Ladungstransportes über ein Benzen-1,4-dithiol (BDT) Molekül, das mit zwei Goldketten kontaktiert ist. Das BDT-Transportsystem ist zu einem Referenzsystem im Experiment und in der Theorie geworden. Trotzdem gibt es signifikante Unterschiede zwischen den Messungen und den Vorhersagen der Theorie, was weitere Forschungen rechtfertigt. Unter anderem stehen die Auswirkungen von starken Korrelationen zwischen Elektronen im BDT-Molekül im Mittelpunkt dieser Arbeit.

Um die Transporteigenschaften berechnen zu können, wird der Dichtefunktionaltheorie (DFT) Code *Quantum Espresso* zum Bestimmen der elektronischen Bandstruktur des Systems verwendet. Die Kohn-Sham Eigenwerte und Eigenfunktionen werden mit dem Code *Wannier90* in eine Basis maximal-lokalisierter Wannierfunktionen (MLWF) transformiert. Diese Vorgehensweise führt zu einem, das Transportsystem beschreibenden, Tight-Binding-Hamiltonian. Starke Korrelationen zwischen den Elektronen können durch ein erweitertes Hubbard-Modell berücksichtigt werden. Die Vielteilchenphysik und Nichtgleichgewichts-Greenfunktionen ermöglichen Transportrechnungen über ein stark-korreliertes Molekül zwischen zwei Kontakten.

Zuerst wird der Ladungstransport über eine Kette von Goldatomen untersucht. Ein Programm zur Berechnung des Stromes durch ein Kontakt-Zentrum-Kontakt System wird implementiert. Durch den Vergleich der elektronischen Bandstruktur der Goldkette mit ihrer Transmissionsfunktion kann der Algorithmus auf Richtigkeit überprüft werden. Dann werden die Transporteigenschaften des Gold-BDT-Gold Systems berechnet. Es stellt sich heraus, dass, bei Verwendung einzelner Goldketten als Kontakte, die Transporteigenschaften nur durch die Orbitale bestimmt werden, die an die Gold *s*-Orbitale koppeln. Der Transport über die Benzen *p_z*-Orbitale wird unterdrückt. Schlussendlich werden starke Korrelationen zwischen den Elektronen in der Zentralregion mit Hilfe der Vielteilchenphysik berücksichtigt. Die Korrelationen reduzieren den Strom durch das Transportsystem.

Acknowledgements

Ich möchte mich bei meinen Betreuern, Prof. Wolfgang von der Linden und Prof. Lilia Boeri, bedanken, die mich im letzten Jahr mit Engagement unterstützt haben, sowohl beim Verstehen und Anwenden der Theorie als auch beim Interpretieren der Ergebnisse. Besonderer Dank gebührt auch Prof. Markus Aichhorn der mit einem Grundstein zu dieser Arbeit legte und stets bereit war sich einzubringen.

Ich möchte mich bei der gesamten Arbeitsgruppe, bestehend aus Prof. Enrico Arrigoni, Gerhard Dorn, Antonius Dorda, Max Sorantin, Delia Fugger, Irakli Titvinidze und Peter Pichler für die Unterstützung und im Besonderen bei Jakob Neumayer für die Zurverfügungstellung von Programmteilen bedanken. Immer ein offenes Ohr für Fragen jeglicher Art hatten auch Gernot Kraberger, Robert Triebel und Manuel Zingl, wofür ich ihnen sehr dankbar bin.

An dieser Stelle möchte ich mich auch bei Andreas Hirczy für die Hilfestellungen beim Umgang mit den Computerressourcen am Institut und bei Brigitte Schwarz für Beistand in allen bürokratischen Dingen bedanken. Dem Zentralen Informatikdienst (ZID) der TU Graz möchte ich für die Zurverfügungstellung von HPC-Ressourcen danken.

Ein besonderer Dank gebührt auch meinen langjährigen Studienkollegen Paul Maierhofer, Markus Bainschab und Ralf Meyer, die zeitgleich am Institut für Experimentalphysik ihre Diplomarbeiten verfasst haben und auch immer für Diskussionen offen standen und Michael Draxler.

Danken möchte ich auch meinen Eltern, Maria und Konrad, die mir das Studieren überhaupt erst ermöglicht haben und mir das Interesse, nicht nur für die Physik, auf meinem Lebensweg mitgegeben haben. Meinem Bruder Johannes danke ich für jeden Kilometer den er mit mir während des Studiums gelaufen ist und mir dabei zugehört hat. Nicht zuletzt möchte ich Monika danken für ihre liebevolle Art und ihre Unterstützung in meinen Vorhaben.

Graz, 2016

Michael Rumetshofer

Contents

1	Introduction	1
2	Theoretical Concepts	5
2.1	Model Hamiltonian	5
2.2	Density Functional Theory	7
2.3	Maximally-localised Wannier functions	9
2.4	Electron interactions	10
2.5	LCR transport system	12
2.6	Green functions	14
2.6.1	Statistical ensembles	14
2.6.2	Non-equilibrium Green functions	15
2.6.3	Lehmann representation	18
2.6.4	Spectral function and occupation number	20
2.7	Coupling Green functions	21
2.7.1	Cluster Perturbation Theory	21
2.7.2	Semi-infinite Chain	23
2.8	Quantum Transport	24
2.8.1	Current between two Systems	24
2.8.2	Current through the LCR System	27
2.8.3	System out of equilibrium	30
2.8.4	Landauer-Büttiker formula	31
2.9	Summary and discussion	34
3	Computational Techniques	37
3.1	Quantum Espresso	37
3.2	Wannier90	38
3.3	Basis states and Hamiltonian	39
3.4	Calculating Green functions	39
3.5	Band Lanczos algorithm	40
3.6	Calculating transport properties	41
4	Application	43
4.1	Gold-Chain	43
4.1.1	The s -model	44
4.1.2	The sd -model	48
4.2	Benzene	53
4.3	Au-BDT-Au system	56
4.3.1	Geometry optimization	57
4.3.2	Hamiltonian and orbitals	59
4.3.3	Transport channels	63
4.3.4	Electron interactions	68
4.3.5	Current-voltage characteristic	70

5 Summary and Prospects

73

Chapter 1

Introduction

Modern computational physics allows to deduce macroscopic properties, e.g. the electrical conductivity, from fundamental equations like the Schrödinger equation. Comparing these calculations with experimental results helps to investigate and improve the theoretical methods and the experimental techniques and leads to deeper insights in the mechanisms of quantum systems. At small scale quantum effects become relevant and there is attempt to use those effects for building molecular devices like a resonant tunneling transistors [1] [2].

An important breakthrough in molecular transport happened in 1997. The groups of Mark Reed at the Yale University and James Tour at the University in South Carolina were able to measure the current-voltage characteristic of a Benzene-1,4-Dithiol (BDT) molecule contacted with gold leads [3]. This experiment is often considered as the first measurement on single molecule junctions. The experiment was done at room temperature in argon atmosphere. BDT became the workhorse in the field of molecular transport and several experiments were done afterwards. For example Lörtscher, Weber and Riel [4] have measured the same system under ultrahigh vacuum conditions at different temperatures (250 K and 50 K). Both experiments used a method called the Mechanically Controllable Break Junction (MCBJ) method. In the MCBJ method a notched metal wire is placed on a flexible substrate. BDT in solution is applied on the metal surface. Bending the substrate until the metal wire breaks and evaporating the solvent produces a self-assembled monolayer (SAM) at the place of fracture. After bending the substrate back until a desired distance between the contacts the current-voltage characteristic can be measured. The distance between the contacts can be determined by using a piezo sensor and the tunneling current. Nowadays there are many more experimental methods, e.g. techniques involving a Scanning Tunneling Microscope (STM) or an Atomic Force Microscope (AFM).

By now many measurements were done on the gold-BDT-gold system. But according to [5] the measured conductances vary between $5 \cdot 10^{-5} G_0$ and $0.1 G_0$. Calculations done for this system predict a conductance between $0.05 G_0$ and $0.4 G_0$. The values are given in units of the conductance quantum $G_0 = 2e^2/h$. Because of this big differences within and between the experimental and theoretical results there is still need to investigate the gold-BDT-gold system in detail. In general the theoretical conductances tend to be higher than the measured ones.

The present work investigates the gold-BDT-gold system drawn in figure 1.1. Even though it is not possible to use single gold chains as leads in an experimental transport system they represent a good model system, because this lead geometry is as simple as possible and it could give deeper insight in the transport mechanisms than using more realistic leads. Keeping the positions of the gold atoms constant and optimizing the positions of the BDT atoms leads to a twisted geometry of the BDT molecule between the gold chains.

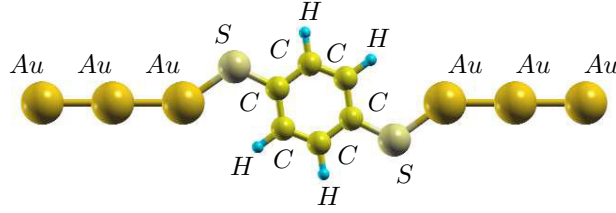


Figure 1.1: Gold-BDT-gold system used for the transport calculation.

The first-principles calculation method chosen in this thesis is an extended version of using Density Functional Theory (DFT) and Non-equilibrium Green functions (NEG). Within DFT the energy levels and wave functions of the transport system including electron correlations at a mean field level can be calculated. Using Maximally Localized Wannier Functions (MLWF) it is possible to reduce the full Hamiltonian of the system to a smaller real-space Hamiltonian which only contains the electronic states relevant for transport. The real-space Hamiltonian can then be rearranged to the Left lead-Center-Right lead (LCR) structure of the transport system. Transport properties through the system can be calculated using NEG. Figure 3.1 sketches the main parts in a DFT+NEG calculation.

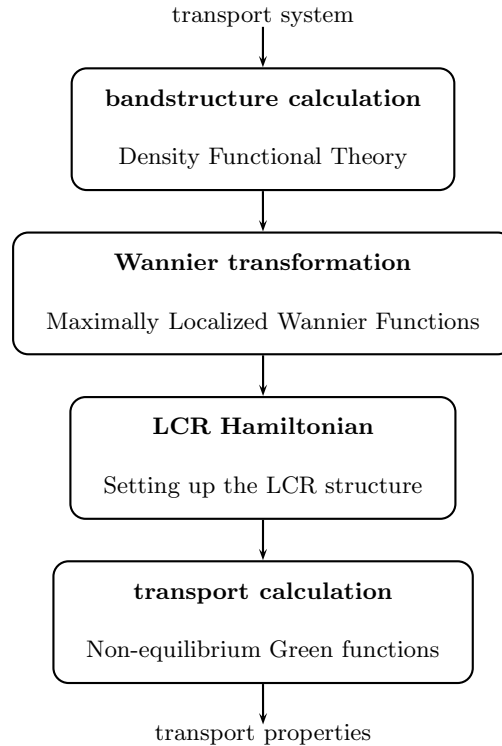


Figure 1.2: Structural model of DFT+NEG.

DFT+NEG is a standard approach [6] and is only able to describe coherent transport. Coherent transport means that the electrons flow elastically without exchanging energy. This is the case if the time that an electron spends on the central molecule of the LCR geometry is shorter than the time it takes to interact with other electrons or phonons. The approximation is correct in the case of large coupling between the leads and the central region. If the coupling is weak electrons stay long enough in the central region to scatter inelastically. In this so-called incoherent transport

regime it is necessary to describe strong correlations between the electrons. This can be done by the use of many-body physics in addition to the DFT+NEG approach [7].

This extended DFT+NEG approach is used in this thesis to be able to describe the transport phenomena in an intermediate regime between strong and weak coupling. In principle the bonds between the gold chains and the sulfur atoms of the BDT molecule are strong and transport should be in the coherent regime, but the large discrepancies between calculated and measured conductances suggest that electronic correlations play an important role in this system.

This thesis is structured as follows. In chapter 2 the theoretical concepts are introduced and discussed, followed by chapter 3 including the computational techniques needed for implementing the concepts. Finally in chapter 4 the theory is applied to the gold-BDT-gold system.

Chapter 2

Theoretical Concepts

This chapter explains how to perform first-principles molecular transport calculations within the method of DFT+NEG including strong electron correlations. Section 2.1 introduces a suitable Hamiltonian for describing quantum systems. How to calculate the model parameters using DFT and MLWFs is discussed in the sections 2.2, 2.3 and 2.5. Within DFT only finite or periodic systems can be calculated and therefore a technique for setting up the Hamiltonian in LCR transport structure is needed. Section 2.4 explains this procedure. The transport calculation in terms of NEG including strong electron correlations is discussed in the sections 2.6, 2.7 and 2.8. Finally section 2.9 illustrates the approximations assumed within this approach.

2.1 Model Hamiltonian

In order to calculate charge transport properties one has to study the movement of charge carriers in the transport system. Here the interest is on electrons interacting with the atomic nuclei and with each other. In quantum mechanics particles are described by their wave functions. The field operators

$$\begin{aligned}\hat{\Psi}^\dagger(\mathbf{r}) &:= \sum_i^N \Psi_i^*(\mathbf{r}) \hat{a}_i^\dagger \\ \hat{\Psi}(\mathbf{r}) &:= \sum_i^N \Psi_i(\mathbf{r}) \hat{a}_i\end{aligned}\tag{2.1.1}$$

denote creation and annihilation of particles in the quantum state described by the wave functions $\Psi_i(\mathbf{r})$. The fermionic commutation rules ensure the anti-symmetry of the electronic states.

$$\begin{aligned}\{\hat{a}_i, \hat{a}_j^\dagger\} &:= \delta_{ij} \\ \{\hat{a}_i, \hat{a}_j\} &:= 0 \\ \{\hat{a}_i^\dagger, \hat{a}_j^\dagger\} &:= 0\end{aligned}\tag{2.1.2}$$

First the electrons are considered to be independent from each other. The model Hamiltonian has to describe the motion of a valence electron through a transport system consisting of effective nuclear potentials. Within the Born-Oppenheimer approximation the atoms are fixed at their equilibrium positions. The kinetic and potential energy term, later called one-particle term, in second quantization is

$$\hat{T} = \int d^3r \hat{\Psi}^\dagger(\mathbf{r}) \left(\frac{-\hbar^2}{2m} \Delta + V(\mathbf{r}) \right) \hat{\Psi}(\mathbf{r}). \quad (2.1.3)$$

Considering the fact that the electrons are interacting with each other due to their Coulomb potential energy U leads to the interaction term

$$\hat{U} = \frac{1}{2} \int d^3r \int d^3r' U(\mathbf{r}, \mathbf{r}') \hat{\Psi}^\dagger(\mathbf{r}) \hat{\Psi}^\dagger(\mathbf{r}') \hat{\Psi}(\mathbf{r}') \hat{\Psi}(\mathbf{r}). \quad (2.1.4)$$

Inserting the definition of the field operators 2.1.1 into the expressions for the kinetic and potential energy term \hat{T} and the interaction term \hat{U} and adding the terms leads to the Hamiltonian

$$\hat{H} = \hat{T} + \hat{U} = \sum_{ij} t_{ij} \hat{a}_i^\dagger \hat{a}_j + \frac{1}{2} \sum_{ijkl} U_{ijkl} \hat{a}_i^\dagger \hat{a}_j^\dagger \hat{a}_k \hat{a}_l \quad (2.1.5)$$

with the parameters

$$\begin{aligned} t_{ij} &= \int d^3r \Psi_i^*(\mathbf{r}) \left(\frac{-\hbar^2}{2m} \Delta + V(\mathbf{r}) \right) \Psi_j(\mathbf{r}) \\ U_{ijkl} &= \int d^3r \int d^3r' U(\mathbf{r}, \mathbf{r}') \Psi_i^*(\mathbf{r}) \Psi_j^*(\mathbf{r}') \Psi_k(\mathbf{r}') \Psi_l(\mathbf{r}). \end{aligned} \quad (2.1.6)$$

This Hamiltonian is so far exact within the Born-Oppenheimer approximation. The Latin index i denotes the wave function \bar{i} and the spin $\sigma \in \{\uparrow, \downarrow\}$. If the wave functions are independent of spin, and the spin of an electron is conserved during a hopping process between two wave functions

$$t_{ij} = t_{\bar{i}\bar{j}} \delta_{\sigma\sigma'} \quad (2.1.7)$$

holds. The Hamiltonian in equation 2.1.5 is very general, but due to the interaction term it is difficult to solve. Knowing the parameters t_{ij} and U_{ijkl} the Hamiltonian can be set up in many-particle space using a suitable basis. However the size of the many-particle space is growing exponentially with the number of wave functions N . This explains why strong electron correlations are usually taken into account in small systems. A possible approximation of the interaction term, which does not reduce the size of the many-particle space but simplifies the calculation, is to consider only density-density correlations

$$\frac{1}{2} \sum_{ijkl} U_{ijkl} \hat{a}_i^\dagger \hat{a}_j^\dagger \hat{a}_k \hat{a}_l \approx \frac{1}{2} \sum_{i \neq j} U_{ij} \hat{n}_i \hat{n}_j \quad (2.1.8)$$

with

$$U_{ij} = \int d^3r \int d^3r' |\Psi_i(\mathbf{r})|^2 |\Psi_j(\mathbf{r}')|^2 U(\mathbf{r}, \mathbf{r}'). \quad (2.1.9)$$

The more localized the wave functions are, the better this approximation is. $U(\mathbf{r}, \mathbf{r}')$ denotes the energy of a screened Coulomb potential

$$U(\mathbf{r}, \mathbf{r}') = \frac{e^2}{4\pi\epsilon|\mathbf{r} - \mathbf{r}'|} \frac{1}{\eta(\mathbf{r}, \mathbf{r}')} \quad (2.1.10)$$

with the screening factor η . The function $\eta(\mathbf{r}, \mathbf{r}')$ represents the screening of the potential due to the remaining mobile charge carriers. To estimate the screening factor the Random Phase Approximation (RPA) [8] can be used. In a first approximation the screening factor can also be estimated by using the Poisson equation

$$\Delta u(\mathbf{r}, \mathbf{r}') = -\frac{\rho(\mathbf{r})}{\epsilon} - \frac{e\delta(\mathbf{r} - \mathbf{r}')}{\epsilon} \quad (2.1.11)$$

where ρ denotes the remaining charge carriers and $u(\mathbf{r}, \mathbf{r}')$ is the potential. In the Thomas-Fermi approximation the charge density is proportional to the potential.

$$\rho(\mathbf{r}) = -\epsilon k_0^2 u(\mathbf{r}, \mathbf{r}') \quad (2.1.12)$$

Solving the Poisson equation in the Thomas-Fermi approximation leads to an exponentially decaying Coulomb potential energy. The screening wave vector k_0 has to be estimated again using techniques like RPA.

$$U(\mathbf{r}, \mathbf{r}') = -eu(\mathbf{r}, \mathbf{r}') = \frac{e^2}{4\pi\epsilon|\mathbf{r} - \mathbf{r}'|} e^{-k_0|\mathbf{r} - \mathbf{r}'|} \quad (2.1.13)$$

A further possible approximation of the interaction part in the Hamiltonian in equation 2.1.5 is to include the interactions only at a mean field level. This is essentially done in DFT calculations.

2.2 Density Functional Theory

In the previous section a suitable model for describing electrons in a solid was introduced. In order to do transport calculations for a real solid within this model one has to determine the hopping parameters t_{ij} and the interaction parameters U_{ijkl} . A widely used approximation to solve the electronic structure problem in real materials is Density Functional Theory (DFT). This section is a short introduction to the theory analogous to the textbook *Theoretische Festkörperphysik* from Czycholl [9]. Starting point is the time-independent Schrödinger equation.

$$\hat{H}\Phi(\mathbf{r}_1, \dots, \mathbf{r}_N) = E\Phi(\mathbf{r}_1, \dots, \mathbf{r}_N) \quad (2.2.1)$$

$\Phi(\mathbf{r}_1, \dots, \mathbf{r}_N)$ is the many-particle wave function, which depends on the position of the N electrons. The full interacting Hamiltonian in the Born-Oppenheimer approximation is

$$\hat{H} = \left(\sum_{i=1}^N \frac{-\hbar^2}{2m} \Delta + \sum_{i=1}^N V(\mathbf{r}_i) + \frac{1}{2} \sum_{\substack{i,j=1 \\ i \neq j}}^N U(\mathbf{r}_i, \mathbf{r}_j) \right), \quad (2.2.2)$$

which is analogous to the Hamiltonian in second quantization in equation 2.1.5. $V(\mathbf{r}_i)$ is the one-particle potential energy for the i th particle and $U(\mathbf{r}_i, \mathbf{r}_j)$ is the interaction energy between the i th and the j th particle. For the present the ground state of the system is considered. DFT introduces a great simplification, because instead of the full many-body wave function $\Phi_0(\mathbf{r}_1, \dots, \mathbf{r}_N)$ it is based on the ground state density $n_0(\mathbf{r})$.

$$n_0(\mathbf{r}) = \int d^3 r_1 \dots \int d^3 r_N \Phi_0^*(\mathbf{r}_1, \dots, \mathbf{r}_N) \sum_{i=1}^N \delta(\mathbf{r} - \mathbf{r}_i) \Phi_0(\mathbf{r}_1, \dots, \mathbf{r}_N) \quad (2.2.3)$$

DFT is based on the papers of Hohenberg and Kohn [10] and Kohn and Sham [11]. The basic theorem of Hohenberg-Kohn says that the groundstate density $n_0(\mathbf{r})$ of a bound system of interacting electrons in some external potential $V(\mathbf{r})$ determines this potential uniquely [12]. A consequence of this theorem is that the ground state energy is a functional of the ground state particle density.

$$E_0 = E[n_0(\mathbf{r})] \quad (2.2.4)$$

Therefore the variational principle

$$\delta E[n_0(\mathbf{r})] = 0 \quad (2.2.5)$$

with the constraint

$$\int d^3r n_0(\mathbf{r}) = N \quad (2.2.6)$$

can be used to obtain the ground state energy of the system. In order to determine the energy functional, one can split the energy into three functionals, the kinetic, the one-particle potential and the interaction term.

$$E[n_0(\mathbf{r})] = T[n_0(\mathbf{r})] + V[n_0(\mathbf{r})] + U[n_0(\mathbf{r})] \quad (2.2.7)$$

For non-interacting electrons the kinetic energy can be written as

$$T[n_0(\mathbf{r})] = \sum_{i=1}^N \int d^3r \Phi_i^*(\mathbf{r}) \left(-\frac{\hbar^2 \Delta}{2m} \right) \Phi_i(\mathbf{r}) \quad (2.2.8)$$

with the particle density

$$n_0(\mathbf{r}) = \sum_{i=1}^N |\Phi_i(\mathbf{r})|^2. \quad (2.2.9)$$

To treat a system with interacting electrons, one introduces some fictitious non-interacting particles, the Kohn-Sham orbitals $\Phi_i(\mathbf{r})$, and drags the rest terms into the functional $U[n_0(\mathbf{r})]$. The one particle potential depends on the particle density as

$$V[n_0(\mathbf{r})] = \int d^3r V(\mathbf{r})n_0(\mathbf{r}). \quad (2.2.10)$$

In comparison with Hartree-Fock theory the interacting functional is

$$U[n_0(\mathbf{r})] = \frac{1}{2} \int d^3r \int d^3r' \frac{e^2}{4\pi\epsilon |\mathbf{r} - \mathbf{r}'|} n_0(\mathbf{r})n_0(\mathbf{r}') + E_{xc}[n_0(\mathbf{r})] \quad (2.2.11)$$

where $E_{xc}[n_0(\mathbf{r})]$ is the exchange correlation functional which contains also the interaction correction to the kinetic energy. The energy functional becomes

$$\begin{aligned} E[n_0(\mathbf{r})] &= \sum_{i=1}^N \int d^3r \Phi_i^*(\mathbf{r}) \left(-\frac{\hbar^2 \Delta^2}{2m} \right) \Phi_i(\mathbf{r}) + \int d^3r V(\mathbf{r})n_0(\mathbf{r}) \\ &\quad + \frac{1}{2} \int d^3r \int d^3r' \frac{e^2}{4\pi\epsilon |\mathbf{r} - \mathbf{r}'|} n_0(\mathbf{r})n_0(\mathbf{r}') + E_{xc}[n_0(\mathbf{r})] \end{aligned} \quad (2.2.12)$$

and the variational principle

$$\delta_{\Phi_i^*} \left\{ E[n_0(\mathbf{r})] - \sum_{j=1}^N \epsilon_j \left(\int d^3r |\Phi_j(\mathbf{r})|^2 - 1 \right) \right\} = 0. \quad (2.2.13)$$

can be used to deduce the Kohn-Sham equations 2.2.14. This equations must be solved self-consistently with equation 2.2.9, which gives the connection between the wave functions and the particle density. Usually the Kohn-Sham equations are solved using a finite set of basis functions to reduce the differential equations to a set of algebraic equations. These equations are typically solved numerically and lead to the Kohn-Sham energies ϵ_i and the wave functions Φ_i .

$$\left\{ -\frac{\hbar^2 \Delta^2}{2m} + V(\mathbf{r}) + \int d^3r' \frac{e^2}{4\pi\epsilon |\mathbf{r} - \mathbf{r}'|} n(\mathbf{r}') + \frac{\delta E_{xc}}{\delta n_0(\mathbf{r})} \right\} \Phi_i(\mathbf{r}) = \epsilon_i \Phi_i(\mathbf{r}) \quad (2.2.14)$$

Finally the problem is to find the right exchange correlation functional $E_{xc}[n_0(\mathbf{r})]$. A widely used approximation for this functional is the Local Density Approximation (LDA). In LDA the exchange correlation functional depends only on the density at the coordinate where the functional is evaluated.

For finite systems the Kohn-Sham equations can be solved in position space as written out in equation 2.2.14. In a periodic crystal it is useful to solve the equations in k -space. In a periodic crystal the Bloch theorem holds and the wave functions can be written as

$$\Phi_i(\mathbf{r}) = \sum_{\mathbf{k}} \underbrace{e^{i\mathbf{k}\mathbf{r}} \varphi_{i\mathbf{k}}(\mathbf{r})}_{\Phi_{i\mathbf{k}}(\mathbf{r})} \quad (2.2.15)$$

where $\Phi_{i\mathbf{k}}(\mathbf{r})$ are Bloch states. A periodic crystal consists of a unit cell of the size $\mathbf{a} \times \mathbf{b} \times \mathbf{c}$ repeated on every lattice vector $\mathbf{R} = n_a \mathbf{a} + n_b \mathbf{b} + n_c \mathbf{c}$ with $n_a, n_b, n_c \in \mathbb{Z}$. $\varphi_{i\mathbf{k}}(\mathbf{r})$ is a periodic function with the periodicity \mathbf{R} .

$$\varphi_{i\mathbf{k}}(\mathbf{r}) = \varphi_{i\mathbf{k}}(\mathbf{r} + \mathbf{R}) \quad (2.2.16)$$

A proof of the Bloch theorem is to show that $\Phi_{i\mathbf{k}}(\mathbf{r})$ is an eigenstate of the translation operator $\hat{T}_{\mathbf{R}}$.

$$\begin{aligned} \hat{T}_{\mathbf{R}} \Phi_{i\mathbf{k}}(\mathbf{r}) &= \hat{T}_{\mathbf{R}} e^{i\mathbf{k}\mathbf{r}} \varphi_{i\mathbf{k}}(\mathbf{r}) \\ &= e^{i\mathbf{k}(\mathbf{r}+\mathbf{R})} \varphi_{i\mathbf{k}}(\mathbf{r} + \mathbf{R}) \\ &= e^{i\mathbf{k}\mathbf{R}} e^{i\mathbf{k}\mathbf{r}} \varphi_{i\mathbf{k}}(\mathbf{r}) \\ &= e^{i\mathbf{k}\mathbf{R}} \Phi_{i\mathbf{k}}(\mathbf{r}) \end{aligned} \quad (2.2.17)$$

2.3 Maximally-localised Wannier functions

Solving the Kohn-Sham equations in k -space results in Bloch states $\Phi_{n\mathbf{k}}(\mathbf{r})$ and the corresponding energies $\epsilon_{n\mathbf{k}}$ with the band index n and the momentum \mathbf{k} . The Bloch states are by definition spreaded out over the crystal structure. With the unitary transformation $U_{mn}^{(\mathbf{k})}$ the system can be transformed to a localized basis using Maximally Localised Wannier Functions (MLWF) $\Psi_{n\mathbf{R}}(\mathbf{r})$ where n is the band index again and \mathbf{R} the lattice vector. The transformation can be written as

$$\Psi_{n\mathbf{R}}(\mathbf{r}) = \frac{V}{(2\pi)^3} \int_{BZ} \left[\sum_m U_{mn}^{(\mathbf{k})} \Phi_{m\mathbf{k}}(\mathbf{r}) \right] e^{-i\mathbf{k}\mathbf{R}} d\mathbf{k} \quad (2.3.1)$$

with V as the unit cell volume. The unitary transformation $U_{mn}^{(\mathbf{k})}$ between Bloch and Wannier functions is not unique, and several methods have been designed to find an optimal recipe. The method of Marzari and Vanderbilt [13] is minimizing the sum of the second moments of the Wannier functions Ω , the so-called spread, to get the transformation matrix.

$$\Omega = \sum_n \left[\langle \Psi_{n\mathbf{0}}(\mathbf{r}) | r^2 | \Psi_{n\mathbf{0}}(\mathbf{r}) \rangle - \langle \langle \Psi_{n\mathbf{0}}(\mathbf{r}) | \mathbf{r} | \Psi_{n\mathbf{0}}(\mathbf{r}) \rangle \rangle^2 \right] \quad (2.3.2)$$

One can distinguish between an gauge invariant term Ω_I and a term $\tilde{\Omega}$ that depends on the choice of the transformation matrix $U_{mn}^{(\mathbf{k})}$.

$$\Omega = \Omega_I + \tilde{\Omega} \quad (2.3.3)$$

with

$$\begin{aligned} \Omega_I &= \sum_n \left[\langle \Psi_{n\mathbf{0}}(\mathbf{r}) | r^2 | \Psi_{n\mathbf{0}}(\mathbf{r}) \rangle - \sum_{\mathbf{R}m} \langle \langle \Psi_{m\mathbf{R}}(\mathbf{r}) | \mathbf{r} | \Psi_{n\mathbf{0}}(\mathbf{r}) \rangle \rangle^2 \right] \\ \tilde{\Omega} &= \sum_n \sum_{\mathbf{R} \neq \mathbf{0}} \langle \langle \Psi_{n\mathbf{R}}(\mathbf{r}) | \mathbf{r} | \Psi_{n\mathbf{0}}(\mathbf{r}) \rangle \rangle^2 + \sum_{m \neq n} \sum_{\mathbf{R}} \langle \langle \Psi_{m\mathbf{R}}(\mathbf{r}) | \mathbf{r} | \Psi_{n\mathbf{0}}(\mathbf{r}) \rangle \rangle^2 \end{aligned} \quad (2.3.4)$$

Therefore the method of Marzari and Vanderbilt is minimizing only the term $\tilde{\Omega}$ with a steepest-descent or a conjugate-gradients algorithm. A brief introduction to MLWFs can be found in the *Wannier90* user guide [14].

The procedure described above is sufficient to obtain MLWFs from an isolated group of bands. Isolated means that there is a finite gap to all the other bands. For a group of bands which is not isolated, so-called entangled bands, one needs an extra procedure [15]. An example where this procedure is needed are the *sd*-bands in gold. To get only the Wannier functions of the *s*-band one needs to disentangle the *s*-band from the *d*-bands. To do so one has to define an energy window which includes at least the N Wannier bands of interest. The bands inside this window are part of the Hilbert space $\mathcal{F}(\mathbf{k})$. Minimizing Ω_I is used to get the right N -dimensional subspace $\mathcal{S}(\mathbf{k}) \subseteq \mathcal{F}(\mathbf{k})$. It turns out that Ω_I measures the *change of character* of the bands. Because minimizing Ω_I is an iterative process an initial guess for the subspace $\mathcal{S}(\mathbf{k})$ is needed. Additional a second energy window, the so-called inner window, can be defined. The bands from the inner window must be included in the subspace $\mathcal{S}(\mathbf{k})$. In a second step one can do the procedure from Marzari and Vanderbilt in the determined subspace $\mathcal{S}(\mathbf{k})$ to get the Wannier functions.

2.4 Electron interactions

The procedure until now allows to determine the parameters \tilde{t}_{ij} in the basis of the MLWFs $\Psi_{i\mathbf{R}}(\mathbf{r})$. The interaction term U_{ij} can be calculated with equation 2.1.6. Since using DFT to determine \tilde{t}_{ij} the mean field part of the electron interactions is already included in \tilde{t}_{ij} . Simply adding the interaction term to the one-particle term would count interactions twice. How to treat this problem, called double counting, is discussed in this section. A possibility to eliminate the double counting is to subtract the mean field part of the electron interactions before adding the full interactions. Starting from the density-density interaction and splitting the sum produces

$$\begin{aligned}
\hat{U} &= \frac{1}{2} \sum_{i \neq j} U_{ij} \hat{n}_i \hat{n}_j \\
&= \frac{1}{2} \sum_{\substack{\bar{i}=\bar{j} \\ \sigma \neq \sigma'}} U_{\bar{i}\bar{j}} \hat{n}_{\bar{i}\sigma} \hat{n}_{\bar{j}\sigma'} + \frac{1}{2} \sum_{\substack{\bar{i} \neq \bar{j} \\ \sigma \sigma'}} U_{\bar{i}\bar{j}} \hat{n}_{\bar{i}\sigma} \hat{n}_{\bar{j}\sigma'}.
\end{aligned} \tag{2.4.1}$$

The indices $i = \{\bar{i}, \sigma\}$ and $j = \{\bar{j}, \sigma'\}$ include the wave function indices \bar{i} and \bar{j} and the spins σ and σ' . The first term describes the interaction of electrons in the same orbital but therefore with different spin. The second term describes the interaction between different orbitals and arbitrary spins. $U_{\bar{i}\bar{j}} = U_{ij}$ because the Coulomb interaction is independent of the spin. In the Hartree-Fock approximation the product of two operators is written like

$$\hat{A}\hat{B} = \underbrace{\left(\hat{A} - \langle \hat{A} \rangle\right) \left(\hat{B} - \langle \hat{B} \rangle\right)}_{\approx 0} + \hat{A} \langle \hat{B} \rangle + \hat{B} \langle \hat{A} \rangle - \langle \hat{A} \rangle \langle \hat{B} \rangle \tag{2.4.2}$$

where the correlations between fluctuations are neglected. Using the Hartree-Fock approximation for the density operators in equation 2.4.1 leads to

$$\hat{U} \approx \frac{1}{2} \sum_{\substack{\bar{i}=\bar{j} \\ \sigma \neq \sigma'}} U_{\bar{i}\bar{j}} (\langle \hat{n}_{\bar{i}\sigma} \rangle \hat{n}_{\bar{j}\sigma'} + \hat{n}_{\bar{i}\sigma} \langle \hat{n}_{\bar{j}\sigma'} \rangle) + \frac{1}{2} \sum_{\substack{\bar{i} \neq \bar{j} \\ \sigma \sigma'}} U_{\bar{i}\bar{j}} (\langle \hat{n}_{\bar{i}\sigma} \rangle \hat{n}_{\bar{j}\sigma'} + \hat{n}_{\bar{i}\sigma} \langle \hat{n}_{\bar{j}\sigma'} \rangle) \tag{2.4.3}$$

where the direct products of expectation values can be canceled because they are just constants. Using the symmetry of the Coulomb interaction $U_{\bar{i}\bar{j}} = U_{\bar{j}\bar{i}}$ and renaming the indices produces the first line of the following equation.

$$\begin{aligned}
\hat{U} &\approx \sum_{\substack{\bar{i}=\bar{j} \\ \sigma \neq \sigma'}} U_{\bar{i}\bar{j}} \hat{n}_{\bar{i}\sigma} \langle \hat{n}_{\bar{j}\sigma'} \rangle + \sum_{\substack{\bar{i} \neq \bar{j} \\ \sigma \sigma'}} U_{\bar{i}\bar{j}} \hat{n}_{\bar{i}\sigma} \langle \hat{n}_{\bar{j}\sigma'} \rangle \\
&= \sum_{\substack{\bar{i} \\ \sigma}} U_{\bar{i}\bar{i}} \hat{n}_{\bar{i}\sigma} \langle \hat{n}_{\bar{i}\sigma} \rangle + 2 \sum_{\substack{\bar{i} \neq \bar{j} \\ \sigma \sigma'}} U_{\bar{i}\bar{j}} \hat{n}_{\bar{i}\sigma} \langle \hat{n}_{\bar{j}\sigma} \rangle
\end{aligned} \tag{2.4.4}$$

In the second line of the equation the sum over σ' is performed using $\langle n_{\bar{i}\sigma'} \rangle = \langle n_{\bar{i}\sigma} \rangle$. Renaming $\langle \hat{n}_{\bar{i}\sigma} \rangle$ by $n_{\bar{i}}^0$ in equation 2.4.4 produces the double counting term.

$$\begin{aligned}
\Delta t_{\bar{i}\bar{i}} &\approx U_{\bar{i}\bar{i}} n_{\bar{i}}^0 + \sum_{\bar{m} \neq \bar{i}} 2U_{\bar{i}\bar{m}} n_{\bar{m}}^0 \\
&= \sum_{\bar{k}} \sum_{\bar{m}}^{N_{occ}} |\{Q^\dagger\}_{\bar{k}\bar{m}}| (U_{\bar{i}\bar{i}} \delta_{\bar{i}\bar{m}} + 2U_{\bar{i}\bar{m}} (1 - \delta_{\bar{i}\bar{m}}))
\end{aligned} \tag{2.4.5}$$

$n_{\bar{i}}^0$ is the equilibrium population without interactions of the i -th orbital. Q is the matrix which diagonalizes the Hamiltonian without interaction and E are the corresponding eigenenergies. The double counting term has to be subtracted from the parameter \tilde{t}_{ij} .

$$\begin{aligned}
t_{\bar{i}\bar{j}} &= \tilde{t}_{\bar{i}\bar{j}} - \Delta t_{\bar{i}\bar{i}} \delta_{\bar{i}\bar{j}} \\
&= \{QE Q^\dagger\}_{\bar{i}\bar{j}} - \Delta t_{\bar{i}\bar{i}} \delta_{\bar{i}\bar{j}}
\end{aligned} \tag{2.4.6}$$

Using DFT and MLWFs and respecting the double counting the model Hamiltonian with defined parameters t_{ij} and U_{ij} for describing a real quantum system is determined.

2.5 LCR transport system

Using a code which has been designed for solids, only periodic systems can be calculated. Figure 2.1 shows three replications of the unit cell used in the DFT calculation for the gold-BDT-gold system.

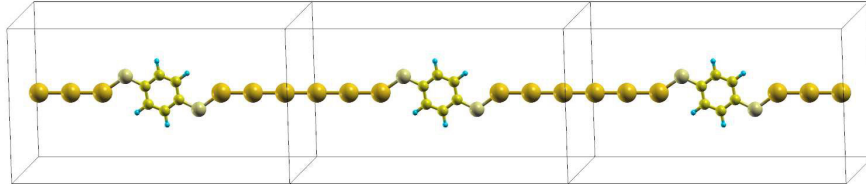


Figure 2.1: Gold-BDT-gold transport system in the DFT calculation.

The goal is to calculate the transport properties of a Left lead-Center-Right lead (LCR) transport system, shown in figure 2.2, which is neither finite nor periodic. Therefore the DFT calculation and the Wannier transformation have to be performed for a periodic or a finite system and one has to restructure the model Hamiltonian afterwards to describe the LCR transport system. A software which does these steps automatically is discussed in [16]. In this thesis a similar procedure is adopted. First the MLWFs of one unit cell are sorted according to their positions. The big advantage of working in a localized basis is that there is a small overlap between MLWFs far away from each other. This is the basic requirement for splitting up the model Hamiltonian into an LCR system.

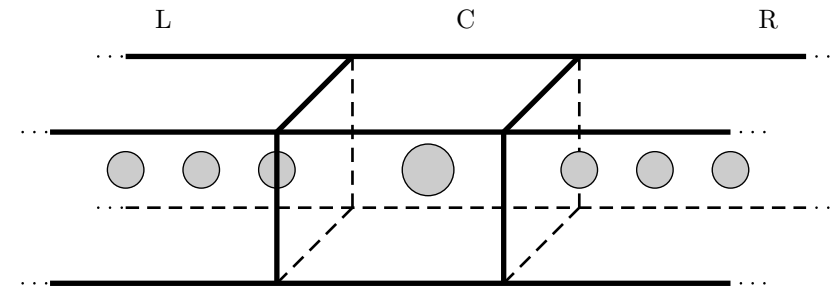


Figure 2.2: Transport over the central region C contacted with the two leads L and R.

Sorting the MLWFs by the position of their centers produces a Hamiltonian schematically written out in equation 2.5.1. The blank spaces denote neglected hopping elements. The splitting has to be chosen in a way that the neglected hopping elements are rather small. The size of the central region H_C should also depend on the magnitude of the hopping parameters V_{LC} and V_{CR} . If the coupling is weak, the hopping parameters V_{LC} and V_{CR} are small and electrons will stay long enough in the central region to scatter inelastically. In this incoherent transport regime it is necessary to include strong electron correlations and electron-phonon coupling in the central region and one has to cut the system at positions where the coupling is weak.

In the *grand canonical ensemble* the system can exchange heat and particles with the environment at fixed temperature, volume and chemical potential. The density operator in the grand canonical ensemble is

$$\hat{\rho} = \frac{1}{Z} e^{-\beta(\hat{H} - \mu\hat{N})} \quad (2.6.5)$$

with the partition function

$$Z = \text{Tr} \left(e^{-\beta(\hat{H} - \mu\hat{N})} \right). \quad (2.6.6)$$

The expectation value can be calculated using again equation 2.6.4. If a system is in equilibrium there is simple connection between the canonical and the grand canonical ensemble, which is presented at the end of section 2.6.3.

2.6.2 Non-equilibrium Green functions

The derivation of the non-equilibrium Green functions in this section is based on a paper from Jauho [19] and a paper from Keldysh [20]. The Hamiltonian 2.6.7 describes a transport system driven out of equilibrium due to the term \hat{h}_t . \hat{h}_t could be a shift in on-site energies or an external electric field. \hat{h}_t is assumed to be switched on at time t_0 . The goal is to calculate how the quantum system evolves in time. \hat{T} is assumed to be the unperturbed Hamiltonian and \hat{V}_t is the perturbation.

$$\hat{H}_t = \hat{T} + \underbrace{\hat{U}_t + \hat{h}_t}_{\hat{V}_t} \quad (2.6.7)$$

In quantum mechanics time evolution can be done either in the states (Schrödinger picture) or in the observables (Heisenberg picture). The Dirac picture, also called interaction representation, is an intermediate representation where the time evolution of \hat{T} is done in the observables and the typically more difficult part \hat{V}_t is time-evolved in the states.

$$|\Psi_D(t)\rangle = \hat{S}_I(t, t_0) |\Psi_D(t_0)\rangle \quad (2.6.8)$$

$$\hat{A}_H(t) = \hat{S}_I^\dagger(t, t_0) \hat{A}_I(t) \hat{S}_I(t, t_0) \quad (2.6.9)$$

The time evolution operator \hat{S}_I connects states at different times in the interaction picture

$$\hat{S}_I(t, t_0) = \mathcal{T} e^{-\frac{i}{\hbar} \int_{t_0}^t dt' \hat{V}_t(t')} \quad (2.6.10)$$

and satisfies the relations

$$\hat{S}_I(t_0, t_0) = 1 \quad (2.6.11)$$

and

$$\hat{S}_I(t_1, t_0) = \hat{S}_I(t_0, t_1)^{-1} = \hat{S}_I(t_0, t_1)^\dagger. \quad (2.6.12)$$

\mathcal{T} denotes the time-ordering operator and is defined as

$$\mathcal{T}\hat{A}(t_1)\hat{B}(t_2) := \begin{cases} \hat{A}(t_1)\hat{B}(t_2), & t_1 > t_2 \\ \hat{B}(t_2)\hat{A}(t_1), & t_2 > t_1 \end{cases}. \quad (2.6.13)$$

The interaction part \hat{U}_t is switched on and off adiabatically. Therefore there is no interaction for $t \rightarrow \pm\infty$ and the interaction attains its full strength at $t = 0$.

$$\hat{U}_t = \hat{U}e^{-0^+|t|} \quad (2.6.14)$$

Assuming that \hat{h}_t is switched on at time t_0 implies that \hat{h}_t is zero for $t < t_0$ and the limes $t_0 \rightarrow -\infty$ is assumed. For simplicity the system is assumed to be at zero temperature and $|\Psi_0\rangle$ is the ground state of \hat{T} . Starting in the Heisenberg picture the time-ordered Green function is

$$G_{\hat{A}\hat{B}}^T(t_1, t_2) = -i \frac{\langle \Psi_0 | \mathcal{T} \hat{A}_H(t_1) \hat{B}_H(t_2) | \Psi_0 \rangle}{\langle \Psi_0 | \Psi_0 \rangle}. \quad (2.6.15)$$

The operators $\hat{A}_H(t_1)$ and $\hat{B}_H(t_2)$ can of course depend on space coordinates and spin but now only the time-dependence is of importance. With equation 2.6.9 the operators in the time-ordered Green function can be transformed from the Heisenberg to the Dirac picture.

$$\begin{aligned} G_{\hat{A}\hat{B}}^T(t_1, t_2) &= -i \frac{\langle \Psi_0 | \hat{S}_I(t_0, \infty) \mathcal{T} \hat{S}_I(\infty, t_1) \hat{A}_I(t_1) \hat{S}_I(t_1, t_2) \hat{B}_I(t_2) \hat{S}_I(t_2, t_0) | \Psi_0 \rangle}{\langle \Psi_0 | \Psi_0 \rangle} \\ &= -i \frac{\langle \Psi_0 | \hat{S}_I(t_0, \infty) \mathcal{T} \hat{S}_I(\infty, t_0) \hat{A}_I(t_1) \hat{B}_I(t_2) | \Psi_0 \rangle}{\langle \Psi_0 | \Psi_0 \rangle} \end{aligned} \quad (2.6.16)$$

The order of the operators on the right side of the time-ordering operator can be changed. In equilibrium the theorem of Gell-Mann and Low holds. The theorem says that if $|\Psi_0\rangle$ is an eigenstate of \hat{T} and when \hat{V}_t is a term which is adiabatically switched on and off then

$$|\infty\rangle = e^{i\phi} |\Psi_0\rangle \quad (2.6.17)$$

holds. Level crossing is not excluded. Therefore in equilibrium one can derive the time-ordered Green function already from equation 2.6.16. In non-equilibrium the theorem of Gell-Mann and Low is not valid anymore because \hat{h}_t is not necessarily switched on adiabatically. The trick is to go back to t_0 on a contour $c \in \{+, -\}$ along the time axis.

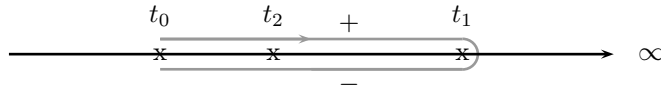


Figure 2.4: Keldysh contour.

In addition to the time the side of the contour $\tau_1 = \{t_1, c_1\}$, $\tau_2 = \{t_2, c_2\}$ has to be specified. Introducing the contour ordering operator as

$$\mathcal{T}_c \hat{A}(t_1, c_1) \hat{B}(t_2, c_2) = \begin{cases} \hat{A}(t_1, c_1) \hat{B}(t_2, c_2), & \{t_1, c_1\} > \{t_2, c_2\} \\ \hat{B}(t_2, c_2) \hat{A}(t_1, c_1), & \{t_2, c_2\} > \{t_1, c_1\} \end{cases} \quad (2.6.18)$$

and using the contour ordering operator instead of the time ordering operator enables permuting all operators and the Green function can be calculated.

$$\begin{aligned} G_{\hat{A}\hat{B}}^{T_c}(t_1, c_1, t_2, c_2) &= -i \frac{\langle \Psi_0 | \mathcal{T}_c \hat{S}_I(t_0, \infty) \hat{S}_I(\infty, t_0) \hat{A}_I(t_1) \hat{B}_I(t_2) | \Psi_0 \rangle}{\langle \Psi_0 | | \Psi_0 \rangle} \\ &= -i \frac{\langle \Psi_0 | \mathcal{T}_c \hat{A}_I(t_1) \hat{B}_I(t_2) | \Psi_0 \rangle}{\langle \Psi_0 | | \Psi_0 \rangle} \end{aligned} \quad (2.6.19)$$

Depending on the contour four different Green functions are generated. The bottom line of this thesis is to calculate charge transport through a quantum mechanical system. It turns out that the transport properties are related to two-point Green functions with the fermionic annihilation and creation operators in the argument. The Green functions can be defined as

$$\begin{aligned} G_{ij}^T(t, t') &:= G_{\hat{a}_i \hat{a}_j^\dagger}^{T_c}(t, +, t', +) = -i \left\langle T \left\{ \hat{a}_i(t) \hat{a}_j^\dagger(t') \right\} \right\rangle && \text{time-ordered} \\ G_{ij}^>(t, t') &:= G_{\hat{a}_i \hat{a}_j^\dagger}^{T_c}(t, +, t', -) = -i \left\langle \hat{a}_i(t) \hat{a}_j^\dagger(t') \right\rangle && \text{greater} \\ G_{ij}^<(t, t') &:= G_{\hat{a}_i \hat{a}_j^\dagger}^{T_c}(t, -, t', +) = i \left\langle \hat{a}_j^\dagger(t') \hat{a}_i(t) \right\rangle && \text{lesser} \\ G_{ij}^{\bar{T}}(t, t') &:= G_{\hat{a}_i \hat{a}_j^\dagger}^{T_c}(t, -, t', -) = -i \left\langle \bar{T} \left\{ \hat{a}_i(t) \hat{a}_j^\dagger(t') \right\} \right\rangle && \text{anti-time-ordered} \end{aligned} \quad (2.6.20)$$

Only three of this four Green functions are linearly independent because of

$$\begin{aligned} G^k &:= G^> + G^< = G^T + G^{\bar{T}} \\ G^r &:= G^T - G^< = G^> - G^{\bar{T}} \\ G^a &:= G^T - G^> = G^< - G^{\bar{T}}. \end{aligned} \quad (2.6.21)$$

This relations between the Green functions can be shown by the use of their definitions. G^k is called the Keldysh, G^r the retarded and G^a the advanced Green function. The Keldysh space can be defined as

$$\mathbf{G} = \begin{pmatrix} G^r & G^k \\ 0 & G^a \end{pmatrix} \quad \text{or} \quad \hat{\mathbf{G}} = \begin{pmatrix} G^T & G^< \\ G^> & G^{\bar{T}} \end{pmatrix}. \quad (2.6.22)$$

\mathbf{G} and $\hat{\mathbf{G}}$ are connected by a linear transformation given by the relations 2.6.21. The retarded and the advanced Green function are

$$G_{ij}^r(t, t') := -i\theta(t - t') \left\langle \left\{ \hat{a}_i(t), \hat{a}_j^\dagger(t') \right\} \right\rangle \quad (2.6.23)$$

$$G_{ij}^a(t, t') := i\theta(t' - t) \left\langle \left\{ \hat{a}_i(t), \hat{a}_j^\dagger(t') \right\} \right\rangle. \quad (2.6.24)$$

There are useful relations between the G^r , G^a and G^k .

$$\begin{aligned} G^a &= (G^r)^\dagger \\ G^k &= -(G^k)^\dagger \end{aligned} \quad (2.6.25)$$

In equilibrium

$$G^k = (G^r - G^a)(1 - 2f) \quad (2.6.26)$$

holds. With the retarded and the advanced Green function it is possible to determine properties like the Density Of States (DOS) or level broadening. To describe kinetic properties the greater Green function $G^>$ and lesser Green function $G^<$ are of importance. In equilibrium the lesser and greater Green function are not independent from the retarded and the advanced Green function. To determine Green functions their definitions, the Lehmann representation or the equation of motion can be used. The Lehmann representation is derived in the next section.

2.6.3 Lehmann representation

In equilibrium the Lehmann representations can be used to calculate Green functions. In order to deduce the Lehmann representation of the retarded Green function the spectral representation of the greater and the lesser Green functions are used. The spectral representations can be reached by inserting a full eigenbasis of the Hamiltonian and involving the operators in time. The Hamiltonian is assumed to be time-independent. First the canonical ensemble is used and the extension to the grand canonical ensemble is shown at the end of this section.

$$\begin{aligned}
G_{ij}^>(t, t') &= \frac{-i}{Z} \sum_n e^{-\beta E_n} \langle n | \hat{a}_i(t) \hat{a}_j^\dagger(t') | n \rangle \\
&= \frac{-i}{Z} \sum_{mn} e^{-\beta E_n} \langle n | e^{i\hat{H}t} \hat{a}_i e^{-i\hat{H}t} | m \rangle \langle m | e^{i\hat{H}t'} \hat{a}_j^\dagger e^{-i\hat{H}t'} | n \rangle \\
&= \frac{-i}{Z} \sum_{mn} e^{-\beta E_n} e^{i(E_n - E_m)(t - t')} \langle n | \hat{a}_i | m \rangle \langle m | \hat{a}_j^\dagger | n \rangle
\end{aligned} \tag{2.6.27}$$

The same calculation can be done for the lesser Green function.

$$G_{ij}^<(t, t') = \frac{i}{Z} \sum_{mn} e^{-\beta E_n} e^{i(E_m - E_n)(t - t')} \langle n | \hat{a}_j^\dagger | m \rangle \langle m | \hat{a}_i | n \rangle \tag{2.6.28}$$

Renaming the indices m and n in the lesser Green function and using the definition 2.6.24 leads to the spectral representation of the retarded Green function.

$$\begin{aligned}
G_{ij}^r(t, t') &= \theta(t - t') (G_{ij}^>(t, t') - G_{ij}^<(t, t')) \\
&= -i\theta(t - t') \frac{1}{Z} \sum_{mn} (e^{-\beta E_n} + e^{-\beta E_m}) e^{i(E_n - E_m)(t - t')} \langle n | \hat{a}_i | m \rangle \langle m | \hat{a}_j^\dagger | n \rangle
\end{aligned} \tag{2.6.29}$$

If the Hamiltonian does not depend explicitly on time the Green functions depend only on the time difference $(t - t')$. In non-equilibrium this is only the case in steady state, meaning long time after bringing the system out of equilibrium. Finally renaming $(t - t')$ by t and defining the Fourier transformation as

$$\begin{aligned}
G_{ij}^r(\omega) &:= \int_{-\infty}^{\infty} G_{ij}^r(t) e^{i\omega t} dt \\
G_{ij}^r(t) &= \frac{1}{2\pi} \int_{-\infty}^{\infty} G_{ij}^r(\omega) e^{-i\omega t} d\omega.
\end{aligned} \tag{2.6.30}$$

leads to the Lehmann representation.

$$\begin{aligned}
G_{ij}^r(\omega) &= \frac{-i}{Z} \sum_{mn} (e^{-\beta E_n} + e^{-\beta E_m}) \langle n | \hat{a}_i | m \rangle \langle m | \hat{a}_j^\dagger | n \rangle \int_0^{\infty} e^{i(\omega + E_n - E_m)t} \\
&= \frac{1}{Z} \sum_{mn} \frac{\langle n | \hat{a}_i | m \rangle \langle m | \hat{a}_j^\dagger | n \rangle}{\omega + E_n - E_m + i0^+} (e^{-\beta E_n} + e^{-\beta E_m})
\end{aligned} \tag{2.6.31}$$

The 0^+ ensures the convergence of the Fourier integral. Introducing the 0^+ is essentially the same as doing a Laplace transformation. Analyzing the retarded Green function in the complex plane gives poles below the real axis and the function is analytically in the upper half plane. From the analyticity in the upper half plane, and therefore from the causality, a relationship between imaginary and real part of the Green function, called Kramers-Kronig relation, can be derived. Changing the sign in front of the $i0^+$ term produces the Lehmann representation of the advanced Green function.

In literature often the grand canonical ensemble is used. In the following the connection between the canonical and the grand canonical ensemble in equilibrium using the example of the lesser Green function is shown. The μ as index of the Green function means treating expectation value and time evolution in the grand canonical ensemble.

$$\begin{aligned} {}^\mu G_{ij}^<(t) &= i \langle \hat{a}_j^\dagger \hat{a}_i(t) \rangle \\ &= i \langle \hat{a}_j^\dagger e^{i(\hat{H}-\mu\hat{N})t} \hat{a}_i e^{-i(\hat{H}-\mu\hat{N})t} \rangle \end{aligned} \quad (2.6.32)$$

In the case of $[\hat{H}, \hat{N}] = 0$ one obtains

$$\begin{aligned} {}^\mu G_{ij}^<(t) &= i \langle \hat{a}_j^\dagger e^{i\hat{H}t} (e^{-i\mu\hat{N}t} \hat{a}_i e^{i\mu\hat{N}t}) e^{-i\hat{H}t} \rangle \\ &= e^{i\mu t} i \langle \hat{a}_j^\dagger e^{i\hat{H}t} \hat{a}_i e^{-i\hat{H}t} \rangle \\ &= e^{i\mu t} G_{ij}^<(t). \end{aligned} \quad (2.6.33)$$

Doing a Fourier transformation leads to the equation

$$\begin{aligned} {}^\mu G_{ij}^<(\omega) &= \frac{1}{2\pi} \int_{-\infty}^{\infty} e^{i\omega t} e^{i\mu t} G_{ij}^<(t) dt \\ &= \frac{1}{2\pi} \int_{-\infty}^{\infty} e^{i(\omega+\mu)t} G_{ij}^<(t) dt \\ &= G_{ij}^<(\omega + \mu). \end{aligned} \quad (2.6.34)$$

The effect of the chemical potential is a shift along the frequency axis. This can also be seen in the Lehmann representation. In the denominator of equation 2.6.31 only the difference of energies $E_n - E_m$ appears where the state $|n\rangle$ consists of N and $|m\rangle$ of $(N+1)$ particles. So the difference of the particle numbers is one and therefore only one times μ appears during the change from the canonical to the grand canonical ensemble, which is again a shift of the frequency axis.

For the lesser Green function

$$\begin{aligned} G_{ij}^<(\omega) &= \int_{-\infty}^{\infty} G_{ij}^<(t) e^{i\omega t} dt \\ &= \int_{-\infty}^{\infty} i \langle \hat{a}_j^\dagger \hat{a}_i(t) \rangle e^{i\omega t} dt \\ &= - \left(\int_{-\infty}^{\infty} i \langle \hat{a}_i^\dagger(t) \hat{a}_j \rangle e^{-i\omega t} dt \right)^* \\ &= - \left(\int_{-\infty}^{\infty} i \langle \hat{a}_i^\dagger \hat{a}_j(t) \rangle e^{i\omega t} dt \right)^* \\ &= - \left(\int_{-\infty}^{\infty} G_{ji}^<(t) e^{i\omega t} dt \right)^* = - (G_{ji}^<(\omega))^* \end{aligned} \quad (2.6.35)$$

holds. This property will be used later on to derive an expression for the current between two systems.

2.6.4 Spectral function and occupation number

The spectral function A is essentially the imaginary part of the retarded Green function.

$$A(\omega) = \text{Tr} (A_{ij}(\omega)) \quad (2.6.36)$$

$$A_{ij}(\omega) := -\frac{1}{\pi} \text{Im} (G_{ij}^r(\omega)) \quad (2.6.37)$$

For real b the relation

$$\text{Im} \frac{1}{b + i0^+} = -\frac{0^+}{b^2 + 0^{+2}} = -\pi\delta(b) \quad (2.6.38)$$

holds. The δ -distribution is approximated by a Lorentzian function with an infinitesimal scale parameter. In order to deduce the spectral representation of the spectral function the Lehmann representation is used.

$$A_{ij}(\omega) = \frac{1}{Z} \sum_{mn} \langle n | \hat{a}_i | m \rangle \langle m | \hat{a}_j^\dagger | n \rangle (e^{-\beta E_n} + e^{-\beta E_m}) \delta(\omega + E_n - E_m) \quad (2.6.39)$$

The spectral function is a weighted sum over δ -distribution with the allowed energy transitions in the argument. Comparing this expression with the Lehmann representation of the retarded Green function leads to the fluctuation dissipation theorem.

$$G_{ij}^r(\omega) = \int_{-\infty}^{\infty} d\omega' \frac{A_{ij}(\omega')}{\omega - \omega' + i0^+} \quad (2.6.40)$$

The fluctuation dissipation theorem connects the spectral function with correlation functions respectively Green functions. Another quantity of interest is the occupation number. To derive an expression for the occupation number depending on Green functions it is useful to evaluate the diagonal elements of the Keldysh Green function.

$$\begin{aligned} G_{ii}^k(t) &= i \langle \hat{a}_i^\dagger \hat{a}_i(t) \rangle - i \langle \hat{a}_i^\dagger(t) \hat{a}_i \rangle \\ &= i \left(2 \langle \hat{a}_i^\dagger \hat{a}_i(t) \rangle - 1 \right) \end{aligned} \quad (2.6.41)$$

Identifying the number of particle operator and doing a Fourier transformation at the time $t = 0$ leads to

$$\hat{n}_i = \langle \hat{a}_i^\dagger \hat{a}_i \rangle = \frac{1}{2} \left(\text{Im} \left(\frac{1}{2\pi} \int_{-\infty}^{\infty} G_{ii}^k(\omega) d\omega \right) + 1 \right). \quad (2.6.42)$$

The spectral function and the occupations number of the orbitals are important tools for analyzing the transport behavior of a quantum system.

2.7 Coupling Green functions

2.7.1 Cluster Perturbation Theory

With the Lehmann representation Green functions in equilibrium can be calculated. Now coupling systems to achieve bigger or even infinite systems is of interest. The simplest way to do this is using Cluster Perturbation Theory (CPT). An introduction to quantum cluster methods in general is given in [21]. The model Hamiltonian in equation 2.1.5 consists of a one-particle part \hat{T} and the correlation part \hat{U} . At first only the one-particle part is treated. \hat{T} is split into a *cluster* part and a *rest* part. The cluster part contains all hoppings within a cluster and the rest part only the hoppings between different clusters.

$$\hat{T} = \sum_{\substack{j \\ \alpha\beta}} t_{\alpha\beta}^{jj} \hat{a}_{j\alpha}^\dagger \hat{a}_{j\beta} + \sum_{\substack{i \neq j \\ ij \\ \alpha\beta}} t_{\alpha\beta}^{ij} \hat{a}_{i\alpha}^\dagger \hat{a}_{j\beta} \quad (2.7.1)$$

The clusters are labeled by Latin indices and the Greek indices denote all quantum numbers within a cluster, e.g. orbital number and spin. An example cluster structure is sketched in figure 2.5.

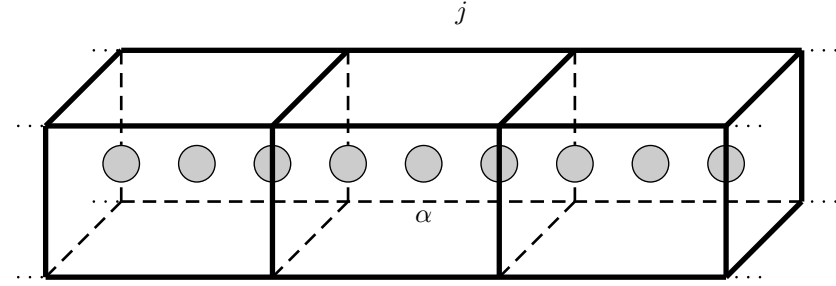


Figure 2.5: Arrangement of clusters in a chain. Each cluster contains more atoms or orbitals.

A possibility for calculating Green functions is the equation of motion method. This equation can be derived using the δ -distribution as the derivative of the Θ -function. 2.7.2 is the equation of motion for the retarded Green function defined in equation 2.6.24.

$$\begin{aligned} i \frac{\partial}{\partial t} G_{\hat{a}_{i\alpha} \hat{a}_{j\beta}^\dagger}^r(t, t') &= \frac{\partial}{\partial t} \theta(t - t') \left\langle \left\{ \hat{a}_{i\alpha}(t), \hat{a}_{j\beta}^\dagger(t') \right\} \right\rangle \\ &= \delta(t - t') \left\langle \left\{ \hat{a}_{i\alpha}(t), \hat{a}_{j\beta}^\dagger(t') \right\} \right\rangle - i \theta(t - t') \left\langle \left[\hat{a}_{i\alpha}(t), \hat{H} \right], \hat{a}_{j\beta}^\dagger(t') \right\rangle \\ &= \delta(t - t') \left\langle \left\{ \hat{a}_{i\alpha}(t), \hat{a}_{j\beta}^\dagger(t') \right\} \right\rangle + G_{[\hat{a}_{i\alpha}, \hat{H}] \hat{a}_{j\beta}^\dagger}^r(t, t') \end{aligned} \quad (2.7.2)$$

The equation also holds for the corresponding advanced Green function. They only obey different boundary conditions.

$$\begin{aligned} G_{\hat{a}_{i\alpha} \hat{a}_{j\beta}^\dagger}^r(t, t') &= 0 \quad \text{for } t < t' \\ G_{\hat{a}_{i\alpha} \hat{a}_{j\beta}^\dagger}^a(t, t') &= 0 \quad \text{for } t > t' \end{aligned} \quad (2.7.3)$$

Doing a Fourier transformation leads to the equation of motion in frequency space.

$$\omega G_{\hat{a}_{i\alpha}\hat{a}_{j\beta}^\dagger}^r(\omega) = \left\langle \left\{ \hat{a}_{i\alpha}, \hat{a}_{j\beta}^\dagger \right\} \right\rangle + G_{[\hat{a}_{i\alpha}, \hat{H}] \hat{a}_{j\beta}^\dagger}^r(\omega) \quad (2.7.4)$$

Here the boundary conditions must be inserted additionally by replacing ω by $\omega + i0^+$ for the retarded Green function respectively by $\omega - i0^+$ for the advanced one. In case of the interacting Hamiltonian \hat{H} the equation of motion leads to higher-order Green functions and therefore a series of equations. To do practically calculations one has to abort the series by hand. Considering only the one-particle Hamiltonian \hat{T} the series aborts itself and the equations are exact. The equation of motion in frequency space leads to

$$\omega G_{\hat{a}_{i\alpha}\hat{a}_{i\beta}^\dagger}^r(\omega) = \delta_{\alpha\beta} + \sum_{\gamma} t_{\alpha\gamma}^{ii} G_{\hat{a}_{i\gamma}\hat{a}_{i\beta}^\dagger}^r(\omega) + \sum_{j\gamma}^{i \neq j} t_{\alpha\gamma}^{ij} G_{\hat{a}_{j\gamma}\hat{a}_{i\beta}^\dagger}^r(\omega). \quad (2.7.5)$$

The so-called cluster Green function g can be calculated by using again the equation of motion respecting only the hoppings within the cluster.

$$\omega g_{\hat{a}_{i\alpha}\hat{a}_{i\beta}^\dagger}^r(\omega) = \delta_{\alpha\beta} + \sum_{\gamma} t_{\alpha\gamma}^{ii} g_{\hat{a}_{i\gamma}\hat{a}_{i\beta}^\dagger}^r(\omega) \quad (2.7.6)$$

Combining the equations 2.7.5 and 2.7.6 leads to the equation

$$G_{\hat{a}_{i\alpha}\hat{a}_{i\beta}^\dagger}^r(\omega) = g_{\hat{a}_{i\alpha}\hat{a}_{i\beta}^\dagger}^r(\omega) + \sum_{j\gamma\delta}^{i \neq j} g_{\hat{a}_{i\alpha}\hat{a}_{i\gamma}^\dagger}^r(\omega) t_{\gamma\delta}^{ij} G_{\hat{a}_{j\delta}\hat{a}_{i\beta}^\dagger}^r(\omega). \quad (2.7.7)$$

Redefining the Green functions to be matrices of the size of their Greek indices leads to the matrix equation 2.7.8. The Green function of the i -th cluster can be calculated knowing the cluster Green function and the Green functions connecting cluster i and j .

$$G^{ii,r}(\omega) = g^{ii,r}(\omega) + \sum_j^{i \neq j} g^{ii,r}(\omega) t^{ij} G^{jj,r}(\omega) \quad (2.7.8)$$

The same procedure can be done to obtain the Green function between cluster i and j .

$$G^{ij,r}(\omega) = \sum_j^{i \neq j} g^{ii,r}(\omega) t^{ij} G^{jj,r}(\omega) \quad (2.7.9)$$

Combining 2.7.8 and 2.7.9 leads to the CPT equation

$$\mathbf{G}^{ij} = \mathbf{g}^{ij} + \sum_{kl} \mathbf{g}^{ik} \mathbf{V}^{kl} \mathbf{G}^{lj} \quad (2.7.10)$$

which also holds in Keldysh space. A cluster Green function \mathbf{g}^{ij} with two different indices $i \neq j$ is zero. The coupling part must be written in block diagonal form.

$$\mathbf{V}^{ij} = \begin{pmatrix} t^{ij} & 0 \\ 0 & t^{ij} \end{pmatrix} \quad (2.7.11)$$

The CPT equation is exact for non-interacting systems. In order to see what happens if the correlation part \hat{U} is treated, equation 2.7.10 is used to write down the full Green function of a cluster.

$$G = g + gVG \quad (2.7.12)$$

V denotes the influence of neighboring clusters. Rewriting the expression leads to

$$G^{-1} = g^{-1} - V. \quad (2.7.13)$$

Interactions are treated within the cluster Green function g by using the cluster self energy Σ_{Cl} . g_0 is the cluster Green function without interactions.

$$g^{-1} = g_0^{-1} - \Sigma_{Cl} \quad (2.7.14)$$

Setting this expression into equation 2.7.13 leads to

$$G^{-1} = \underbrace{g_0^{-1}}_{G_0^{-1}} - V - \Sigma_{Cl}. \quad (2.7.15)$$

Defining G_0 to be the coupled Green function without interaction produces

$$G = G_0 + G_0 \Sigma_{Cl} G \quad (2.7.16)$$

which looks similar to the famous Dyson equation

$$G = G_0 + G_0 \Sigma G. \quad (2.7.17)$$

Comparing equation 2.7.16 and 2.7.17 shows that the approximation done within CPT is to replace the full self energy Σ by the cluster self energy Σ_{Cl} .

2.7.2 Semi-infinite Chain

As an example in this section CPT is used for calculating the Green function \mathbf{G}^{11} of a semi-infinite chain. The structure of a semi-infinite chain consisting of equal clusters is drawn in figure 2.6.

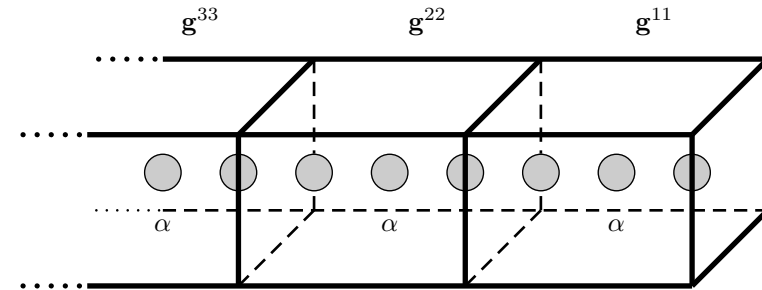


Figure 2.6: Arrangement of clusters in a semi-infinite chain.

\mathbf{G}^{11} is the Green function of the first cluster coupled to the rest of the semi-infinite chain. Therefore using the CPT equation leads to

$$\mathbf{G}^{11} = \mathbf{g}^{11} + \mathbf{g}^{11} \mathbf{V}^{12} \mathbf{G}^{21} \quad (2.7.18)$$

where \mathbf{g}^{11} is the Green Function of the single cluster. The coupling \mathbf{V}^{ij} exists only between neighboring clusters and therefore j is restricted to $j = i \pm 1$. In the case of the semi-infinite chain the first cluster has only one neighbor. The CPT equation can be used again to produce the Green Function \mathbf{G}^{21} .

$$\mathbf{G}^{21} = \mathbf{g}^{22} \mathbf{V}^{21} \mathbf{G}^{11} \quad (2.7.19)$$

Combining the equations 2.7.18 and 2.7.19 leads to

$$\mathbf{G}^{11} = \mathbf{g}^{11} + \mathbf{g}^{11} \mathbf{V}^{12} \mathbf{g}^{22} \mathbf{V}^{21} \mathbf{G}^{11}. \quad (2.7.20)$$

The cluster Green function \mathbf{g}^{22} can be seen again as a Green function for a semi-infinite chain, therefore $\mathbf{g}^{22} = \mathbf{G}^{11}$. This leads to an equation for \mathbf{G}^{11} depending only on the cluster Green function and the coupling matrix between the clusters.

$$\mathbf{G}^{11} = \left((\mathbf{g}^{11})^{-1} - \mathbf{V}^{12} \mathbf{G}^{11} \mathbf{V}^{21} \right)^{-1} \quad (2.7.21)$$

The equation must be solved iteratively and will be used later on to calculate the Green functions of the leads in the transport system.

2.8 Quantum Transport

The goal of this section is to find an expression for calculating the current flowing through a transport system. First a formula for the current between two systems is derived. This formula can also be applied for calculating the current through the LCR transport system. Finally the Landauer-Büttiker formula is deduced.

"Usually when we think about a current flowing, we imagine the electrons as particles moving along. Really we should be thinking about how the occupation of the wave like eigenstates is changing." [22]

2.8.1 Current between two Systems

A closed quantum system consisting of system I and system II is assumed. The current between the systems can be expressed by the derivative of the number of particles operator of one of the systems.

$$j = q \frac{d}{dt} \langle \hat{N}_I \rangle = q \left\langle \frac{d}{dt} \hat{N}_I \right\rangle \quad (2.8.1)$$

Using the Heisenberg picture the observables have to satisfy the Heisenberg equation. This leads to an expression for the current

$$j = q \left\langle \frac{d}{dt} \hat{N}_I \right\rangle = \frac{iq}{\hbar} \left\langle [\hat{H}, \hat{N}_I] \right\rangle. \quad (2.8.2)$$

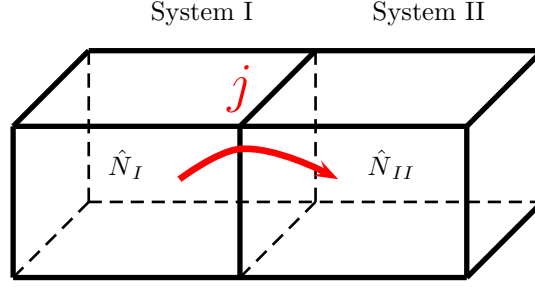


Figure 2.7: Current between two systems.

Each of the two systems consists of clusters which are labeled by Latin indices. Every cluster contains more orbitals with spins labeled by Greek indices. In this notation the total number of particle operator of system I is

$$\hat{N}_I = \sum_{\substack{l \in I \\ \gamma}} \hat{n}_{l\gamma}. \quad (2.8.3)$$

The full interacting Hamiltonian 2.1.5 in this index notation is

$$\hat{H} = \sum_{\substack{ij \\ \alpha\beta}} t_{\alpha\beta}^{ij} \hat{a}_{i\alpha}^\dagger \hat{a}_{j\beta} + \frac{1}{2} \sum_{\substack{ijkl \\ \alpha\beta\gamma\delta}} U_{\alpha\beta\gamma\delta}^{ijkl} \hat{a}_{i\alpha}^\dagger \hat{a}_{j\beta}^\dagger \hat{a}_{k\gamma} \hat{a}_{l\delta} \quad (2.8.4)$$

where the first term describes the hopping between the orbitals and the second term introduces the electron-electron correlations. To calculate the current between the systems I and II the commutator of \hat{N}_I and \hat{H} is needed. The sums can be extracted from the commutator because of linearity. Due to the commutation rules of number operators the commutator with the interaction part of the Hamiltonian vanishes.

$$\left[\hat{H}, \hat{N}_I \right] = \sum_{\substack{ij \\ \alpha\beta}} \sum_{\substack{l \in I \\ \gamma}} t_{\alpha\beta}^{ij} \left[\hat{a}_{i\alpha}^\dagger \hat{a}_{j\beta}, \hat{n}_{l\gamma} \right] \quad (2.8.5)$$

By use of the commutation relations

$$\begin{aligned} [\hat{a}_{i\alpha}, \hat{n}_{j\beta}] &= \delta_{ij} \delta_{\alpha\beta} \hat{a}_{i\alpha} \\ [\hat{a}_{i\alpha}^\dagger, \hat{n}_{j\beta}] &= -\delta_{ij} \delta_{\alpha\beta} \hat{a}_{i\alpha}^\dagger \end{aligned} \quad (2.8.6)$$

the commutator can be solved. There are four possibilities to distribute the two indices i and j at the two systems I and II. Distinguishing this cases leads to four terms.

$$\begin{aligned}
[\hat{H}, \hat{N}_I] &= \sum_{\substack{i \in I \\ j \in I \\ \alpha \beta}} \sum_{\substack{l \in I \\ \gamma}} t_{\alpha\beta}^{ij} \left(\hat{a}_{i\alpha}^\dagger \hat{a}_{j\beta} \delta_{jl} \delta_{\beta\gamma} - \hat{a}_{i\alpha}^\dagger \hat{a}_{j\beta} \delta_{il} \delta_{\alpha\gamma} \right) \\
&+ \sum_{\substack{i \in I \\ j \in II \\ \alpha \beta}} \sum_{\substack{l \in I \\ \gamma}} t_{\alpha\beta}^{ij} \left(\hat{a}_{i\alpha}^\dagger \hat{a}_{j\beta} \delta_{jl} \delta_{\beta\gamma} - \hat{a}_{i\alpha}^\dagger \hat{a}_{j\beta} \delta_{il} \delta_{\alpha\gamma} \right) \\
&+ \sum_{\substack{i \in II \\ j \in I \\ \alpha \beta}} \sum_{\substack{l \in I \\ \gamma}} t_{\alpha\beta}^{ij} \left(\hat{a}_{i\alpha}^\dagger \hat{a}_{j\beta} \delta_{jl} \delta_{\beta\gamma} - \hat{a}_{i\alpha}^\dagger \hat{a}_{j\beta} \delta_{il} \delta_{\alpha\gamma} \right) \\
&+ \sum_{\substack{i \in II \\ j \in II \\ \alpha \beta}} \sum_{\substack{l \in I \\ \gamma}} t_{\alpha\beta}^{ij} \left(\hat{a}_{i\alpha}^\dagger \hat{a}_{j\beta} \delta_{jl} \delta_{\beta\gamma} - \hat{a}_{i\alpha}^\dagger \hat{a}_{j\beta} \delta_{il} \delta_{\alpha\gamma} \right) \tag{2.8.7}
\end{aligned}$$

The first term adds up to zero. The δ -functions are restricting the sums. Therefore the first part in the second term, the second part in the third term and the last term are zero too. The remaining terms are

$$[\hat{H}, \hat{N}_I] = - \sum_{\substack{i \in I \\ j \in II \\ \alpha \beta}} t_{\alpha\beta}^{ij} \hat{a}_{i\alpha}^\dagger \hat{a}_{j\beta} + \sum_{\substack{i \in II \\ j \in I \\ \alpha \beta}} t_{\alpha\beta}^{ij} \hat{a}_{i\alpha}^\dagger \hat{a}_{j\beta}. \tag{2.8.8}$$

Renaming the indices of the second sum and applying 2.8.2 produces an expression for the current. Also the fact that t is hermitian is used, which must hold because \hat{H} is observable.

$$j = -\frac{q}{\hbar} \sum_{\substack{i \in I \\ j \in II \\ \alpha \beta}} \left(t_{\alpha\beta}^{ij} i \langle \hat{a}_{i\alpha}^\dagger \hat{a}_{j\beta} \rangle - t_{\alpha\beta}^{ij*} i \langle \hat{a}_{j\beta}^\dagger \hat{a}_{i\alpha} \rangle \right) \tag{2.8.9}$$

The current depends on correlation functions of annihilation and creation operators. By use of the definition of the lesser Green function 2.6.20 and doing a Fourier transformation defined in 2.6.30 one can rewrite the expectation values in formula 2.8.9. Using

$$i \langle \hat{a}_i^\dagger \hat{a}_j \rangle = G_{ij}^<(t=0) = \frac{1}{2\pi} \int_{-\infty}^{\infty} G_{ij}^<(\omega) d\omega \tag{2.8.10}$$

and the relation 2.6.35 leads to

$$\begin{aligned}
j &= -\frac{q}{\hbar} \sum_{\substack{i \in I \\ j \in II \\ \alpha \beta}} \left(t_{\alpha\beta}^{ij} G_{\alpha\beta}^{ij,<} - t_{\alpha\beta}^{ij*} G_{\beta\alpha}^{ji,<} \right) \\
&= -\frac{q}{\hbar} \int_{-\infty}^{\infty} \sum_{\substack{i \in I \\ j \in II \\ \alpha \beta}} \left(t_{\alpha\beta}^{ij} G_{\alpha\beta}^{ij,<}(\omega) - t_{\alpha\beta}^{ij*} G_{\beta\alpha}^{ji,<}(\omega) \right) d\omega \\
&= -\frac{q}{\hbar} \int_{-\infty}^{\infty} \sum_{\substack{i \in I \\ j \in II \\ \alpha \beta}} 2 \operatorname{Re} \left(t_{\alpha\beta}^{ij} G_{\alpha\beta}^{ij,<}(\omega) \right) d\omega \tag{2.8.11}
\end{aligned}$$

The Green function between the systems I and II is needed and therefore $i \neq j$. Under this conditions $G^< = G^>$ is true and therefore $G^K = 2G^<$.

$$j = -\frac{q}{h} \int_{-\infty}^{\infty} \sum_{\substack{i \in I \\ j \in II \\ \alpha\beta}} \text{Re} \left(t_{\alpha\beta}^{ij} G_{\alpha\beta}^{ij,k}(\omega) \right) d\omega \quad (2.8.12)$$

An expression for the current depending on the Keldysh Green function in frequency space is derived. More often than not $t_{\alpha\beta}^{ij} \in \mathbb{R}$ is true. This would not be the case in applying a magnetic field.

2.8.2 Current through the LCR System

In particular the quantity of interest is the current flowing through a molecule contacted by two leads which is described by the LCR transport system drawn in figure 2.2. For technical reasons electron correlations are considered only in the central system. According to equation 2.8.12 the Keldysh part of \mathbf{G}^{LC} is responsible for the current between the left lead and the central region. \mathbf{G}^{LC} can be calculated using the CPT equation.

$$\mathbf{G}^{LC} = \mathbf{g}^{LL} \mathbf{V}^{LC} \mathbf{G}^{CC} \quad (2.8.13)$$

The same equation holds for the Green function between the right contact and the central region. Therefore

$$\mathbf{G}^{\nu C} = \mathbf{g}^{\nu\nu} \mathbf{V}^{\nu C} \mathbf{G}^{CC} \quad \text{with } \nu \in \{L, R\} \quad (2.8.14)$$

holds which is exact for considering interactions only in the central region. Due to equation 2.8.13 two further Green functions are needed to calculate \mathbf{G}^{LC} . As cluster Green function for the leads \mathbf{g}^{LL} the Green function \mathbf{G}^{11} in equation 2.7.21 is used. \mathbf{G}^{CC} can be calculated by using the CPT equation again.

$$\begin{aligned} \mathbf{G}^{CC} &= \mathbf{g}^{CC} + \sum_{\nu \in \{L, R\}} \mathbf{g}^{CC} \mathbf{V}^{C\nu} \mathbf{G}^{\nu C} \\ &= \mathbf{g}^{CC} + \sum_{\nu \in \{L, R\}} \mathbf{g}^{CC} \mathbf{V}^{C\nu} \mathbf{g}^{\nu\nu} \mathbf{V}^{\nu C} \mathbf{G}^{CC} \\ &= \mathbf{g}^{CC} + \underbrace{\mathbf{g}^{CC} \sum_{\nu \in \{L, R\}} \mathbf{V}^{C\nu} \mathbf{g}^{\nu\nu} \mathbf{V}^{\nu C}}_{\Delta^{CC}} \mathbf{G}^{CC} \end{aligned} \quad (2.8.15)$$

Equation 2.8.15 is not exact anymore. It turns out that it is a first-order result in doing strong-coupling perturbation theory [21]. To include the transition regions \mathbf{g}^{TL} and \mathbf{g}^{TR} in the transport calculation they should be coupled to the semi-infinite leads in equation 2.7.21. Then the Green functions \mathbf{G}^{TL} and \mathbf{G}^{TR} represent the new leads.

$$\begin{aligned} \mathbf{G}^{TL} &= \left((\mathbf{g}^{TL})^{-1} - \mathbf{V}^{TL} \mathbf{g}^{LL} \mathbf{V}^{LT} \right)^{-1} \\ \mathbf{G}^{TR} &= \left((\mathbf{g}^{TR})^{-1} - \mathbf{V}^{TR} \mathbf{g}^{RR} \mathbf{V}^{RT} \right)^{-1} \end{aligned} \quad (2.8.16)$$

At this point in principle all equations for calculating the current through the LCR system are derived. The following paragraphs are analytical simplifications of this formulas. In a first step

calculating the equations for the retarded, advanced and keldysh Green function separate saves computational effort. The retarded part of \mathbf{G}^{CC} produces

$$G^{CC,r} = g^{CC,r} + g^{CC,r} \Delta^{CC,r} G^{CC,r} \quad (2.8.17)$$

with the solution

$$G^{CC,r} = \left((g^{CC,r})^{-1} - \Delta^{CC,r} \right)^{-1}. \quad (2.8.18)$$

The advanced part can be calculated similar to the retarded part and results in

$$G^{CC,a} = \left((g^{CC,a})^{-1} - \Delta^{CC,a} \right)^{-1}. \quad (2.8.19)$$

The Keldysh part is more difficult to calculate.

$$\begin{aligned} G^{CC,k} &= g^{CC,k} + g^{CC,k} \Delta^{CC,a} G^{CC,a} \\ &\quad + g^{CC,r} \Delta^{CC,k} G^{CC,a} \\ &\quad + g^{CC,r} \Delta^{CC,r} G^{CC,k} \end{aligned} \quad (2.8.20)$$

where $(ABC)^k = A^k B^a C^a + A^r B^k C^a + A^r B^r C^k$ is used.

$$\begin{aligned} (1 - g^{CC,r} \Delta^{CC,r}) G^{CC,k} &= g^{CC,k} + g^{CC,k} \Delta^{CC,a} G^{CC,a} \\ &\quad + g^{CC,r} \Delta^{CC,k} G^{CC,a} \end{aligned} \quad (2.8.21)$$

Using equation 2.8.18 and 2.8.19 to substitute $\Delta^{CC,r}$ and $\Delta^{CC,a}$ leads to

$$\begin{aligned} G^{CC,k} &= G^{CC,r} \left((g^{CC,r})^{-1} g^{CC,k} (g^{CC,a})^{-1} + \Delta^{CC,k} \right) G^{CC,a} \\ &= \underbrace{G^{CC,r} (g^{CC,r})^{-1} g^{CC,k} (g^{CC,a})^{-1} G^{CC,a}}_{\Lambda} + G^{CC,r} \Delta^{CC,k} G^{CC,a}. \end{aligned} \quad (2.8.22)$$

In equilibrium the Keldysh Green function is proportional to the Fermi function f and the difference of advanced and retarded Green function. Equation 2.6.26 can be used to derive

$$\begin{aligned} (g^{CC,r})^{-1} g^{CC,k} (g^{CC,a})^{-1} &= (1 - 2f^C) (g^{CC,r})^{-1} (g^{CC,a} - g^{CC,r}) (g^{CC,a})^{-1} \\ &= (1 - 2f^C) \left((g^{CC,r})^{-1} - (g^{CC,a})^{-1} \right) \\ &= 2i0^+ (1 - 2f^C) \end{aligned} \quad (2.8.23)$$

where the structure of retarded and advanced cluster Green function

$$\begin{aligned} (g^{CC,r})^{-1} &= \omega - T_{Cl} - \Sigma_{ee} + i0^+ \\ (g^{CC,a})^{-1} &= \omega - T_{Cl} - \Sigma_{ee} - i0^+ \end{aligned} \quad (2.8.24)$$

is used in the last line. T_{Cl} denotes the hopping part inside the cluster and Σ_{ee} is the electron self energy. According to the Lehmann representation the Green Function of a finite system has

only real poles and the imaginary part is simply due to $i0^+$. Therefore the anti-hermitian part of the self energy in finite size systems is always proportional to 0^+ . The full Green function of the center can be calculated including also the lead-induced self energy.

$$\begin{aligned}(G^{CC,r})^{-1} &= \omega - T_{Cl} - \Sigma_{ee} - \Sigma^r + i0^+ \\ (G^{CC,a})^{-1} &= \omega - T_{Cl} - \Sigma_{ee} - \Sigma^a - i0^+\end{aligned}\quad (2.8.25)$$

The lead-induced self energy Σ can be split up into a hermitian part R and an anti-hermitian part $\frac{i}{2}\Gamma$.

$$\begin{aligned}\Sigma^r &= R - \frac{i}{2}\Gamma \\ \Sigma^a &= R + \frac{i}{2}\Gamma\end{aligned}\quad (2.8.26)$$

The matrices R and Γ are both hermitian. R and Γ represent the influence of both leads and therefore

$$\begin{aligned}R &= \sum_{\nu \in \{L,R\}} R^\nu \\ \Gamma &= \sum_{\nu \in \{L,R\}} \Gamma^\nu\end{aligned}\quad (2.8.27)$$

holds. Splitting up the hermitian and the anti-hermitian part in equation 2.8.25 leads to

$$\begin{aligned}(G^r)^{-1} &= (\omega - B) + i\left(0^+ + \frac{\Gamma}{2}\right) \\ (G^a)^{-1} &= (\omega - B) - i\left(0^+ + \frac{\Gamma}{2}\right)\end{aligned}\quad (2.8.28)$$

with

$$B = T_{Cl} + \Sigma_{ee} + R \quad (2.8.29)$$

and an expression for Λ follows.

$$\begin{aligned}\Lambda &= 2i0^+(1 - 2f^C)G^{CC,r}G^{CC,a} \\ &= 2i(1 - 2f^C)\frac{0^+}{(\omega - B)^2 + (0^+ + \frac{\Gamma}{2})^2}\end{aligned}\quad (2.8.30)$$

Now two cases have to be distinguished.

$\Gamma \neq 0$: In this case Λ is proportional to 0^+ .

$\Gamma = 0$: For orbitals that do not couple to the leads Λ is proportional to the δ -distribution.

$$\begin{aligned}\Lambda &= 2i(1 - 2f^C)\frac{0^+}{(\omega - B)^2 + (0^+)^2} \\ &= 2i(1 - 2f^C)\pi\delta(\omega - B)\end{aligned}\quad (2.8.31)$$

In the case of calculating the current the Keldysh Green function is multiplied by the coupling matrix and therefore $\Lambda = 0$ holds. Due to $\Lambda = 0$ the Fermi function of the center does not enter the transport calculation at this point. Using equation 2.6.26 again shows that the Fermi functions of the leads enter in $\Delta^{CC,k}$.

$$\begin{aligned}\Delta^{CC,k} &= \sum_{\nu \in \{L,R\}} V^{C\nu} g^{\nu\nu,k} V^{\nu C} \\ &= \sum_{\nu \in \{L,R\}} (1 - 2f^\nu) V^{C\nu} (g^{\nu\nu,a} - g^{\nu\nu,r}) V^{\nu C}\end{aligned}\quad (2.8.32)$$

The result is an equation to calculate the Keldysh part of the central Green function.

$$G^{CC,k} = G^{CC,r} \Delta^{CC,k} G^{CC,a} \quad (2.8.33)$$

The Green function \mathbf{G}^{LC} separated in retarded, advanced and Keldysh component produces

$$G^{LC,r} = g^{LL,r} V^{LC} G^{CC,r} \quad (2.8.34)$$

$$G^{LC,a} = g^{LL,a} V^{LC} G^{CC,a} \quad (2.8.35)$$

$$G^{LC,k} = g^{LL,r} V^{LC} G^{CC,k} + g^{LL,k} V^{LC} G^{CC,a}. \quad (2.8.36)$$

As mentioned above the Green functions of the leads $\mathbf{g}^{\nu\nu}$ can be calculated using equation 2.7.21. The retarded component is

$$G^{11,r} = \left((g^{11,r})^{-1} - V^{12,r} G^{11,r} V^{21,r} \right)^{-1} \quad (2.8.37)$$

The leads are always in equilibrium and therefore the equations 2.6.25 and 2.6.26 can be used for calculating the advanced and the Keldysh component.

2.8.3 System out of equilibrium

The theory of a quantum system out of equilibrium was already introduced in section 2.6.2. Now the goal is to apply the theory on the LCR transport system. The LCR transport system can be driven out of equilibrium by applying a voltage across the system. This is done by shifting the Green functions of the leads on the frequency axis against each other. Due to keeping the filling of the leads to be constant also the chemical potentials μ_L and μ_R are shifted. In equilibrium $\mu = \mu_L = \mu_C = \mu_R$ holds and μ can be determined calculating the Fermi energy within DFT.

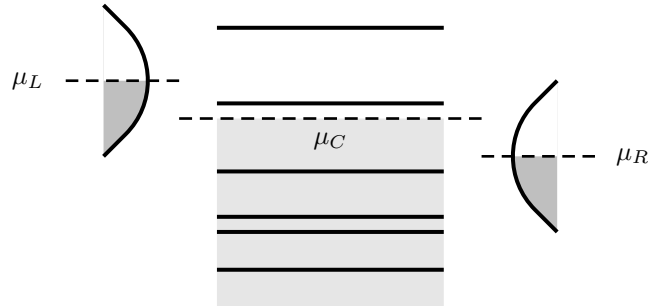


Figure 2.8: The LCR transport system out of equilibrium.

The current through the system can be calculated using equation 2.8.12 where the Keldysh Green function between the left lead and the center contributes. The last sections have showed how to calculate this Green function within CPT. The chemical potentials of the leads μ_L and μ_R enters the transport calculation within the Fermi function in the Keldysh component of the lead Green functions. The filling of the central region should be adjusted automatically by the formalism during the transport calculation. Therefore the initial chemical potential of the central region μ_C should not enter the transport calculation. This is really the case in having a non-interacting central region. In the case of interaction in the central region the cluster Green functions $g^{CC,r}$ and $g^{CC,a}$ depend on the electron self energy Σ_{ee} which depends on the filling of the system and therefore μ_C enters. In order to fix this problem one has to solve the transport system for the electron self energy Σ_{ee} and the filling of the central region consistently.

2.8.4 Landauer-Büttiker formula

Formula 2.8.11 can be used as starting point to deduce the Landauer-Büttiker formula, which is intuitively understandable and has advantages in the computational calculation.

$$j = -\frac{q}{h} \int_{-\infty}^{\infty} \sum_{\substack{i \in I \\ j \in II \\ \alpha\beta}} 2 \operatorname{Re} \left(V_{\alpha\beta}^{ij} G_{\alpha\beta}^{ij,<}(\omega) \right) d\omega \quad (2.8.38)$$

Calculating the current between the left lead ($i \in I = L$) and the central region ($j \in II = C$) leads to the matrix equation

$$j^{LC} = -\frac{2q}{h} \int_{-\infty}^{\infty} \operatorname{Re} \left(\operatorname{Tr} \left(V^{CL} G^{LC,<}(\omega) \right) \right) d\omega. \quad (2.8.39)$$

In analogy to the previous section the CPT equation leads to

$$\mathbf{G}^{LC} = \mathbf{g}^{LL} \mathbf{V}^{LC} \mathbf{G}^{CC}. \quad (2.8.40)$$

This equation is exact in the case of non-interacting leads. Using the Langreth theorem

$$G^{LC,<} = g^{LL,<} V^{LC} G^{CC,a} + g^{LL,r} V^{LC} G^{CC,<} \quad (2.8.41)$$

and defining the lead-induced self energies Σ^ν with $\nu \in \{L, R\}$ leads to

$$\begin{aligned} j^{LC} &= -\frac{2q}{h} \int_{-\infty}^{\infty} \left\{ \operatorname{Re} \left(\operatorname{Tr} \left(\underbrace{V^{CL} g^{LL,<} V^{LC}}_{\Sigma^{L,<}} G^{CC,a} + \underbrace{V^{CL} g^{LL,r} V^{LC}}_{\Sigma^{L,r}} G^{CC,<} \right) \right) \right\} d\omega \\ &= -\frac{2q}{h} \int_{-\infty}^{\infty} \left\{ \underbrace{\operatorname{Re} \left(\operatorname{Tr} \left(\Sigma^{L,<} G^{CC,a} \right) \right)}_{j_1} + \underbrace{\operatorname{Re} \left(\operatorname{Tr} \left(\Sigma^{L,r} G^{CC,<} \right) \right)}_{j_2} \right\} d\omega. \end{aligned} \quad (2.8.42)$$

Simplifying the term j_1 :

The lesser Green function in the non-interacting case is

$$\begin{aligned}
g_k^{\nu\nu,<}(\omega) &= i \int_{-\infty}^{\infty} e^{i\omega t} \langle \hat{a}_k^\dagger(t) \hat{a}_k(0) \rangle \\
&= i \int_{-\infty}^{\infty} e^{i\omega t} \langle e^{i\hat{H}t} \hat{a}_k^\dagger e^{-i\hat{H}t} \hat{a}_k \rangle \\
&= 2\pi i f_\nu(\omega) \delta(\omega - \omega_{k,\nu}).
\end{aligned} \tag{2.8.43}$$

Therefore the lesser part of the lead-induced self energy is

$$\begin{aligned}
\Sigma^{\nu,<}(\omega) &= V^{C\nu} g^{\nu\nu,<}(\omega) V^{\nu C} \\
&= i f_\nu(\omega) \Gamma^\nu(\omega).
\end{aligned} \tag{2.8.44}$$

Plugging 2.8.44 into the j_1 term produces

$$\begin{aligned}
j_1 &= \text{Re} \left(\text{Tr} (\Sigma^{L,<} G^{CC,a}) \right) \\
&= \text{Re} \left(\text{Tr} (i f_L \Gamma^L G^{CC,a}) \right).
\end{aligned} \tag{2.8.45}$$

The next step is to compute the full interacting Green function of the central region. One can use the CPT equation to write down

$$\mathbf{G}^{CC} = \mathbf{g}^{CC} + \mathbf{g}^{CC} \sum_{\nu \in \{L,R\}} \underbrace{\mathbf{V}^{C\nu} \mathbf{g}^{\nu\nu} \mathbf{V}^{\nu C}}_{\Sigma^\nu} \mathbf{G}^{CC}. \tag{2.8.46}$$

This expression is not exact anymore for a correlated central region. Using the CPT-approximation to write down the advanced part of the Green function produces

$$\begin{aligned}
G^a &= G^r (G^r)^{-1} G^a \\
&= G^r (g^r)^{-1} G^a - G^r \Sigma^r G^a \\
&= G^r (g^r)^{-1} G^a - G^r R G^a + \frac{i}{2} G^r \Gamma G^a.
\end{aligned} \tag{2.8.47}$$

According to equation 2.8.26 the self energy is split up into a hermitian part R and an anti-hermitian part $\frac{i}{2}\Gamma$. Plugging 2.8.47 into the equation 2.8.45 leads to

$$\begin{aligned}
j_1 &= \underbrace{\text{Re} \left(\text{Tr} (i f_L \Gamma^L G^{CC,r} (g^{CC,r})^{-1} G^{CC,a}) \right)}_{j_1^a} - \underbrace{\text{Re} \left(\text{Tr} (i f_L \Gamma^L G^{CC,r} R G^{CC,a}) \right)}_{j_1^b} \\
&\quad - \frac{1}{2} \underbrace{\text{Re} \left(\text{Tr} (f_L \Gamma^L G^{CC,r} \Gamma G^{CC,a}) \right)}_{j_1^c}.
\end{aligned} \tag{2.8.48}$$

In the term j_1^a one can substitute

$$(g^{CC,r})^{-1} = \underbrace{\omega - h - \Sigma_{ee}}_A + i0^+. \tag{2.8.49}$$

So j_1^a again splits up into two terms, the one with A and the $i0^+$ -term. In the A -term A is hermitian and the trace

$$\begin{aligned}
b &= \text{Tr}(\Gamma G^r A G^a) \\
b^* &= \text{Tr}(G^{a\dagger} A^\dagger G^{r\dagger} \Gamma) \\
&= -\text{Tr}(G^r A G^a \Gamma) \\
&= -\text{Tr}(\Gamma G^r A G^a) = b
\end{aligned} \tag{2.8.50}$$

is always $b \in \mathbb{R}$. Therefore the A -term is zero. Also the $i0^+$ -term is zero because the 0^+ always dominates the rest part.

$$0^+ \text{Re} \left(\text{Tr} (f_L \Gamma^L G^{CC,r} G^{CC,a}) \right) \xrightarrow{0^+ \rightarrow 0} 0 \tag{2.8.51}$$

j_1^b cancels for the same reason as the A -term in j_1^a . So the remaining part is

$$\begin{aligned}
j_1 &= -j_1^c = -\frac{1}{2} \text{Re} \left(\text{Tr} (f_L \Gamma^L G^{CC,r} \Gamma G^{CC,a}) \right) \\
&= -\frac{1}{2} \text{Tr} (f_L \Gamma^L G^{CC,r} \Gamma G^{CC,a}) \\
&= -\frac{1}{2} \sum_{\nu \in \{L,R\}} \text{Tr} (f_L \Gamma^L G^{CC,r} \Gamma^\nu G^{CC,a}).
\end{aligned} \tag{2.8.52}$$

Simplifying the term j_2 :

The j_2 term depends on the lesser Green function of the center $G^{CC,<}$. The Keldysh version of the Kadanoff-Baym theorem is

$$G^{<} = G^r (g^r)^{-1} g^{<} (g^a)^{-1} G^a + G^r \Sigma^{<} G^a. \tag{2.8.53}$$

In analogy to the equations 2.6.26 the cluster lesser Green function for the center is

$$g^{CC,<} \propto f_C (g^{CC,a} - g^{CC,r}) \tag{2.8.54}$$

and therefore

$$G^{CC,<} = f_C G^{CC,r} \underbrace{(g^{CC,r})^{-1} (g^{CC,a} - g^{CC,r}) (g^{CC,a})^{-1}}_{(g^{CC,r})^{-1} - (g^{CC,a})^{-1}} G^{CC,a} + G^{CC,r} \Sigma^{<} G^{CC,a}. \tag{2.8.55}$$

The first part of the sum is zero due to the same reason as j_1^a . The second part remains.

$$\begin{aligned}
j_2 &= \text{Re} \left(\text{Tr} (\Sigma^{L,r} G^{CC,r} \Sigma^{<} G^{CC,a}) \right) \\
&= \sum_{\nu \in \{L,R\}} \text{Re} \left(\text{Tr} (i f_\nu \Sigma^{L,r} G^{CC,r} \Gamma^\nu G^{CC,a}) \right) \\
&= \frac{1}{2} \sum_{\nu \in \{L,R\}} \text{Re} \left(\text{Tr} (f_\nu \Gamma^L G^{CC,r} \Gamma^\nu G^{CC,a}) \right) \\
&= \frac{1}{2} \sum_{\nu \in \{L,R\}} \text{Tr} (f_\nu \Gamma^L G^{CC,r} \Gamma^\nu G^{CC,a})
\end{aligned} \tag{2.8.56}$$

Summing up j_1 and j_2 leads to the Landauer-Büttiker formula.

$$\begin{aligned} j^{LC} &= -\frac{2q}{h} \int_{-\infty}^{\infty} d\omega (j_1 + j_2) \\ &= -\frac{q}{h} \int_{-\infty}^{\infty} d\omega (f_R(\omega) - f_L(\omega)) \text{Tr} (\Gamma^L G^r \Gamma^R G^a) \end{aligned} \quad (2.8.57)$$

Meir and Wingreen have deduced this formula in [23]. Defining the transmission function

$$T(\omega) = \text{Tr} (\Gamma^L G^r \Gamma^R G^a) \quad (2.8.58)$$

leads to

$$j^{LC} = -\frac{q}{h} \int_{-\infty}^{\infty} d\omega (f_R(\omega) - f_L(\omega)) T(\omega) \quad (2.8.59)$$

the Landauer Büttiker formula proposed by Rolf Landauer in 1957 [24]. In applying a voltage across the transport system the Fermi functions of the leads are shifted against each other. If there is a finite transmission in this energy region current can flow.

2.9 Summary and discussion

This chapter introduced the basic theoretical concepts used in this thesis. First the many-body Hamiltonian which describes the electrons in the gold-BDT-gold system was introduced. The Hamiltonian consists of a one-body part (kinetic and potential energy) and a two-body term, which describes the interaction between the electrons. Then the methods used to estimate the model parameters ab-initio were described. In this thesis Density Functional Theory (DFT) and Maximally Localized Wannier Functions (MLWF) were used. The following sections explained how to setup the geometry of the transport system, the so-called LCR geometry. Finally the formalism of Non-equilibrium Green functions (NEG) and Cluster Perturbation Theory (CPT) were introduced. The concepts will be used to implement the transport equations.

The novelty of this thesis is to combine all this aspects to solve a realistic model of transport through a molecular system, including many-body effects. Before going further the approximations made within this work are discussed critically in the following paragraphs.

- 1.) **Density Functional Theory (DFT):** To construct the eigenvalues and eigenfunctions of the model system DFT was employed. There one assumes that the Kohn-Sham orbitals represents a good approximation for the non-interacting quasi-particles in the system. Although this is formally not exact, several empirical and theoretical (Koopmans' theorem) arguments justify this assumption. DFT and many-body methods are widely used in many fields of theoretical physics [25] and provide a very powerful tool to realistically describe systems with strong electron correlations. Besides the Kohn-Sham orbital problem there is the aspect of the choice of the exchange-correlation functional. This can influence, for example, the equilibrium geometry and the band gap of the benzene molecule. One has to chose a functional which produces reasonable results.
- 2.) **Non-equilibrium:** In this thesis all DFT calculations were done with the transport system in equilibrium. But by applying a voltage the system is driven out of equilibrium. Therefore the charge density changes compared to the equilibrium one. One can include this effect by

calculating NEG and DFT self-consistently with respect to the charge density. This is done by first guessing a charge density and using the Poisson equation to calculate the potential. Doing a DFT calculation within this potential produces the parameters for using the NEG technique to calculate the charge density again. The procedure has to be repeated until the charge density converges [5].

- 3.) **Cluster Perturbation Theory (CPT):** A further approximation done with this approach is to use CPT for coupling Green functions which is not exact anymore in the case of having strong electron correlations. Depending on the coupling strength compared to the interaction strength one has to go beyond the CPT approximation. By including strong electronic correlations there is also the problem in determining the screening factor.

Chapter 3

Computational Techniques

The following sections explain the computational techniques used to implement the LCR transport calculation. All electronic band structures calculations were done with the Open Source code *Quantum Espresso* [26] which is based on plane waves and pseudopotentials. The Open Source code *Wannier90* [14] was used for computing the MLWFs. The sections 3.1 and 3.2 specify the parameters for the *Quantum Espresso* and *Wannier90* calculations. How to implement NEG technique is introduced in the sections 3.3, 3.4, 3.5 and 3.6.

3.1 Quantum Espresso

In this thesis the Open Source code *Quantum Espresso* was used for performing the Density Functional Theory (DFT) calculations. *Quantum Espresso* is a band structure code written for solids. In principle, the only physical input parameters are the size of the unit cell and the desired atom configuration within this unit cell. Because of periodicity the Kohn-Sham equations are solved in k -space. *Quantum Espresso* uses a Plane Wave (PW) basis set for solving the Kohn-Sham equations. In order to reduce the basis size, the electron-ion interaction is treated in the pseudopotential approximation. For doing reliable calculations a set of parameters has to be found. In this thesis all parameters are converged with respect to the total energy.

- **Vacuum distance:**

For calculating non-periodic structures with a code written for solids one has to introduce vacuum distances in the directions where the structure should not be periodic.

- **Cut-off energy:**

Using PWs to describe the Bloch states leads to

$$\begin{aligned}
 \Phi_i(\mathbf{r}) &= \sum_{\mathbf{k}} e^{i\mathbf{k}\mathbf{r}} \varphi_{i\mathbf{k}}(\mathbf{r}) \\
 &= \sum_{\mathbf{k}} e^{i\mathbf{k}\mathbf{r}} \sum_{\mathbf{G}} c_{\mathbf{k}+\mathbf{G}} e^{i\mathbf{G}\mathbf{r}} \\
 &= \sum_{\mathbf{kG}} c_{\mathbf{k}+\mathbf{G}} e^{i(\mathbf{k}+\mathbf{G})\mathbf{r}}.
 \end{aligned} \tag{3.1.1}$$

In practice one has to use a finite number of PWs. This can be done by taking only plane waves with an energy smaller than a cut off energy E_{cut} . Therefore only wave functions which satisfy

$$\left| \frac{\hbar^2(\mathbf{k} + \mathbf{G})^2}{2m} \right| < E_{cut} \quad (3.1.2)$$

are used within the calculation. For the charge density, equation 2.2.9, this implies

$$\left| \frac{\hbar^2(\mathbf{k} + \mathbf{G})^2}{2m} \right| < 4E_{cut}. \quad (3.1.3)$$

for non-ultrasoft pseudopotentials. The number of plane waves which enters a given physical problem is determined by its smallest length-scale oscillations. These are reduced substantially if the full potential generated by the ionic cores is replaced by a pseudopotential which coincides with the atomic potential outside a given core radius and is smooth inside.

- ***k*-grid:**

Within DFT calculating integrals over the Brillouin-zone are necessary. This can be done numerically by replacing the integrals by weighted sums over a special *k*-grid. A common choice is to take a uniform grid of *k*-points. The number of *k*-points has to be chosen big enough. For calculating the Density Of States (DOS) or the Fermi level the tetrahedron method was used.

- **Smearing parameter:**

In metallic systems integrals over functions that are discontinuous at the Fermi-level appear. Therefore a smearing technique which replaces the functions by smoother ones is necessary. Standard techniques are a Gaussian smearing or the Methfessel-Paxton method.

The Perdew Zunger (PZ) exchange correlation functional within Local Density Approximation (LDA), the ultrasoft pseudopotential *van_ak* and the Methfessel-Paxton smearing technique are used for calculating the gold-BDT-gold transport system. The functional and the pseudopotential are chosen according to paper [27] where comparable band structure problems are calculated.

3.2 Wannier90

The Open Source code *Wannier90* was used for performing the Wannier transformation of a subset of bands of a given electronic structure. In principle the program determines the transformation matrix in equation 2.3.1 by minimizing the spread of the MLWFs. The basic parameters for doing the transformation successfully are the energy windows and the starting orbitals.

- **Energy windows:** For choosing the orbitals to be transformed to a localized basis an inner and an outer window have to be defined. The inner window should contain as many bands as the number of Wannier orbitals wanted to be extracted. The outer window restricts the energy range of the Wannier bands. In practice, it is necessary to adjust the windows until the PW bands desired to transform are reproduced by the Wannier bands.
- **Starting orbitals:** The starting orbitals $|g_n\rangle$ are important to guide the minimization procedure to the MLWFs if there are entangled bands. They should already be a good guess of the MLWFs.

Wannier90 is compatible with *Quantum Espresso* and uses the overlaps between the cell periodic part of the Bloch states $M_{mn}^{(\mathbf{k}, \mathbf{b})} = \langle \varphi_{m\mathbf{k}} | \varphi_{n\mathbf{k}+\mathbf{b}} \rangle$ and the projections of the initial guess for the localised orbitals on the Bloch states $A_{mn}^{(\mathbf{k})} = \langle \Phi_{m\mathbf{k}} | g_n \rangle$ as input parameters for the Wannier transformation.

3.3 Basis states and Hamiltonian

The next challenge after determining all model parameters is finding the ground state and the corresponding eigenvector of the many-particle Hamiltonian. Therefore one has to represent the Hamiltonian in the many-particle basis. If there are L MLWFs in the system then the number of many-particle basis states is 2^{2L} . A common technique for setting up the basis vectors is using a decimal representation of the bit sequence of the occupation. As example 3.3.1 shows a state with $L = 4$, $N_{\uparrow} = 3$ and $N_{\downarrow} = 2$ in binary and decimal notation.

$$|115\rangle = \underbrace{|0, 1, 1, 1\rangle}_{\text{up}} \underbrace{|0, 0, 1, 1\rangle}_{\text{down}} \quad (3.3.1)$$

N_{σ} is the total number of electrons with spin σ in the system. In this example the sites one and two are fully occupied, on site three there is only an up-electron and site four is empty. This bit sequence is equal to the decimal number 115. Before setting up the Hamiltonian one should care about symmetries. The commutators

$$\begin{aligned} [\hat{H}, \hat{N}_{\uparrow}] &= 0 \\ [\hat{H}, \hat{N}_{\downarrow}] &= 0 \end{aligned} \quad (3.3.2)$$

hold. Therefore the Hamiltonian splits up in sectors with fixed particle numbers N_{\uparrow} and N_{\downarrow} . The number of basis states in each sector is given by dl .

$$dN_{\uparrow} = \binom{L}{N_{\uparrow}} \quad dN_{\downarrow} = \binom{L}{N_{\downarrow}} \quad (3.3.3)$$

$$dl = dN_{\uparrow} dN_{\downarrow} \quad (3.3.4)$$

Further symmetries would reduce the size of the sectors. Setting up the Hamiltonian can be done in each particle sector $l = \{N_{\uparrow}, N_{\downarrow}\}$ separately.

$$\hat{H} = \bigoplus_l \hat{H}^{(l)} \quad (3.3.5)$$

$$H_{\mu\nu}^{(l)} = \langle \omega_{\mu}^{(l)} | \hat{H} | \omega_{\nu}^{(l)} \rangle \quad (3.3.6)$$

Instead of programming a loop over μ and ν it is faster to generate the possible states $\langle \omega_{\mu}^{(l)} |$ corresponding to $|\omega_{\nu}^{(l)}\rangle$ and search them in a list. There are only few entries in the matrices therefore sparse matrices should be used.

In addition the up and the down sector in the Hamiltonian are decoupled. Therefore the Hamilton matrices can be calculated separately and combined using the Kronecker product. The decoupled up and down sectors are also used in the Band Lanczos algorithm.

3.4 Calculating Green functions

The Green function in the ground state $|\Omega\rangle$ of the Hamiltonian is of interest. Using the spectral representations 2.6.27 and 2.6.28 at zero temperature and the definition of the retarded Green function 2.6.21 leads to

$$G_{ij}(\omega) = \langle \Omega | \hat{a}_i \frac{1}{\omega - \hat{H} + E_0} \hat{a}_j^\dagger | \Omega \rangle + \langle \Omega | \hat{a}_j^\dagger \frac{1}{\omega + \hat{H} - E_0} \hat{a}_i | \Omega \rangle. \quad (3.4.1)$$

The first term is called electron part and the second one hole part. Photoelectron Spectroscopy (PES) and Inverse Photoemission Spectroscopy (IPES) can be used to measure these terms directly. Here only the electron part will be discussed. The hole part can be calculated in a similar way. Let $|\omega_l\rangle$ be the many-particle basis of the Hamiltonian then the ground state can be written as

$$|\Omega\rangle = \sum_l b_l |\omega_l\rangle. \quad (3.4.2)$$

As mentioned above the Hamiltonian is block diagonal within a fixed number of particles. Therefore $|\Omega\rangle$ is in the N -particle subspace. Inserting the eigenbasis of the $N + 1$ -particle subspace of the Hamiltonian leads to a matrix equation for the electron part of the Green function

$$\begin{aligned} \langle \Omega | \hat{a}_i \frac{1}{\omega - \hat{H} + E_0} \hat{a}_j^\dagger | \Omega \rangle &= \sum_{lmn} b_m b_l^* \langle \omega_m | \hat{a}_i | \beta_n \rangle \langle \beta_n | \frac{1}{\omega - E_n + E_0} | \beta_n \rangle \langle \beta_n | \hat{a}_j^\dagger | \omega_l \rangle \\ &= \sum_n Q_{in}^{(e)} \frac{1}{\omega - E_n + E_0} Q_{nj}^{(e)\dagger} \\ &= \left\{ Q^{(e)} \frac{1}{\omega - E - E_0} Q^{(e)\dagger} \right\}_{ij} \end{aligned} \quad (3.4.3)$$

with the matrix

$$Q_{in}^{(e)} = \sum_m b_m \langle \omega_m | \hat{a}_i | \beta_n \rangle. \quad (3.4.4)$$

The dimension of the many-body Hamiltonian, even in particle subspace, grows exponentially with the system size and solving the eigenvalue problem gets a challenge. Very powerful tools for solving huge eigenvalue problems are exact diagonalization algorithms.

3.5 Band Lanczos algorithm

A method for setting up Green functions directly is the Band Lanczos algorithm. The following brief introduction to the Band Lanczos algorithm is taken from [21]. The Band Lanczos algorithm is a generalized Lanczos procedure where the Krylov subspace is spanned not by one, but by many states. As starting vectors

$$|\Phi_i\rangle = \hat{a}_i^\dagger |\Omega\rangle \quad (3.5.1)$$

are used. Because the Hamiltonian is decoupled in spin, the spins up and down can be treated separately. Therefore i runs from 1 to L and let \hat{H}' be the corresponding Hamiltonian. The Krylov subspace is spanned by the application of \hat{H}' on the starting vectors and orthonormalizing the new vectors with respect to the previous ones.

$$\left\{ |\Phi_1\rangle, \dots, |\Phi_L\rangle, \hat{H}' |\Phi_1\rangle, \dots, \hat{H}' |\Phi_L\rangle, \dots, \hat{H}'^m |\Phi_1\rangle, \dots, \hat{H}'^m |\Phi_L\rangle \right\} \quad (3.5.2)$$

The orthogonalization procedure can become a problem. A practical rule is to control the number of iterations m by looking on the convergence of the lowest eigenvalue.

The projected Hamiltonian \mathcal{H} on the Krylov subspace has $2L$ diagonals around the central diagonal and can be diagonalized using standard techniques. The Band Lanczos procedure provides directly the $Q^{(e)}$ matrices in equation 3.4.3. Doing the same procedure for the hole part leads to the Green function.

$$G_{ij}(\omega) = \sum_n \frac{Q_{in}^{(e)} Q_{nj}^{(e)\dagger}}{\omega - E_n + E_0} + \sum_m \frac{Q_{im}^{(h)} Q_{mj}^{(h)\dagger}}{\omega + E_m - E_0} \quad (3.5.3)$$

3.6 Calculating transport properties

All formulas for calculating the transport properties of the LCR transport system are treated in chapter 2. Although implementing the calculation is straightforward, there are some points to take care of.

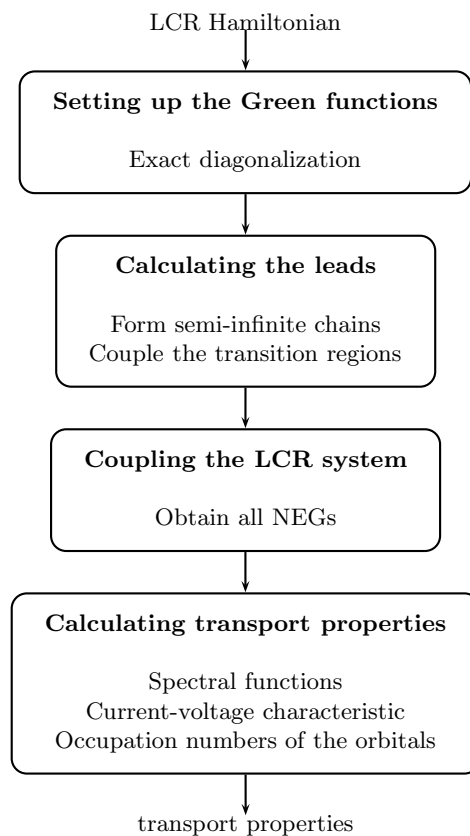


Figure 3.1: Calculation scheme of the NEG method.

First of all the size of the Green functions is reduced by a factor of two using the retarded, advanced and Keldysh Green functions separately and not Keldysh space. In principle then the Green functions are matrices of size $2L \times 2L$, where L is the number of orbitals in the cluster. To halve the size of the matrices a second time the spins can be treated separately.

In order to calculate the Green functions of the semi-infinite chains, equation 2.7.21 has to be solved iteratively. In every step a Green function has to be inverted and problems occur if the matrix is close to singular. In general it is recommendable to use the relations between the retarded,

advanced and Keldysh Green function instead of calculating the Green functions separately to avoid numerical problems.

In addition the Green functions depend on the frequency ω . The spectral function or the transmission in dependence of ω can be calculated directly from the obtained Green functions. The calculation of the current or the occupation numbers of the orbitals is more troublesome, because one has to integrate over the Green functions. Because of calculating a realistic system the Green functions can vary rapidly as a function of energy. The simplest way to do the integration is using a fixed ω -grid and the trapezoidal method. The artificial level broadening 0^+ must be chosen as small as possible. Taking the Landauer-Büttiker formula instead of the integration over the Keldysh Green function is advantageous because in the derivation of the Landauer-Büttiker formula terms proportional to 0^+ were already canceled. Making 0^+ small is no problem in calculating the current, but for computing the occupation numbers the resolution in ω must be in the order of 0^+ and therefore the computational effort is high. More sophisticated approaches are adaptive integration methods or a integration routine which takes care about both parameters, the artificial level broadening 0^+ and the grid size.

Chapter 4

Application

Calculating the transport properties through the Benzene-1,4-Dithiol (BDT) molecule connected by two gold chains is divided into three parts. First the leads, single gold chains, are studied within different approximations in section 4.1. Strong electron correlations are neglected in all gold atoms. Second, the benzene molecule is discussed in section 4.2. Finally, in section 4.3 the focus is on the full gold-BDT-gold system. Strong electron correlations are treated in the BDT molecule.

4.1 Gold-Chain

A convergence analysis leads to the choice of a cut-off energy for the wavefunction of $32 Ry$ and the charge density of $128 Ry$. All the parameters are converged with respect to the total energy ($5 meV$). The Perdew Zunger (PZ) exchange correlation functional within local density approximation (LDA) and an ultrasoft pseudopotential (Au.pz-van_ak.UPF) are used in the calculation. Because gold is a metal also a smearing technique is necessary. Methfessel-Paxton with a smearing parameter of $0.01 Ry$ is chosen.

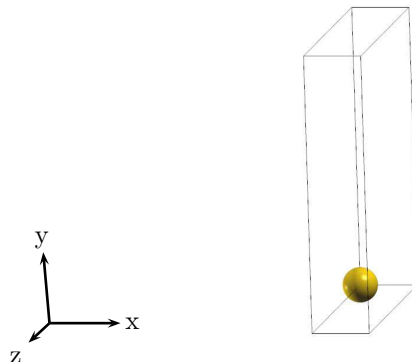


Figure 4.1: Unit cell of the gold chain.

Due to using a code designed for solids a vacuum distance in the directions perpendicular to the gold chain has to be introduced. The vacuum distance must be chosen big enough ($d_{vac} = 12\text{\AA}$) to avoid the effect of periodicity in the y and z direction. The unit cell is shown in figure 4.1. The calculated equilibrium gold distance in this regime is $d_{Au} = 2.4699 \text{\AA}$. So the size of the tetragonal unit cell is $d_{Au} \times d_{vac} \times d_{vac}$.

126 k-points are used to calculate the bandstructure in figure 4.2. The Density Of States (DOS) is calculated using the tetrahedron method and 1260 k-points. Gold has the electron configuration [Xe] 4f14 5d10 6s1. All energies are given in the energy scale of the *Quantum Espresso* calculation. The Fermi energy is $E_{Fermi} = -5.725 \text{ eV}$. For the transport calculations the bands near the Fermi level are important. There are one *s*-band (green) and five *d*-bands (blue). How the electrical conductance, especially the transmission function, is influenced by considering only the *s*-band is the first point of the investigation.

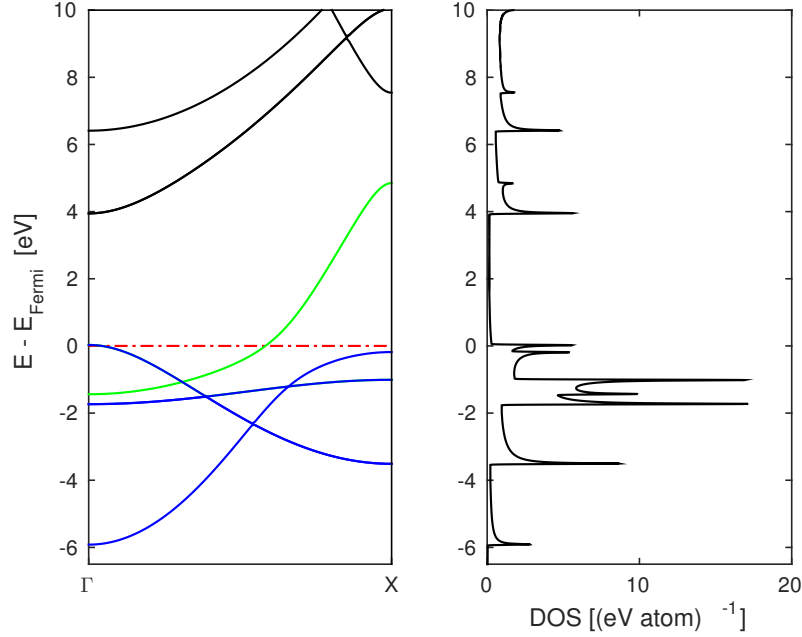


Figure 4.2: Bandstructure and DOS of a gold chain. The *s*-band is marked green and the *d*-bands are drawn in blue. The Fermi level is at the zero of the energy scale.

4.1.1 The *s*-model

A Wannier transformation is used to get a maximally localized orbital for the *s*-band. As a starting guess for the orbital an *s*-orbital centered on the gold atom is used. The inner and the outer window are the dotted lines in figure 4.4. The red line is the result of the Wannier transformation. The resulting Wannier orbital is shown in figure 4.3. The starting *s*-orbital centered at the gold atom has been shifted in-between two gold atoms and forms therefore a σ -bond.

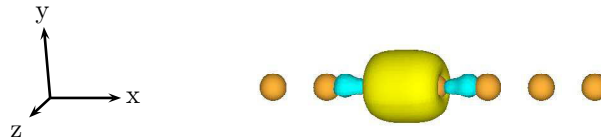


Figure 4.3: Gold Wannier orbital in the *s*-model.

The Wannier orbitals are not eigenfunctions of the Hamiltonian anymore. Therefore the Hamiltonian in the Wannier basis has off-diagonal elements, hoppings to neighboring atoms, in addition to the on-site energies. Table 4.1 shows the on-site energy ϵ and the hopping parameters t_i , where

t_i is the hopping to the i -th neighbour. Due to the DFT calculation all energies are given within an accuracy of ± 5 meV.

Table 4.1: Hopping parameters in the s -model.

ϵ [eV]	t_1 [eV]	t_2 [eV]	t_3 [eV]	t_4 [eV]	t_5 [eV]	t_6 [eV]
-5.293	-1.290	0.523	-0.237	0.097	-0.045	0.035

The hopping parameter decreases with the distance due to the reduced overlap of the orbitals. A possible way to reduce the number of parameters in the subsequent transport calculation is to truncate the expansion at the point where the hopping parameter falls under a defined threshold value. A second possibility is to include only hopping parameter up to a defined hopping distance. The convergence of the expansion can be judged from a comparison of the achieved tight binding model with the actual band structure shown in figure 4.4. The dashed curves show the s -bands in different tight binding (TB) regimes. TB i includes all hopping smaller or equal to the i -th neighbor. The dashed band which is furthest away from the original band at the X point is TB1. The next one is TB2 and so on.

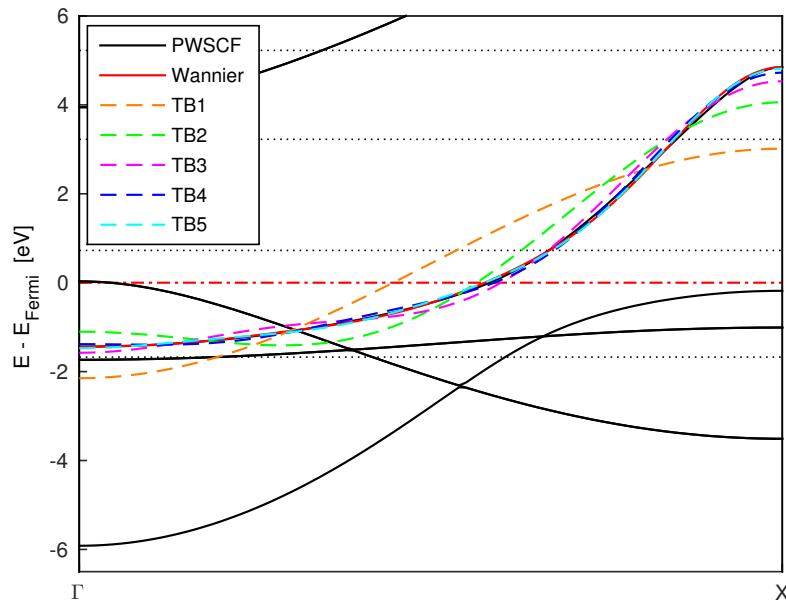


Figure 4.4: Bandstructure in the s -model. The black lines are the actual PWSCF band structure, the dashed lines are calculated with a TB model with different numbers of neighbors and the dotted lines present the inner and outer Wannier window.

The s -model in TB1 is the easiest case to calculate the conductance in the gold chain. The cluster Green function is plotted in figure 4.5 and shows a resonance at the onsite energy ϵ because there is only one atom in the cluster.

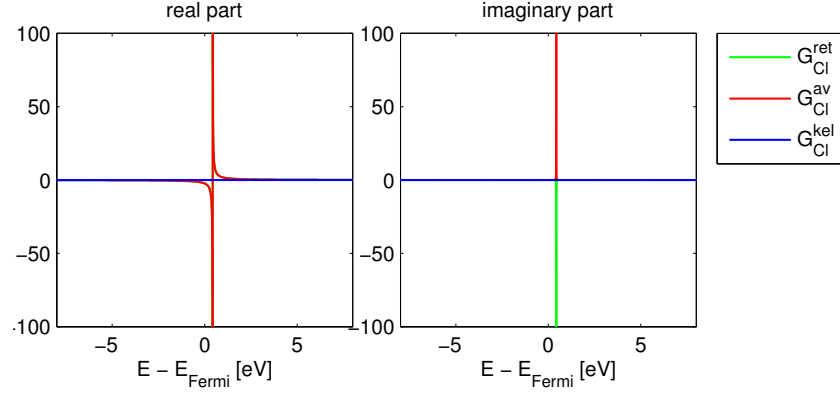


Figure 4.5: Cluster Green function of a transport calculation over a gold chain in the s -model considering only nearest neighbor hoppings.

Forming an semi-infinite chain out of the cluster Green function \mathbf{G}_{Cl} shows a semicircular imaginary part in \mathbf{G}_{LL} , in figure 4.6. The semicircle has its center at ϵ and a diameter of $4t_1$. The imaginary part of the full central Green function \mathbf{G}_{CC} shows the typically $1d$ -DOS behavior.

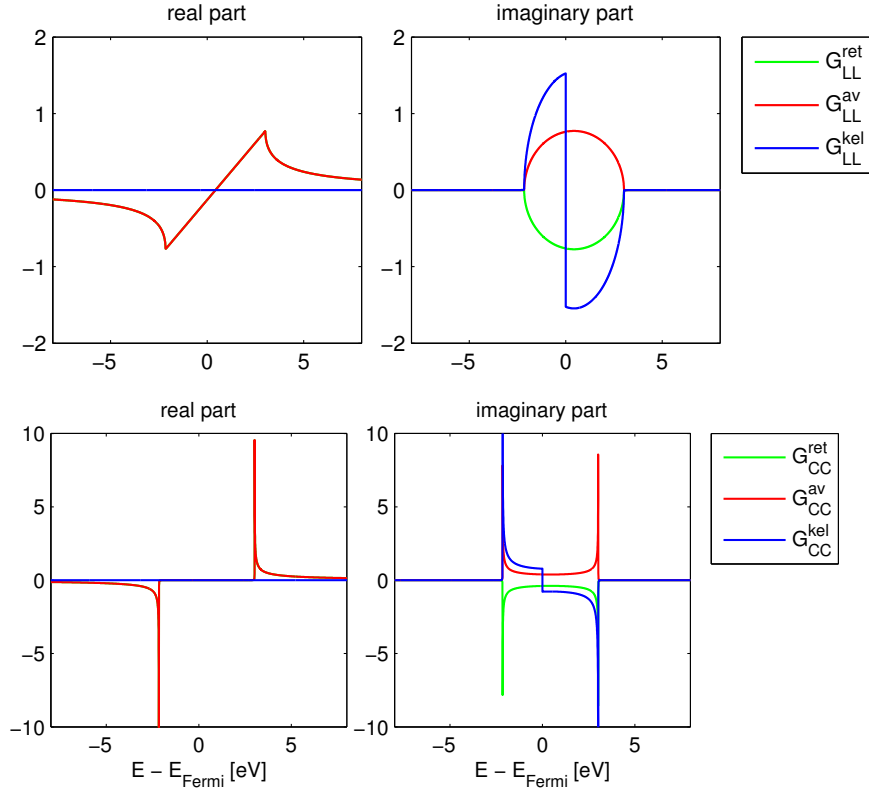


Figure 4.6: Full Green functions of a transport calculation over a gold chain in the s -model considering only nearest neighbor hoppings.

The Green function \mathbf{G}_{LC} and the lead-induced self energy Σ are plotted in figure 4.7.

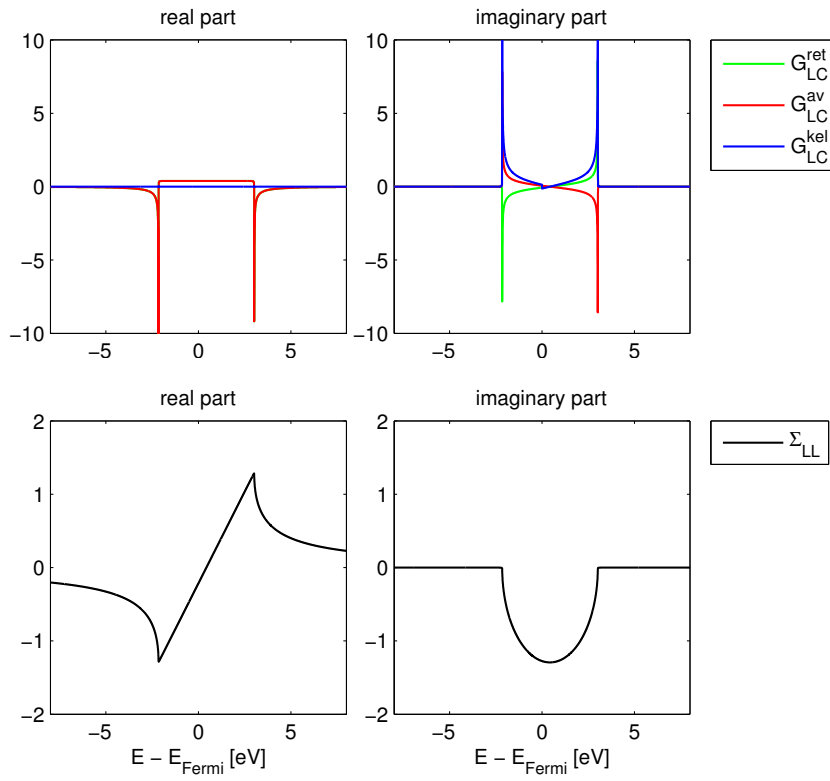


Figure 4.7: Lead-induced self energy of a transport calculation over a gold chain in the s -model considering only nearest neighbor hoppings.

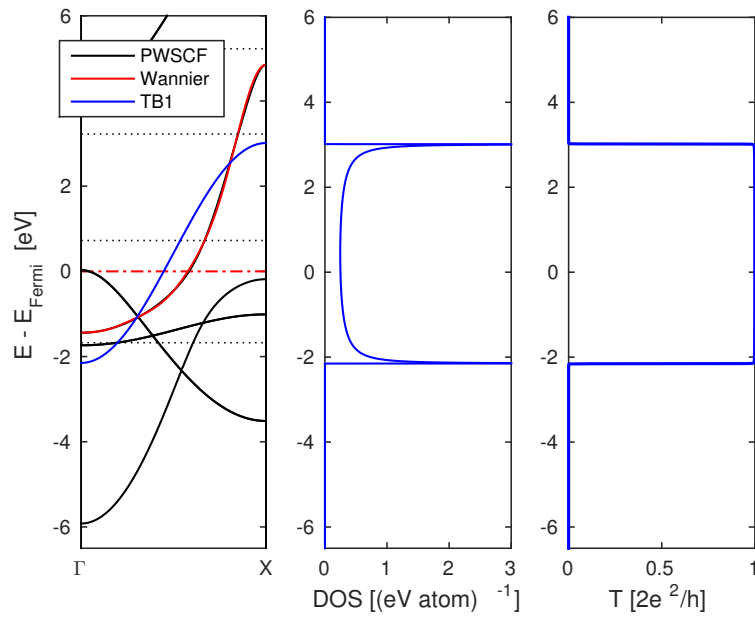


Figure 4.8: Band structure, DOS and transmission of a gold chain with nearest neighbor hoppings in the s -model.

The band structure, the DOS and the conductance are shown in figure 4.8. With this arrangement of the plots it is easy to understand the results of the conductance calculation and to see the approximation which is done by just using nearest neighbor hoppings. The figure clearly shows that there is a finite conductance if there is a band at a certain energy.

4.1.2 The sd -model

The sd -model includes the s -band and five d -bands per gold atom. Therefore the Hamiltonian can be divided in 6×6 matrices where ϵ is the Hamiltonian of one isolated gold atom and t_i are the hopping matrices to the neighboring gold atoms. The Wannier orbitals are not orthogonal per definition therefore off-diagonal elements appear. The s -orbital is highlighted in orange and the d -orbitals in blue. The energies are again given in eV and an accuracy of $5 meV$.

$$\epsilon = \begin{pmatrix} -6.685 & 0.645 & 0 & 0 & -0.645 & 0 \\ 0.645 & -7.167 & 0 & 0 & 0.063 & 0 \\ 0 & 0 & -7.664 & 0 & 0 & 0 \\ 0 & 0 & 0 & -7.104 & 0 & 0 \\ -0.645 & 0.063 & 0 & 0 & -7.167 & 0 \\ 0 & 0 & 0 & 0 & 0 & -7.664 \end{pmatrix} \quad (4.1.1)$$

Due to the Wannier transformation matrices with complex numbers can appear. The complex values can be transformed to real numbers using the arbitrary phase of each wavefunction. This is already done here.

$$\langle \tilde{\Psi}_m | \hat{H} | \tilde{\Psi}_n \rangle = \langle \Psi_m | e^{i\phi_m} \hat{H} e^{-i\phi_m} | \Psi_n \rangle = \langle \Psi_m | \hat{H} | \Psi_n \rangle \quad (4.1.2)$$

The matrix ϵ must be symmetric, or hermitian in case of a complex matrix. The matrices 4.1.3 and 4.1.4 are the hopping matrices to the next two neighbors.

$$t_1 = \begin{pmatrix} -2.151 & 0.089 & 0 & 0 & -0.089 & 0 \\ 0.645 & -0.408 & 0 & 0 & 0.227 & 0 \\ 0 & 0 & 0.863 & 0 & 0 & 0 \\ 0 & 0 & 0 & -0.181 & 0 & 0 \\ -0.645 & 0.227 & 0 & 0 & -0.408 & 0 \\ 0 & 0 & 0 & 0 & 0 & 0.863 \end{pmatrix} \quad (4.1.3)$$

$$t_2 = \begin{pmatrix} 0.427 & -0.023 & 0 & 0 & 0.023 & 0 \\ 0.089 & 0.014 & 0 & 0 & -0.011 & 0 \\ 0 & 0 & 0.092 & 0 & 0 & 0 \\ 0 & 0 & 0 & 0.003 & 0 & 0 \\ -0.089 & -0.011 & 0 & 0 & 0.014 & 0 \\ 0 & 0 & 0 & 0 & 0 & 0.092 \end{pmatrix} \quad (4.1.4)$$

In the further calculations one has to pay attention that each orbital has as many neighbor orbitals on the right as on the left side due to symmetry. Therefore for a calculation with nearest neighbors some matrix elements in t_1 have to be set to zero (gray marked values) and no matrix t_2 is used. For a calculation with next nearest neighbors one has to delete the gray marked values in t_2 and use the full matrix t_1 . In case of not deleting these values the s -orbital would have more

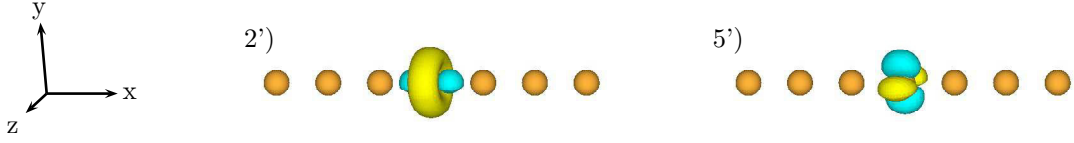


Figure 4.10: Wannier orbitals calculated by diagonalizing the d -orbital part in ϵ .

Diagonalizing the whole ϵ matrix leads to the eigenfunctions in figure 4.11. In orbital 1* and 2* one can see the hybridization between the s -orbital and the d -orbital.

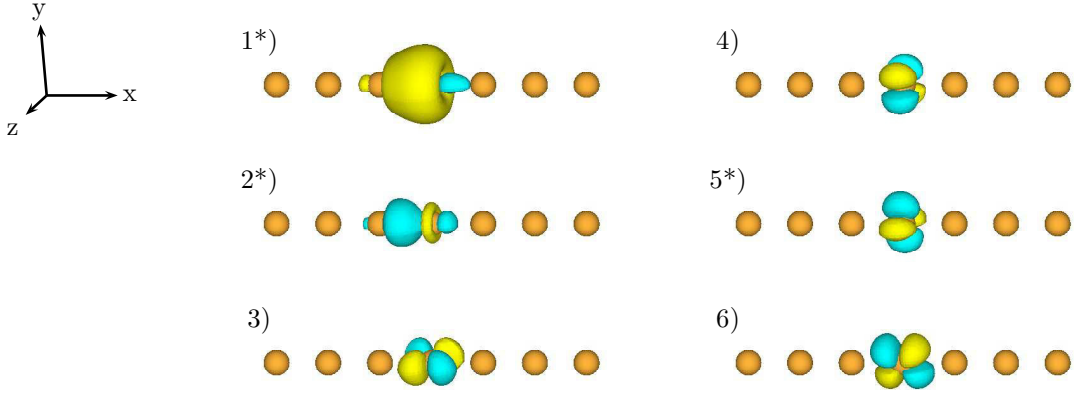


Figure 4.11: The hybridized gold orbitals.

Using the eigenbasis produces the on-site matrix $\tilde{\epsilon}$ and the hopping matrix \tilde{t}_1 . Due to rotational symmetry of the gold chain the orbitals 4 and 5* and the orbitals 3 and 6 have the same energy.

$$\tilde{\epsilon} = \begin{pmatrix} -7.909 & 0 & 0 & 0 & 0 & 0 \\ 0 & -6.005 & 0 & 0 & 0 & 0 \\ 0 & 0 & -7.664 & 0 & 0 & 0 \\ 0 & 0 & 0 & -7.104 & 0 & 0 \\ 0 & 0 & 0 & 0 & -7.104 & 0 \\ 0 & 0 & 0 & 0 & 0 & -7.664 \end{pmatrix} \quad (4.1.7)$$

$$\tilde{t}_1 = \begin{pmatrix} -1.613 & 1.313 & 0 & 0 & 0 & 0 \\ 0.401 & -1.173 & 0 & 0 & 0 & 0 \\ 0 & 0 & 0.863 & 0 & 0 & 0 \\ 0 & 0 & 0 & -0.181 & 0 & 0 \\ 0 & 0 & 0 & 0 & -0.181 & 0 \\ 0 & 0 & 0 & 0 & 0 & 0.863 \end{pmatrix} \quad (4.1.8)$$

Therefore the cluster Green function shown in figure 4.12 is diagonal. Of course the excitation energies are at the energies in $\tilde{\epsilon}$. Due to the non-diagonal hopping matrices the full Green functions and the lead-induced self energy are not diagonal anymore. But in the case of considering only nearest neighbor hoppings only one off-diagonal element is non-zero.

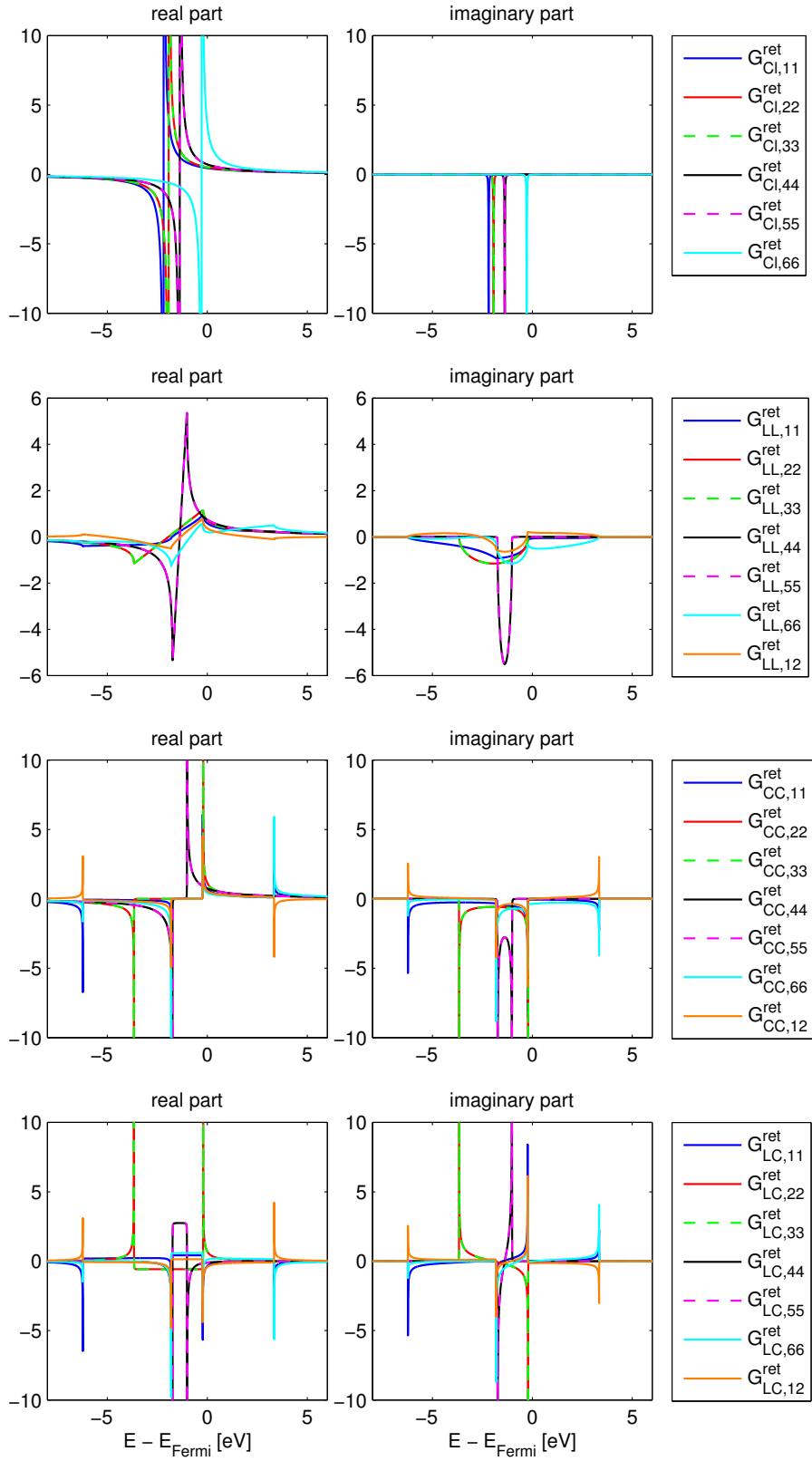


Figure 4.12: Green functions of a transport calculation over a gold chain in the *sd*-model considering only nearest neighbor hoppings.

As one can see in the figures 4.12 and 4.13 the four elements which are diagonal in \tilde{t}_1 show the typical tight binding behavior from the s -model. The imaginary part of the lead Green function is a semi-circle and the imaginary part of the full center Green function looks like a 1d-DOS.

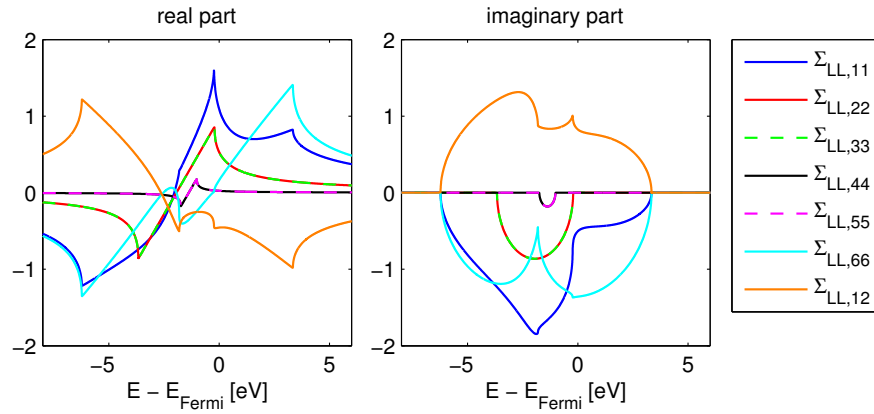


Figure 4.13: Lead-induced self energy of a transport calculation over a gold chain in the sd -model considering only nearest neighbor hoppings.

The bandstructure, the DOS and the transmission are plotted in figure 4.14. There is a simple connection between these plots. The transmission is the number of bands (channels) at a certain energy.

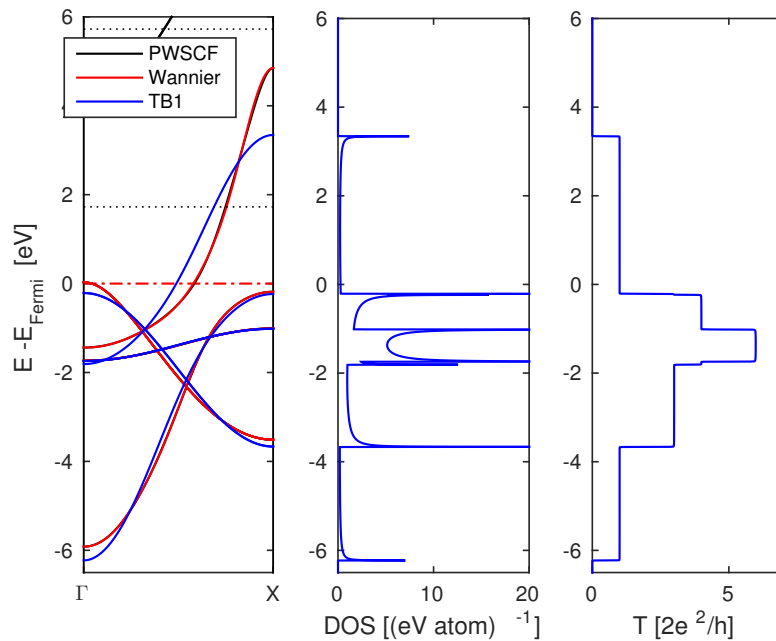


Figure 4.14: Bandstructure, DOS and transmission of a gold chain with nearest neighbor hoppings.

Figure 4.15 results from a next nearest neighbor calculation.

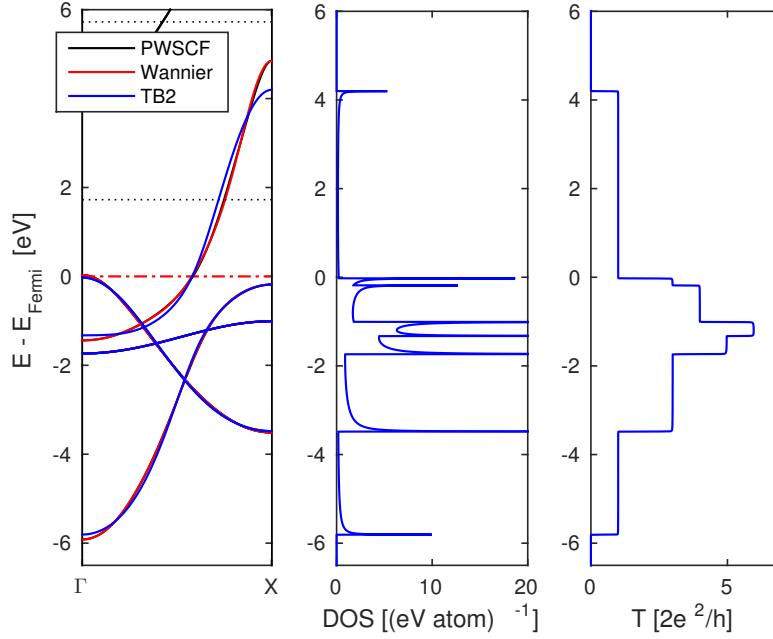


Figure 4.15: Bandstructure, DOS and transmission of a gold chain with next nearest neighbor hoppings.

4.2 Benzene

Benzene is a well studied molecule. Because of its symmetries it is possible to predict the pattern of the main levels using the Hückel model. A general Hamiltonian in the Born-Oppenheimer approximation is

$$\hat{H} = \sum_{i=1}^N \left(-\frac{\hbar^2 \nabla_i^2}{2m} - \sum_{l=1}^N \frac{Z_l e^2}{4\pi\epsilon |r_i - R_l|} \right) + \frac{1}{2} \sum_{\substack{i,j=1 \\ i \neq j}}^N \frac{e^2}{4\pi\epsilon |r_i - r_j|} = \sum_{i=1}^N \hat{H}_i \quad (4.2.1)$$

where the indices i and j run over the electrons and R_l are the positions of the atoms. It is assumed that there is one electron per atom. In a further approximation the electron correlation can be treated by using an effective one-particle Hamiltonian \hat{H}_i for each electron. In doing this approximations the Hamiltonian can be separated into Hamiltonians \hat{H}_i , also called molecular orbital Hamiltonian \hat{H}_{MO} , for each electron i which can be solved by linear combination of atomic orbitals. In this regime the total wavefunction is approximated by a linear combination of the atomic orbitals of the atoms in the molecule.

$$|\Psi_{MO}\rangle = \sum_{j=1}^N c_j |\phi_j\rangle \quad (4.2.2)$$

Starting from the time-independent Schrödinger equation

$$\hat{H}_{MO} |\Psi_{MO}\rangle = E |\Psi_{MO}\rangle \quad (4.2.3)$$

the coefficients c_j are defined by the extended eigenvalue problem

$$\sum_{j=1}^N \langle \phi_i | \hat{H}_{MO} | \phi_j \rangle c_j = E \sum_{j=1}^N \langle \phi_i | \phi_j \rangle c_j. \quad (4.2.4)$$

The Hückel model now assumes that the atomic wave functions are orthogonal $\langle \phi_i | \phi_j \rangle = \delta_{ij}$ to each other. For the benzene molecule it is obvious to take a p_z -orbital out of the plane for each carbon atom. Therefore the diagonal matrix elements $\langle \phi_i | H_{MO} | \phi_i \rangle = \alpha$ are all the same. Respecting only overlap between nearest neighbor orbitals $\langle \phi_i | H_{MO} | \phi_{i+1} \rangle = \beta$ the Hückel model applied to benzene leads to the eigenvalue problem

$$\begin{pmatrix} \alpha - E & \beta & 0 & 0 & 0 & \beta \\ \beta & \alpha - E & \beta & 0 & 0 & 0 \\ 0 & \beta & \alpha - E & \beta & 0 & 0 \\ 0 & 0 & \beta & \alpha - E & \beta & 0 \\ 0 & 0 & 0 & \beta & \alpha - E & \beta \\ \beta & 0 & 0 & 0 & \beta & \alpha - E \end{pmatrix} \begin{bmatrix} c_1 \\ c_2 \\ c_3 \\ c_4 \\ c_5 \\ c_6 \end{bmatrix} = \mathbf{0}. \quad (4.2.5)$$

It turns out that the overlap β has a negative sign. The energy levels of benzene are arranged like

$$E = \{\alpha - 2\beta, \alpha - \beta, \alpha - \beta, \alpha + \beta, \alpha + \beta, \alpha + 2\beta\} \quad (4.2.6)$$

from the highest to the lowest energy. Level two and three are degenerated, also the energy levels four and five. The difference between these energies is the HOMO-LUMO gap. The corresponding eigenvectors are

$$\mathbf{c} = \left\{ \underbrace{\begin{pmatrix} -1 \\ 1 \\ -1 \\ 1 \\ -1 \\ 1 \end{pmatrix}}_{B_{2g}}, \underbrace{\begin{pmatrix} -1 \\ 0 \\ 1 \\ -1 \\ 0 \\ 1 \end{pmatrix}, \begin{pmatrix} 1 \\ -2 \\ 1 \\ 1 \\ -2 \\ 1 \end{pmatrix}}_{E_{2u}}, \underbrace{\begin{pmatrix} 1 \\ 0 \\ -1 \\ 0 \\ 1 \\ 1 \end{pmatrix}, \begin{pmatrix} 1 \\ 2 \\ 1 \\ -1 \\ -2 \\ -1 \end{pmatrix}}_{E_{1g}}, \underbrace{\begin{pmatrix} 1 \\ 1 \\ 1 \\ 1 \\ 1 \\ 1 \end{pmatrix}}_{A_{2u}} \right\}. \quad (4.2.7)$$

The first three eigenenergies respectively eigenvectors are the antibonding, the last three the bonding ones. The point group of benzene is D_{6h} and the irreducible representation is B_{2g} , E_{2u} , E_{1g} and A_{2u} . The orbitals are typically named by their symmetry.

Figure 4.16 presents the molecular orbitals obtained by doing a full ab-initio DFT calculation for the benzene molecule with a Generalized Gradient Approximation (GGA) functional. The orbitals are sorted by their energies.

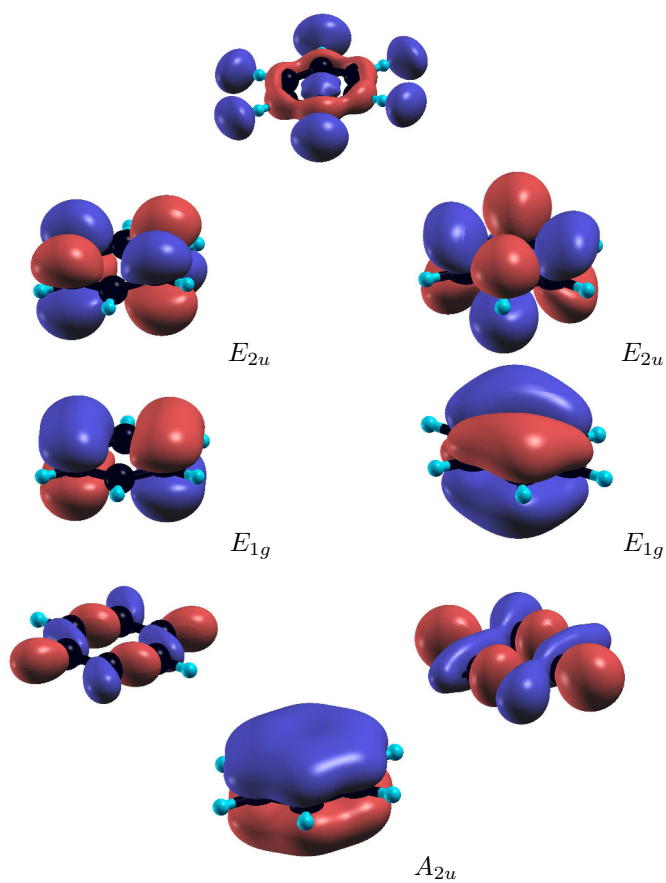


Figure 4.16: Benzene orbitals sorted by their energies.

The orbitals E_{2u} , E_{1g} and A_{2u} can be identified with orbitals from the DFT calculation. The B_{2g} orbital must be searched at higher energies. Planar orbitals cannot be described by the p_z -orbitals used in the Hückel model. The energy levels corresponding to the orbitals in figure 4.16 and the comparison the Hückel model are shown in figure 4.17. The Hückel parameters are fitted using the energy difference of the HOMO-LUMO gap.

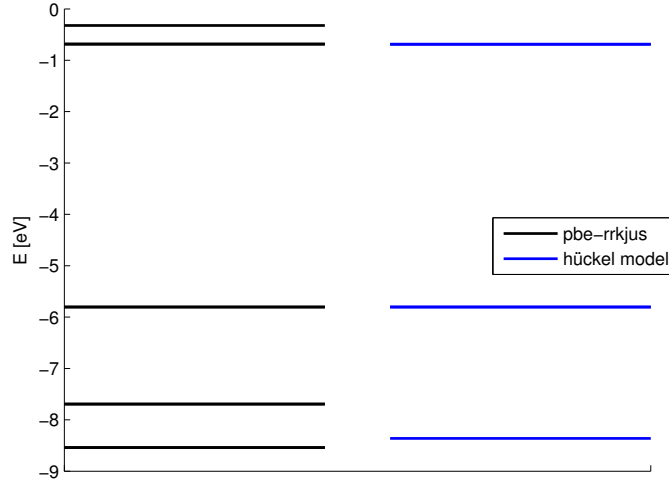


Figure 4.17: Benzene energy levels.

The energies depend on the functional chosen in the DFT calculation. Table 4.2 compares the HOMO-LUMO gap and the distances d_{CC} and d_{CH} calculated with different functionals to measured values.

Table 4.2: Comparison of different functionals to experimental results.

	GGA (pbe-rrkjus)	LDA (pz-van_ak)	experimental [28]
HOMO-LUMO gap	5.1151 eV	5.1840 eV	4.9 eV
d_{CC}	1.394 Å	1.384 Å	1.396 Å
d_{CH}	1.090 Å	1.094 Å	1.083 Å

The Perdew Zunger (PZ) exchange correlation functional and an ultrasoft pseudopotential (pz-van_ak) are used in the further calculations analog to paper [27].

4.3 Au-BDT-Au system

In this section the transport through a gold-BDT-gold system is discussed. For simplicity rigid gold chains with equal distances between the gold atoms, as calculated in section 4.1, are assumed as leads. Nearest neighbor hoppings between the gold atoms are assumed. The transport system is drawn in figure 4.18.



Figure 4.18: Gold-BDT-gold system used for the transport calculation.

At first different configurations of the BDT between the gold leads are discussed. After choosing the geometry a Wannier transformation is performed to generate the Hamiltonian in a maximally localized basis. The Hamiltonian is used to do the molecular transport calculation. Finally electron-electron interactions will be included.

4.3.1 Geometry optimization

The unit cell used for performing the DFT calculations is shown in figure 4.19. The distance between the gold atoms in the chain d_{Au} and the vacuum distance d_{vac} are chosen according to section 4.1.

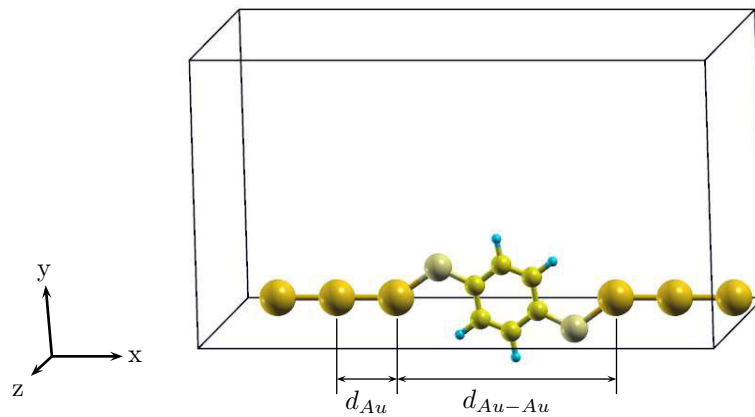


Figure 4.19: Unit cell of the gold-BDT-gold system.

Doing geometry optimizations for particular distances d_{Au-Au} between the contacts results in different configurations for the BDT atoms. The configurations are shown in figure 4.20.

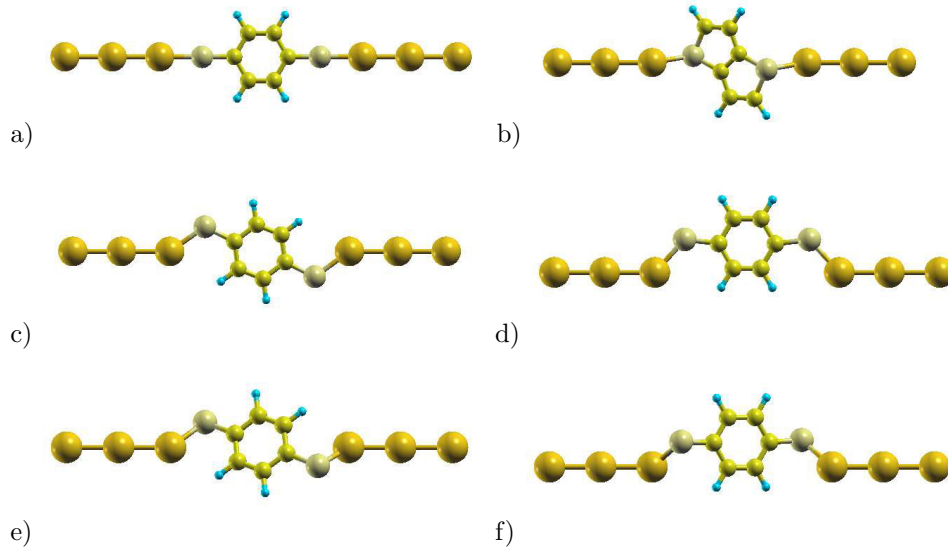


Figure 4.20: The line (a), thienothiophene (b), twisted (c), atop (d), twisted-twisted (e) and the atop-twisted (f) configuration of BDT.

The total energies E_{tot} of the configurations depending on different distances d_{Au-Au} between the contacts are drawn in figure 4.21.

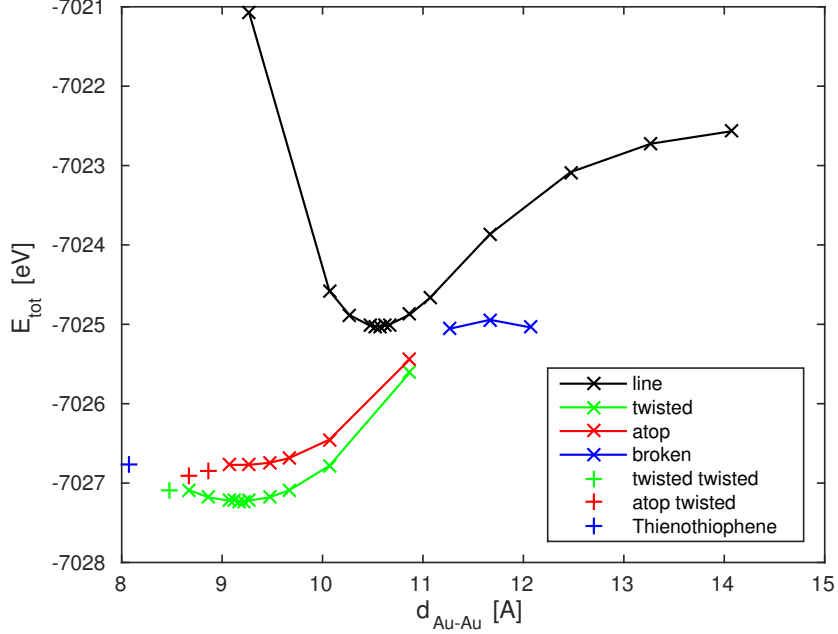


Figure 4.21: The total energy E_{tot} for different geometries and distances d_{Au-Au} between the contacts.

At large distances ($d_{Au-Au} > 11 \text{ \AA}$) the broken configuration is energetically preferred. In the broken geometry the BDT is placed at one contact and not in-between the two contacts. At narrow distances ($11 \text{ \AA} > d_{Au-Au} > 8.5 \text{ \AA}$) the twisted configuration is favored. At even smaller distances ($8.5 \text{ \AA} > d_{Au-Au}$) the twisted-twisted geometry is preferred until the atoms rearrange and form the molecule thienothiophene. For the transport calculations the twisted geometry at a distance of $d_{Au-Au} = 9.17 \text{ \AA}$ is chosen, because this is the geometry with the lowest total energy.

Quantum Espresso is a code written for periodic materials therefore the number of gold atoms per unit cell has to be chosen large enough to reduce periodic effects in the DFT calculation and that the BDT molecule relaxes like coupled to two semi-infinite gold chains. The results of doing Wannier transformations with different numbers of gold atoms N_{Au} per unit cell are summarized in table 4.3.

Table 4.3: Convergence of the energies as a function of the number of gold atoms N_{Au} per unit cell.

N_{Au}	4		6		8	
	gold	benzene	gold	benzene	gold	benzene
	-2.59	-5.39	-2.01	-5.21	-2.02	-5.21
	-1.96	-2.81	-1.84	-2.65	-1.81	-2.65
	-1.85	-2.50	-1.74	-2.32	-1.74	-2.32
	-1.33	1.87	-1.26	2.03	-1.22	2.02
	-1.33	2.81	-1.26	2.98	-1.22	2.98
	-0.64	5.78	-0.23	6.01	-0.23	6.00

The *gold* columns present the eigenenergies of a gold atom as far as possible away from the BDT. The energies of the benzene B_{2g} , E_{2u} , E_{1g} and A_{2u} states are in the *benzene* columns. The values seem to be already converged using six gold atoms per unit cell.

4.3.2 Hamiltonian and orbitals

For the Wannier transformation an energy window and a starting guess for the orbitals is needed. It turns out that the starting orbitals have to be chosen carefully. According to section 4.1 an s -orbitals and the five d -orbitals are used as starting guess for the gold atoms. But now it is important to place the s -orbitals in-between the gold atoms to get the σ -bonds. For the sulfur atoms p_x -, p_y - and p_z -orbitals are chosen and for the carbon atoms p_z -orbitals, which point out of the ring plane. The remaining functions are chosen randomly. An inner energy window narrowed by -5.95 eV and 3.16 eV and an outer window bounded by -5.95 eV and 7.46 eV produce suitable results. The Wannier transformation is only done for the Γ -point.

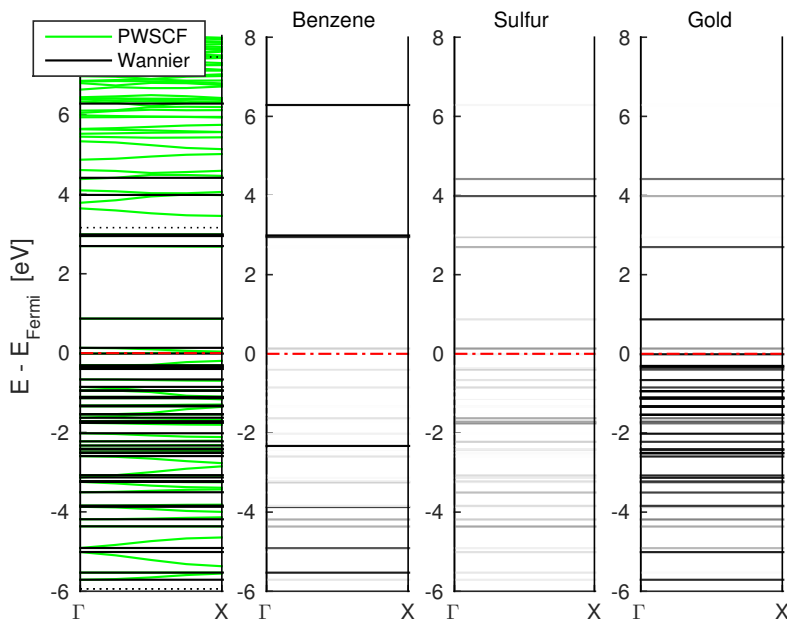


Figure 4.22: Wannier transformation of the gold-BDT-gold system.

The Fermi energy is $E_{Fermi} = -4.898$. Again all energies are given in the energy scale of the *Quantum Espresso* calculation. In figure 4.22 the band structure (green) calculated with *Quantum Espresso* is compared to the levels (black) of the Wannier orbitals. At the Γ -point almost all levels seem to agree with a band from the PWSCF calculation. Also the projected bands are shown to see to which sort of atom the levels belong to. The darker the lines are the more contribution to the particular atom sort is present. In principle, the bands near the Fermi level are important for the transport properties. Therefore the gold s - and d -orbitals and the BDT orbitals near the Fermi level should be included in the Wannier transformation.

The Wannier transformation produces 49 orbitals and therefore a Hamiltonian of the size 49×49 . For further calculations one has to sort the Wannier orbitals by their centers and symmetries. The structure of the sorted Hamiltonian is

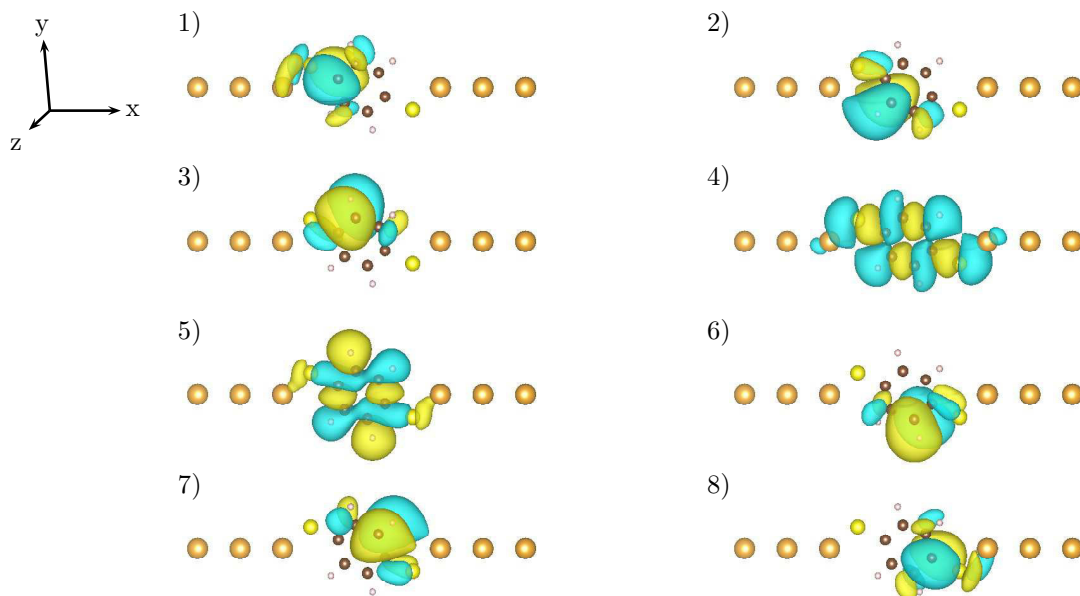


Figure 4.23: Benzene orbitals in the Wannier basis.

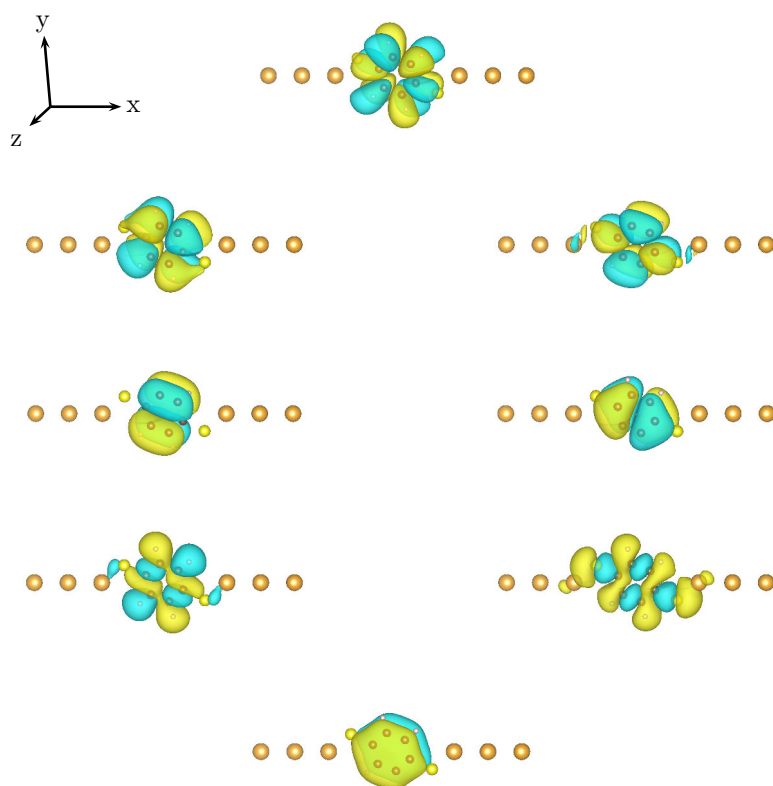


Figure 4.24: Benzene orbitals in the eigenbasis.

Six of the 49 orbitals belong to the sulfur atoms. Therefore the left sulfur Hamiltonian H_S is of size 3×3 .

$$H_S = \begin{pmatrix} \boxed{-3.07} & 0 & \boxed{1.21} \\ 0 & \boxed{-6.43} & 0 \\ \boxed{1.21} & 0 & \boxed{-7.23} \end{pmatrix} \quad (4.3.3)$$

The basis of the Hamiltonian H_S are orbital 1, 2 and 3 in figure 4.25. The orbitals 4, 5, and 6 belong to the right sulfur atom. The Hamiltonian for the right sulfur atom looks similar to 4.3.3 and is therefore not written out here. Orbital 2 and 5 are p_z -like orbitals. The others are in the plane of the benzene ring.

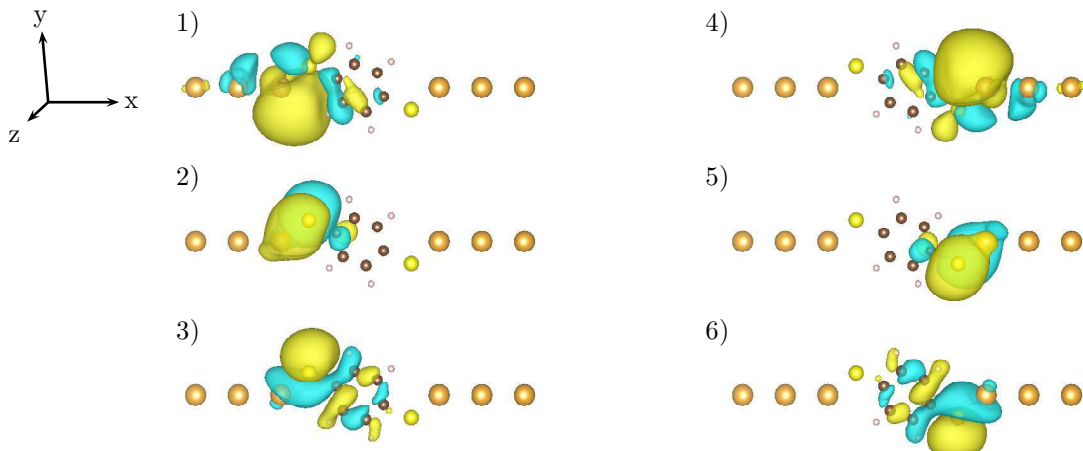


Figure 4.25: Sulfur orbitals in the Wannier basis.

The coupling matrix between the left sulfur atom and the benzene is

$$V_{SB} = \begin{pmatrix} 0 & 0 & 0 & \boxed{0.20} & \boxed{0.19} & 0 & 0 & 0 \\ \boxed{-2.11} & \boxed{0.23} & \boxed{0.15} & 0 & 0 & \boxed{0.03} & \boxed{0.03} & \boxed{0.04} \\ 0 & 0 & 0 & \boxed{-0.09} & \boxed{0.38} & 0 & 0 & 0 \end{pmatrix}. \quad (4.3.4)$$

All p_z -orbitals (blue) are coupled to each other but not to the planar ones (orange). Equations 4.3.5 and 4.3.6 describe the coupling between the gold atoms and between a gold atom and the central region.

$$V_{AuS} = \begin{pmatrix} \boxed{-1.79} & 0 & \boxed{0.33} \\ \boxed{0.45} & 0 & \boxed{-0.09} \\ 0 & \boxed{-1.08} & 0 \\ 0 & \boxed{-0.74} & 0 \\ \boxed{1.50} & 0 & \boxed{1.62} \\ \boxed{0.73} & 0 & \boxed{0.53} \end{pmatrix} \quad (4.3.5)$$

$$V_{AuB} = \begin{pmatrix} 0 & 0 & 0 & 0.31 & -0.11 & 0 & 0 & 0 \\ 0 & 0 & 0 & -0.02 & -0.00 & 0 & 0 & 0 \\ 0.13 & -0.19 & 0.01 & 0 & 0 & 0.07 & -0.03 & -0.01 \\ 0.14 & 0.01 & -0.01 & 0 & 0 & -0.03 & -0.01 & 0.01 \\ 0 & 0 & 0 & 0.16 & 0.01 & 0 & 0 & 0 \\ 0 & 0 & 0 & 0.51 & -0.09 & 0 & 0 & 0 \end{pmatrix} \quad (4.3.6)$$

So the observed symmetry even holds at the contact to the gold chains and within the gold chain. There are two transport channels through the system. p_z -like orbitals determine the first channel. The second channel is constructed by the hybridized s -orbitals in the gold chain and the planar sulfur and benzene orbitals. All orbitals in the second channel have inversion symmetry with respect to the xy -plane.

4.3.3 Transport channels

As discussed above there are two separate transport channels through the system. In the non-interacting case it is possible to do the transport calculation for the channels separately.

Channel I:

Channel I consists of orbital 1, 2, 3, 6, 7 and 8 in figure 4.23 and 2 and 5 in figure 4.25. They are all p_z -like orbitals and therefore for symmetry reasons decoupled from the orbitals with inversion symmetry with respect to the xz -plane. In a first step the Green functions of the left and the right leads have to be calculated. The third gold atom on the left hand of the center is formed to a semi-infinite chain as the left lead. Then successive the transition regions 1, 2 and 3 are added. The spectral function of the left lead is plotted in figure 4.26.

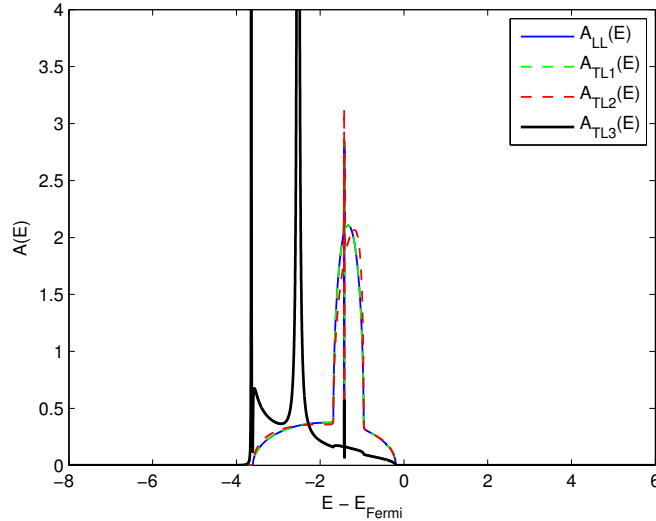


Figure 4.26: Channel I - Spectral density of the left lead.

The right lead must be calculated using the same procedure. The result for the right lead is nearly

the same as for the left one and plotted in figure 4.27. The differences result from the fact that the BDT molecule is not arranged perfectly symmetric between the gold chains.

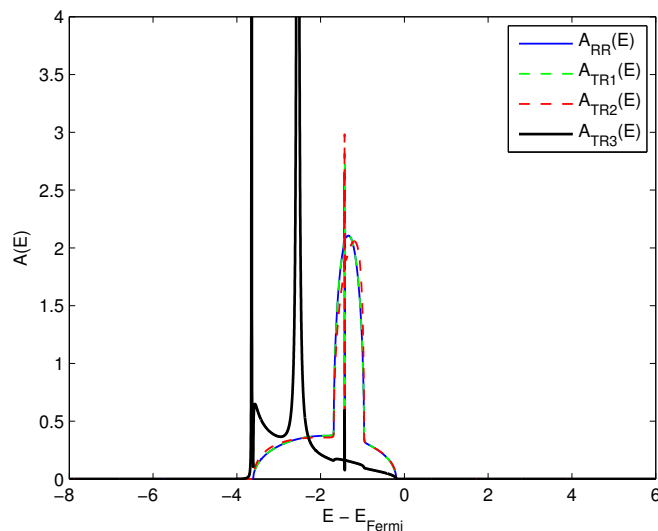


Figure 4.27: Channel I - Spectral density of the right lead.

The spectral densities of the leads are filled up to the Fermi energy. Applying a voltage across the transport system shifts the lead spectral functions against each other. In channel I the leads are completely filled with electrons. Therefore even if a voltage is applied there is no current flowing because there are no empty states for the electrons to hop into. Channel I is not conducting at all but for the sake of completeness the central region will be discussed too. The spectral function of the central region has its resonances at the eigenvalues of the corresponding Hamiltonian.

$$E_{Center}^I - E_{Fermi} = \{-5.55, -3.96, -2.39, -2.09, -0.51, 2.78, 2.92, 6.20\} \quad (4.3.7)$$

The spectral function of the isolated central region is drawn in figure 4.28.

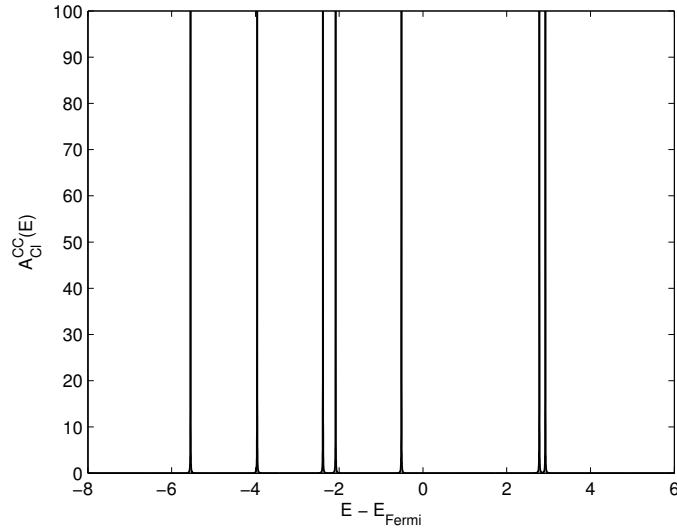


Figure 4.28: Channel I - Uncoupled spectral density of the center.

Coupling the leads to the center and applying voltage leads to the spectral functions in figure 4.29.

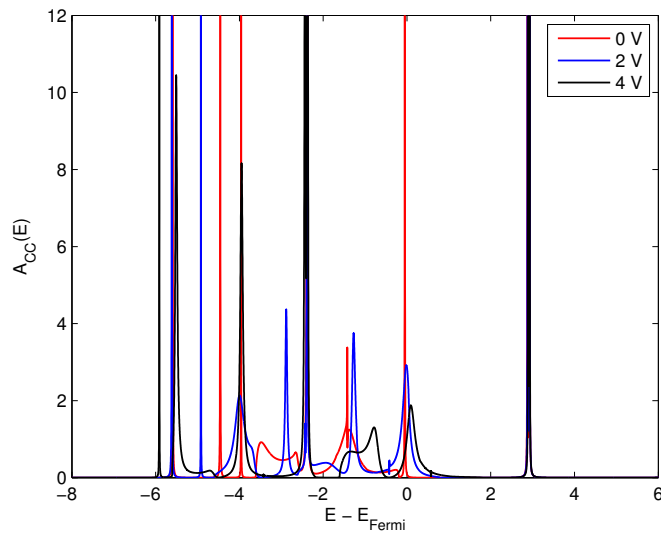


Figure 4.29: Channel I - Coupled spectral density of the center.

In the weak coupling regime the molecular orbitals of the central region are only weakly disturbed by the leads and sequential-tunneling processes are responsible for the conductance. The molecular orbitals are hybridized with the states in the leads in the large coupling regime and coherent transport happens. Comparing figure 4.28 and the 0 V curve in figure 4.29 shows that due to the coupling of the central region to the leads the peaks are broadened and shifted and there is additional structure from the leads in the spectral density. Therefore the investigated transport system is not in the small coupling regime.

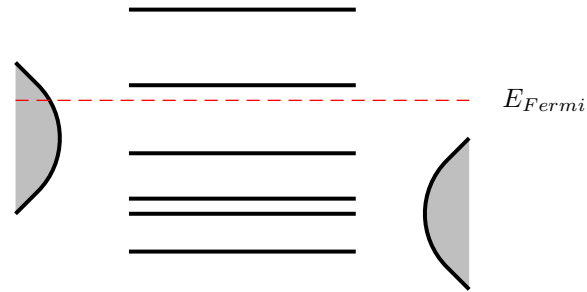


Figure 4.30: Channel I - Transport over a weak coupled central region.

Figure 4.30 illustrates the transport behavior in the case of full occupied leads. The red dashed line is the Fermi energy.

Channel II:

Channel II consists of orbital 4 and 5 in figure 4.23 and 1, 3, 4 and 6 in figure 4.25. Figure 4.31 presents the spectral function of the left lead calculated through coupling the transition layers to the semi-infinite gold chain.

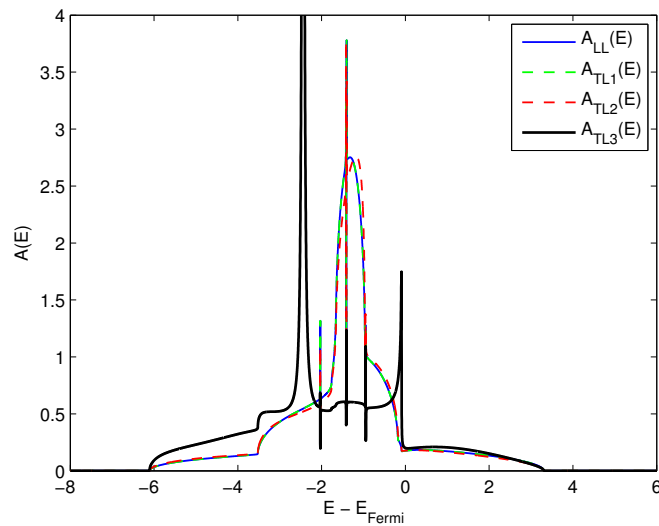


Figure 4.31: Channel II - Spectral density of the left lead.

The behavior in the right lead is nearly the same and plotted in figure 4.32.

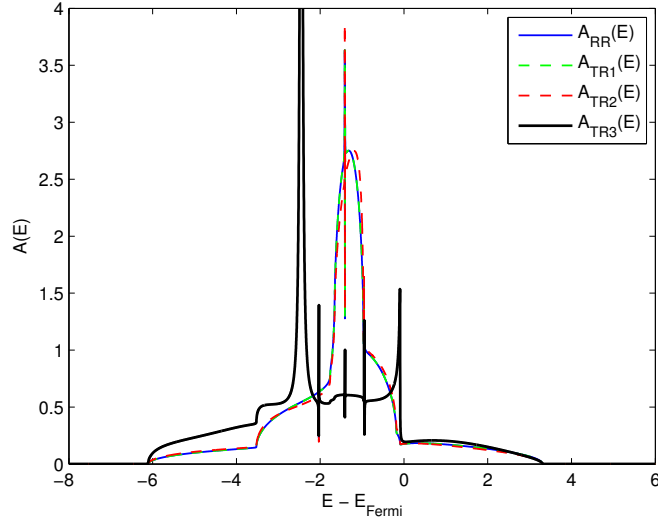


Figure 4.32: Channel II - Spectral density of the right lead.

Diagonalizing the channel II part of the center Hamiltonian leads to the eigenvalues

$$E_{Center}^{II} - E_{Fermi} = \{-4.76, -4.01, -2.67, -2.53, 2.11, 2.20\} \quad (4.3.8)$$

The peaks of the uncoupled spectral function of the center are at these eigenvalues.

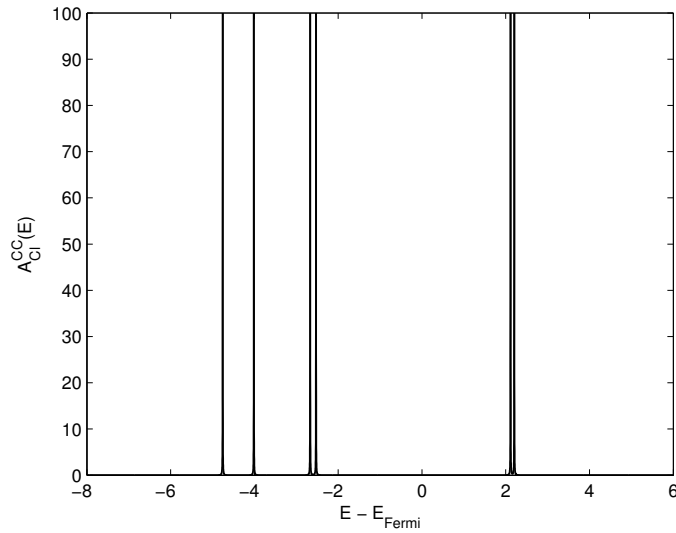


Figure 4.33: Channel II - Uncoupled spectral density of the center.

Coupling the leads to the center and applying different voltages produces the spectral functions in figure 4.34.

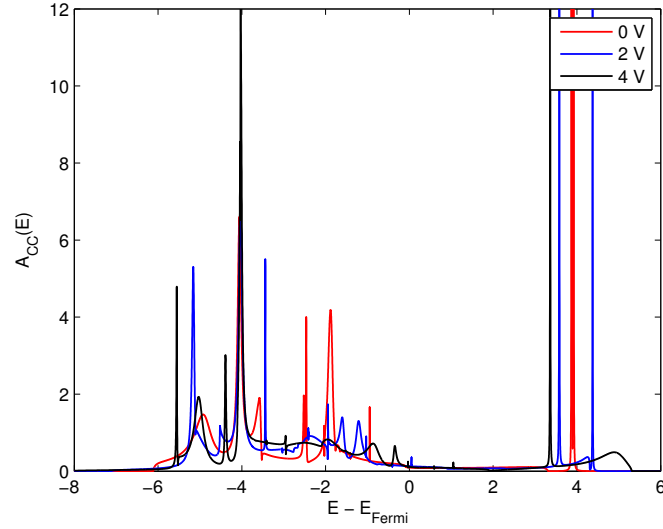


Figure 4.34: Channel II - Coupled spectral density of the center.

In channel II there are full and empty states in the leads. Due to this fact and because the spectral density of the central region has a finite value at the Fermi level there is transport in Channel II. Figure 4.35 sketches a typical transport behavior in the weak coupling regime. Applying a voltage shifts the lead Green functions against each other. If there are states in the central region current can flow through the system.

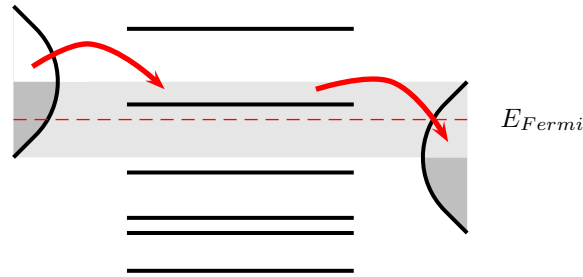


Figure 4.35: Channel II - Transport over a weak coupled central region.

The gold-BDT-gold transport system, in the configuration as treated within this thesis is not in the weak coupling regime.

4.3.4 Electron interactions

Electron-electron interactions were calculated using the Wannier orbitals and formula 2.1.9. A constant screening parameter of $\eta = 1.5$ is chosen according to [7]. To calculate the interaction parameter the integration was done numerically using the wave functions given on a lattice ($67 \times 50 \times 50$). The calculated interaction parameters are

$$U = \begin{pmatrix} \boxed{6.14} & 3.81 & \boxed{3.68} & 3.25 & 3.40 & 2.24 & \boxed{2.70} & \boxed{2.46} & 2.34 & 1.82 & 1.84 & \boxed{1.51} & 1.43 & \boxed{1.26} \\ 3.81 & \boxed{7.90} & 7.05 & 4.93 & 3.25 & 3.32 & 3.39 & 2.90 & 2.27 & 2.28 & 2.00 & 1.60 & \boxed{1.50} & 1.43 \\ \boxed{3.68} & 7.05 & \boxed{7.94} & 5.10 & 3.50 & 3.71 & \boxed{3.60} & \boxed{3.23} & 2.48 & 2.50 & 2.17 & \boxed{1.71} & 1.60 & \boxed{1.52} \\ 3.25 & 4.93 & 5.10 & \boxed{9.00} & \boxed{5.18} & \boxed{5.23} & 4.47 & 4.49 & \boxed{3.42} & \boxed{3.37} & \boxed{2.96} & 2.17 & 2.00 & 1.85 \\ 3.40 & 3.25 & 3.50 & \boxed{5.18} & \boxed{8.54} & \boxed{3.41} & 4.47 & 4.55 & \boxed{5.22} & \boxed{2.97} & \boxed{3.37} & 2.50 & 2.28 & 1.83 \\ 2.24 & 3.32 & 3.71 & \boxed{5.23} & \boxed{3.41} & \boxed{8.91} & 4.43 & 4.80 & \boxed{3.03} & \boxed{5.22} & \boxed{3.42} & 2.48 & 2.27 & 2.36 \\ \boxed{2.70} & 3.39 & \boxed{3.60} & 4.47 & 4.47 & 4.43 & \boxed{4.67} & \boxed{4.47} & 4.45 & 4.45 & 4.48 & \boxed{3.62} & 3.40 & \boxed{2.71} \\ \boxed{2.46} & 2.90 & 3.23 & 4.49 & 4.55 & 4.80 & \boxed{4.47} & 5.11 & 4.79 & 4.56 & 4.49 & \boxed{3.23} & 2.90 & \boxed{2.48} \\ 2.34 & 2.27 & 2.48 & \boxed{3.42} & \boxed{5.22} & \boxed{3.03} & 4.45 & 4.79 & \boxed{8.92} & \boxed{3.41} & \boxed{5.23} & 3.70 & \boxed{3.32} & 2.25 \\ 1.82 & 2.28 & 2.51 & \boxed{3.37} & \boxed{2.97} & \boxed{5.22} & 4.45 & 4.56 & \boxed{3.41} & \boxed{8.52} & \boxed{5.18} & 3.50 & 3.26 & 3.43 \\ 1.84 & 2.00 & 2.17 & \boxed{2.96} & \boxed{3.37} & \boxed{3.42} & 4.48 & 4.49 & \boxed{5.23} & \boxed{5.18} & \boxed{9.00} & 5.10 & 4.93 & 3.27 \\ \boxed{1.51} & 1.60 & \boxed{1.71} & 2.17 & 2.50 & 2.48 & \boxed{3.62} & \boxed{3.23} & 3.70 & 3.50 & 5.10 & \boxed{7.94} & 7.05 & \boxed{3.69} \\ \boxed{1.43} & \boxed{1.50} & 1.60 & 2.00 & 2.28 & 2.27 & 3.40 & 2.90 & \boxed{3.32} & \boxed{3.26} & \boxed{4.93} & 7.05 & \boxed{7.90} & 3.81 \\ \boxed{1.26} & 1.43 & \boxed{1.52} & 1.85 & 1.83 & 2.36 & \boxed{2.71} & \boxed{2.48} & 2.25 & 3.43 & 3.27 & \boxed{3.69} & 3.81 & \boxed{6.16} \end{pmatrix}. \quad (4.3.9)$$

The values are given in eV with an accuracy of $\pm 0.1 eV$. Again all orbitals corresponding to channel I are marked blue, channel II is marked in orange. The two channels are coupled by the interaction term.

The results can be compared to the Pariser-Parr-Pople (PPP) Model for π -electron systems with only nearest neighbor hoppings and Coulomb interaction. There the most used values for describing benzene are $t = 2.40 eV$ and $U = 11.26 eV$ [29] which is in agreement with the obtained U using a smaller screening parameter η . The Matago-Nishimoto approximation [30] makes it possible to estimate the off-diagonal from the diagonal elements.

$$U_{\alpha\beta} = \frac{e^2}{4\pi\epsilon_0 d_{\alpha\beta} + \frac{2e^2}{U_{\alpha\alpha} + U_{\beta\beta}}} \quad (4.3.10)$$

The results are shown in equation 4.3.11. The nearest neighbor C -distance is assumed to be $d_{CC} = 1.40 \text{ \AA}$.

$$U = \begin{pmatrix} 9.00 & 4.74 & 4.80 & 3.58 & 3.55 & 3.28 \\ 4.74 & 8.54 & 3.54 & 4.73 & 3.22 & 3.55 \\ 4.80 & 3.54 & 8.91 & 3.27 & 4.73 & 3.58 \\ 3.58 & 4.73 & 3.27 & 8.92 & 3.54 & 4.80 \\ 3.55 & 3.22 & 4.73 & 3.54 & 8.52 & 4.74 \\ 3.28 & 3.54 & 3.58 & 4.80 & 4.74 & 9.00 \end{pmatrix} \quad (4.3.11)$$

The calculated values are in agreement with the red values in equation 4.3.9.

Although channel I and channel II are coupled by the electron correlations interactions are only treated in channel II. Channel I is not conducting and therefore ignored in the further calculations. The approximation makes sense because due to the DFT calculation the influence of channel I on channel II is already treated at a mean field level.

Channel II:

In this case U_{ij} is the orange part of matrix 4.3.9. In the interacting case the levels get pushed away from the Fermi energy. This can be seen by comparing the uncoupled spectral functions in figure 4.33 and figure 4.36.

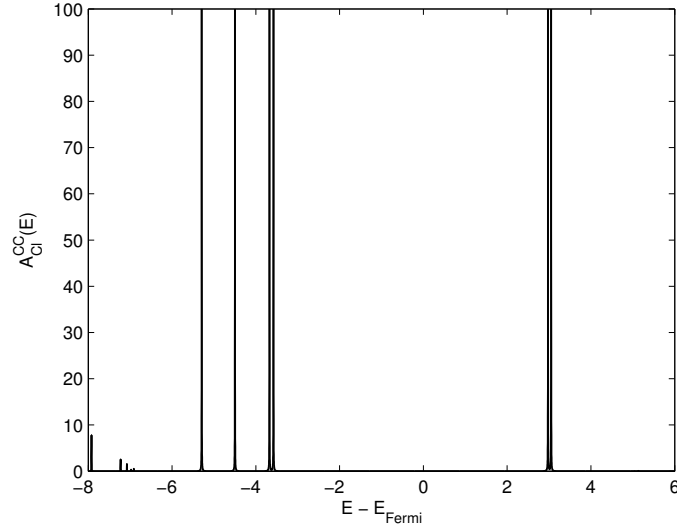


Figure 4.36: Channel II + electron interactions - Uncoupled spectral density of the center.

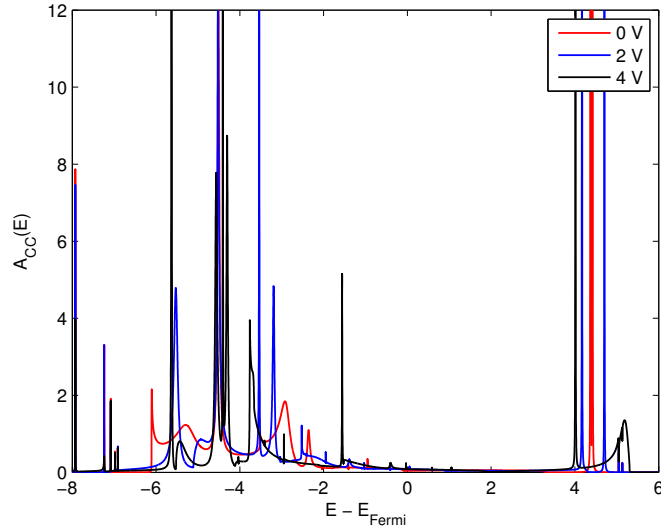


Figure 4.37: Channel II + electron interactions - Coupled spectral density of the center.

The coupled spectral function plotted in figure 4.37 has a lower value in the transport window than the coupled spectral function without interaction. Therefore the conductance in the case of including strong electron correlations will be smaller.

4.3.5 Current-voltage characteristic

Finally figure 4.38 presents the current-voltage characteristic with and without electron interactions in the central region. Due to the fact that channel I is not conducting the current is only calculated using channel II. The current is mainly due to the strong-coupling leads. Even if there are no states in the transport region of the spectral density of the decoupled central region the

leads are able to induce transmission.

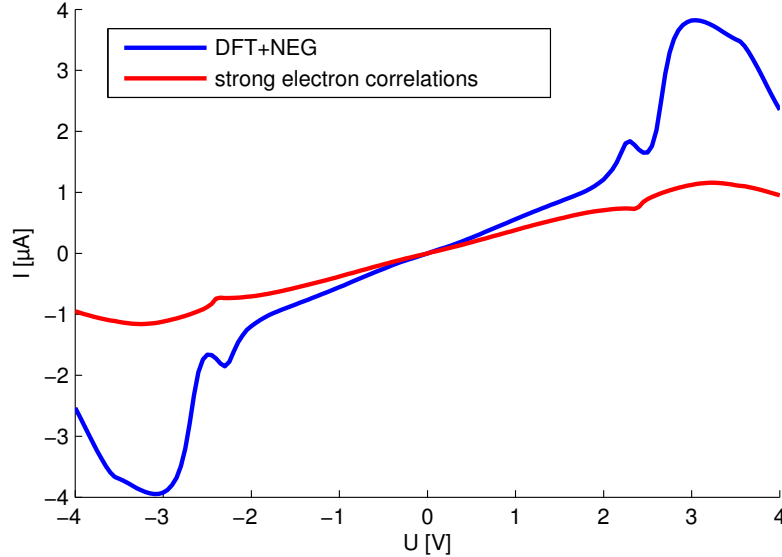


Figure 4.38: Current-voltage characteristic of the gold-BDT-gold system.

The current-voltage characteristic is only valid for $|U| < 2$ V. Looking at the band structure of the gold chain in figure 4.2 shows that one has to include the gold p -orbitals for higher voltages.

The experimental measurements of Reed and Tour [3] and of Lörtscher, Weber and Riel [4] show a non-linear behavior of the current-voltage characteristic. Reed and Tour have detected a rise of the current at $U = \pm 0.7$ V at room temperature, see figure 4.39, and Lörtscher, Weber and Riel at $U = \pm 0.45$ V at 250 K and $U = \pm 0.3$ V at 50 K. If the coupling of the leads is small enough the spectral function of channel I in figure 4.28 suggests non-linear behavior within channel I, because there is an energy level near the Fermi energy.

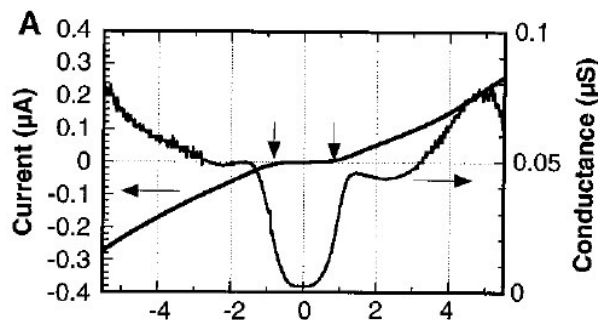


Figure 4.39: Current-voltage characteristic of the gold-BDT-gold system measured by Reed and Tour [3].

In theoretical investigations it turns out that the transport strongly depends on the type of the junction and the leads and it is not known how the contact geometry in the experiments really

looks like. For example Kondo, Kino, Nara, Ozaki and Ohno [31] have investigated the dependence of the transmission on the contact geometry in a gold bulk-BDT-gold bulk system. They have coupled the BDT molecule at different places in different rotation angles at the Au(111) surfaces and came to the result that a p_z -type LUMO orbital mainly contributes to the transport properties and the coupling to this orbital depends on the contact geometry. Also Ventra, Pantelides and Lang [32] have obtained similar results. They have modeled the leads as homogeneous electron gas and showed that the current is more than two orders of magnitude smaller if a single gold atom is put in-between each metal-molecule contact. The reason is that the gold s -states couple only to sulfur p -states perpendicular to the metal surface and therefore a channel closes in placing the single gold atom in-between the metal-molecule contacts. This is in agreement with the results of this thesis.

Comparing figure 4.38 with the experimental measurement in figure 4.39 shows, that even in contacting the BDT molecule with single gold atoms, the calculated current is still higher than in the current in the experiment. Therefore it is necessary to include strong electron correlations and electron-phonon coupling in calculations. The current-voltage characteristic in figure 4.38 shows clearly that including electron-electron interactions reduces the current.

Chapter 5

Summary and Prospects

In this thesis the transport properties through a benzene-1,4-dithiol (BDT) molecule connected to two semi-infinite gold chains were investigated. The calculation was done using Density Functional Theory (DFT) and Non-equilibrium Green functions (NEG) and including strong electron correlations in the BDT molecule. First the technique was used to study a single gold chain. By comparing the electronic band structure of the gold chain with their transmission function, it is possible to check the algorithm. Connecting two gold chains to the BDT molecule led to the gold-BDT-gold system investigated within this thesis. It turns out that in the gold-BDT-gold system transport takes place in two decoupled channels. Channel I consists of p_z -like orbitals but is not conducting due to the symmetry of the leads. The transport properties of channel II consisting of orbitals with inversion symmetry with respect to the xy -plane are mainly determined by the structure of the leads. Including strong electron correlations reduces the current.

There are a few points which would be worth the effort of further investigations on the gold-BDT-gold system.

- First it would be interesting to improve the gold-BDT-gold system transport calculation including more than nearest-neighbor coupling in the gold atoms.
- Numerical difficulties in integrations over the Keldysh Green functions causes problems by calculating the occupation numbers of the orbitals.
- A third improvement of the existing technique would be to calculate the screening parameter in the interaction potentials consistently.
- The experiment of Lörtscher, Weber and Riel [4] shows that the current decreases with temperature which suggests to perform calculations at finite temperatures.

Further steps imply changing the system of investigation. For instance contacts which couple to channel I can be taken. This can be done by using gold bulks or gold tips as leads instead of the semi-infinite gold chains or by replacing the gold atoms by platinum or aluminum atoms.

List of Figures

1.1	Gold-BDT-gold transport system.	2
1.2	Structural model of DFT+NEG.	2
2.1	Gold-BDT-gold transport system in the DFT calculation.	12
2.2	LCR transport system.	12
2.3	Extended LCR transport system.	13
2.4	Keldysh contour.	16
2.5	Arrangement of clusters in a chain.	21
2.6	Arrangement of clusters in a semi-infinite chain.	23
2.7	Current between two systems.	25
2.8	LCR transport system out of equilibrium.	30
3.1	Calculation scheme of the NEG method.	41
4.1	Unit cell of the gold chain.	43
4.2	Bandstructure and DOS of a gold chain.	44
4.3	Gold Wannier orbital in the s -model.	44
4.4	Bandstructure in the s -model.	45
4.5	Cluster Green function in the s -model.	46
4.6	Full Green functions in the s -model.	46
4.7	Lead-induced self energy in the s -model.	47
4.8	Band structure, DOS and transmission in the s -model.	47
4.9	Gold Wannier orbitals in the sd -model.	49
4.10	Gold d -orbitals.	50
4.11	Hybridized gold orbitals.	50
4.12	Green functions in the sd -model.	51
4.13	Lead-induced self energy in the sd -model.	52
4.14	Bandstructure, DOS and transmission in the sd -model (TB1).	52
4.15	Bandstructure, DOS and transmission in the sd -model (TB2).	53
4.16	Benzene orbitals.	55
4.17	Benzene energy levels.	56
4.18	Gold-BDT-gold transport system.	56
4.19	Unit cell of the gold-BDT-gold system.	57
4.20	Configurations of the BDT.	57
4.21	Total energies of the BDT configurations.	58
4.22	Wannier transformation of the gold-BDT-gold system.	59
4.23	Benzene orbitals in the Wannier basis.	61
4.24	Benzene orbitals in the eigenbasis.	61
4.25	Sulfur orbitals in the Wannier basis.	62
4.26	Channel I - Spectral density of the left lead.	63
4.27	Channel I - Spectral density of the right lead.	64
4.28	Channel I - Uncoupled spectral density of the center.	65

4.29 Channel I - Coupled spectral density of the center.	65
4.30 Channel I - Transport over a weak coupled central region.	66
4.31 Channel II - Spectral density of the left lead.	66
4.32 Channel II - Spectral density of the right lead.	67
4.33 Channel II - Uncoupled spectral density of the center.	67
4.34 Channel II - Coupled spectral density of the center.	68
4.35 Channel II - Transport over a weak coupled central region.	68
4.36 Channel II + electron interactions - Uncoupled spectral density of the center. . . .	70
4.37 Channel II + electron interactions - Coupled spectral density of the center.	70
4.38 Current-voltage characteristic of the gold-BDT-gold system.	71
4.39 Current-voltage characteristic measured by Reed and Tour.	71

List of Tables

4.1	Hopping parameters in the s -model.	45
4.2	Comparison of different functionals to experimental results.	56
4.3	Convergence of the energies as a function of the number of gold atoms per unit cell.	58

Bibliography

- [1] M. Di Ventra, S. T. Pantelides, N. D. Lang. *The benzene molecule as a resonant-tunneling transistor*. Appl. Phys. Lett. 76, 3448 (2000).
- [2] F. Schwarz, G. Kastlunger, F. Lissel, C. Egler-Lucas, S. N. Semenov, K. Venkatesan, H. Berke, R. Stadler, E. Lörtscher. *Field-induced conductance switching by charge-state alternation in organometallic single-molecule junctions*. Nat. Nanotechnol. 11, 170–176 (2016).
- [3] M. A. Reed, C. Zhou, C. J. Muller, T. P. Burgin, J. M. Tour. *Conductance of a Molecular Junction*. Science 278, 5336, 252-254 (1997).
- [4] E. Lörtscher, H. B. Weber, H. Riel. *Statistical Approach to Investigating Transport through Single Molecules*. Phys. Rev. Lett. 98, 176807 (2007).
- [5] J. C. Cuevas, E. Scheer. *Molecular Electronics, An Introduction to Theory and Experiment*. World Scientific Publishing Company (2010). ISBN 978-9814282581.
- [6] A. Calzolari, N. Marzari, I. Souza, M. Buongiorno Nardelli. *Ab initio transport properties of nanostructures from maximally localized Wannier functions*. Phys. Rev. B. 69, 035108 (2004).
- [7] D. A. Ryndyk, A. Donarini, M. Grifoni, K. Richter. *Many-body localized molecular orbital approach to molecular transport*. arXiv:1210.5615v1 (2012).
- [8] D. Bohm, D. Pines. *A Collective Description of Electron Interactions: III. Coulomb Interactions in a Degenerate Electron Gas*. Phys. Rev. 92, 609 (1953).
- [9] G. Czycholl. *Theoretische Festkörperphysik Band 1*. Springer (2016). ISBN 9783662471418.
- [10] P. Hohenberg, W. Kohn. *Inhomogeneous electron gas*. Phys. Rev. 136, B864 (1964).
- [11] W. Kohn, L. J. Sham. *Self-consistent equations including exchange and correlation effects*. Phys. Rev. 140, A1133 (1965).
- [12] W. Kohn. *Electronic structure of matter - wave functions and density functionals*. Nobel Lecture (1999).
- [13] N. Marzari, D. Vanderbilt. *Maximally localized Wannier functions for composite energy bands*. Phys. Rev. B 56, 12847 (1997).
- [14] A. A. Mostofi, J. R. Yates, Y.-S. Lee, I. Souza, D. Vanderbilt and N. Marzari. *Wannier90: A Tool for Obtaining Maximally-Localized Wannier Functions*. Comput. Phys. Commun. 178, 685 (2008).
- [15] I. Souza, N. Marzari, and D. Vanderbilt. *Maximally localized Wannier functions for entangled energy bands*. Phys. Rev. B 65, 035109 (2001).
- [16] M. Shelley, Nicolas Poilvert, Arash A. Mostofi, Nicola Marzari. *Automated quantum conductance calculations using maximally-localised Wannier functions*. Comput. Phys. Commun. 182, 10, 2174-2183 (2011).

- [17] W. Nolting. *Grundkurs Theoretische Physik 7: Viel-Teilchen-Theorie*. Springer (2009). ISBN 9783642016066.
- [18] D. A. Ryndyk, R. Gutierrez, B. Song, G. Cuniberti. *Green function techniques in the treatment of quantum transport at the molecular scale*. arXiv:0805.0628v2 (2008).
- [19] A. Jauho. *Introduction to the Keldysh nonequilibrium Green function technique*. <https://nanohub.org/resources/1877> (2006).
- [20] L. V. Keldysh. *Diagram technique for nonequilibrium processes*. Sov. Phys. JETP 20, 4 (1965).
- [21] D. Sénéchal. *An introduction to quantum cluster methods*. arXiv:0806.2690v2 (2008).
- [22] P. Headley. *Course in Advanced Solid State Physics at TU Graz*. <http://www.if.tugraz.at> (2014).
- [23] Y. Meir, N. S. Wingreen. *Landauer formula for the current through an interacting electron region*. Phys. Rev. Lett. 68, 2512 (1992).
- [24] R. Landauer. *Spatial Variation of Currents and Fields Due to Localized Scatterers in Metallic Conduction*. IBM J. Res. Dev. 1, 223–231 (1957).
- [25] V. I. Anisimov, F. Aryasetiawan, A. I. Lichtenstein. *First-principles calculations of the electronic structure and spectra of strongly correlated systems: the LDA + U method*. J. Phys.: Condens. Matter 9, 767-808 (1997).
- [26] <http://www.quantum-espresso.org> (2016).
- [27] G. Scauzero, A. Dal Corso, A. Smogunov. *Interaction of CO with an Au monoatomic chain at different strains: Electronic structure and ballistic transport*. Phys. Rev. B. 85, 165411 (2012).
- [28] K. Yabana, G. F. Bertsch. *Time-dependent local-density approximation in real time: Application to conjugated molecules*. Int. J. Quant. Chem. 75, 55-66 (1999).
- [29] R. J. Bursill, C. Castleton, W. Barford. *Optimal parametrisation of the Pariser-Parr-Pople Model for benzene and biphenyl*. Chem. Rev. Let. 294, 305-313 (1998).
- [30] B. Muralidharan, A. W. Ghosh, S. K. Pati, S. Datta. *Theory of high bias Coulomb Blockade in ultrashort molecules*. arXiv:0610244v1 (2006).
- [31] H. Kondo, H. Kino, J. Nara, T. Ozaki, T. Ohno. *Contact-structure dependence of transport properties of a single organic molecule between Au electrodes*. Phys. Rev. B 73, 235323 (2006).
- [32] M. Di Ventra, S. T. Pantelides, N. D. Lang. *First-Principles Calculation of Transport Properties of a Molecular Device*. Phys. Rev. Let. 84, 979 (1999).